AN INVESTIGATION OF THE PRINCIPLES OF LABORATORY-SCALE
PARTICLE-BED COMMINUTION

A THESIS SUBMITTED TO
THE GRADUATE SCHOOL OF NATURAL AND APPLIED SCIENCES
OF
MIDDLE EAST TECHNICAL UNIVERSITY

BY

HANDE CİMİLLİ

IN PARTIAL FULFILLMENT OF THE REQUIREMENTS
FOR
THE DEGREE OF MASTER OF SCIENCE
IN
MINING ENGINEERING

MAY 2008

Approval of thesis:

AN INVESTIGATION OF THE PRINCIPLES OF LABORATORY-SCALE PARTICLE-BED COMMINUTION

submitted by **HANDE CİMİLLİ** in partial fulfillment of the requirements for the degree of **Master of Science in Mining Engineering Department, Middle East Technical University** by,

Prof. Dr. Canan Özgen
Dean, Graduate School of **Natural and Applied Sciences** _____

Prof. Dr. Celal Karpuz
Head of Department, **Mining Engineering** _____

Prof. Dr. Çetin Hoşten
Supervisor, **Mining Engineering Dept., METU** _____

Examining Committee Members:

Prof. Dr. M. Ümit Atalay
Mining Engineering Dept., METU _____

Prof. Dr. Çetin Hoşten
Mining Engineering Dept., METU _____

Prof. Dr. Ali İhsan Arol
Mining Engineering Dept., METU _____

Prof. Dr. Yavuz Topkaya
Metallurgical and Materials Engineering Dept., METU _____

Dr. Çağatay Avşar
Metso Minerals Dış Ticaret Ltd. Şirketi _____

Date: 9 May 2008

I hereby declare that all information in this document has been obtained and presented in accordance with academic rules and ethical conduct. I also declare that, as required by these rules and conduct, I have fully cited and referenced all material and results that are not original to this work.

Name, Last name: Hande Cimilli

Signature   :

ABSTRACT

AN INVESTIGATION OF THE PRINCIPLES OF LABORATORY-SCALE PARTICLE BED COMMINUTION

Cimilli, Hande

M. Sc., Department of Mining Engineering

Supervisor: Prof. Dr. Çetin Hoşten

May 2008, 120 pages

The objective of this thesis is to investigate the principles of laboratory-scale particle bed comminution in a piston-die-press. The feed materials used in this investigation are quartz and calcite which were stage-crushed and dry screened to produce 3.35 x 2.36, 2.36 x 1.7, 1.7 x 1.18, 1.18 x 0.85, and minus 0.85mm size fractions. First, these narrow size fractions (excluding minus 0.85mm fraction) were comminuted under different pressures to determine the baseline for energy utilization. Then, these size fractions and minus 0.85mm size fraction were proportionately mixed to produce feeds of three different size distributions having three different Gates-Gaudin-Schuhmann (GGS) size distribution moduli (m=0.5, 0.7, and 0.9), and comminuted under different bed pressures of appropriate magnitudes to generate a reasonable range of specific breakage energy inputs.

As a result of the experiments carried out, it can be concluded that higher amounts of fines were obtained from calcite samples than quartz at all narrow-range size fractions and distribution moduli. Furthermore, experimental results showed that the feed material having the widest size distribution (m = 0.5) showed more resistance to

size reduction when compared with narrow-size fractions, which led to increase in energy consumption due to the presence of higher amounts of fines. Tests samples with distribution moduli of 0.7 and 0.9 showed higher resistance to size reduction than narrow-size samples, but the reduction ratios achieved with the size distributed samples were higher than those achieved with the narrow-size samples. In addition, by using t-curves (t_{50} and t_{10}) the amounts of breakage of different samples were compared. Consequently, the distribution modulus of 0.9 gave better breakage results in terms of expended energy and amount of breakage than all narrow-size fractions, especially for the relatively soft mineral calcite.

ÖZ

LABORATUVAR ÖLÇEKLİ TANE YATAKLARINDA KIRILMA İLKELERİNİN İNCELENMESİ

Cimilli, Hande

Yüksek Lisans, Maden Mühendisliği Bölümü

Tez Yöneticisi: Prof. Dr. Çetin Hoşten

Mayıs 2008, 120 sayfa

Bu çalışmada, laboratuvar ölçekli sıkıştırılmış yataklarda tane ufalanması ilkelerinin piston-kalıp basma düzeneğinde incelenmesi amaçlanmıştır. Deneylerde kullanılan kuvars ve kalsit numuneleri kırılıp elenerek 3,35 x 2,36; 2,36 x 1,7; 1,7 x 1,18; 1,18 x 0,85 ve 0,85mm'den ince tane boyutlarındaki numuneler elde edilmiştir. Öncelikli olarak bu tane boyutlarındaki numuneler (850 mikrondan ince malzeme hariç) farklı basınçlar altında kırılarak enerji kullanımı ile ilgili temel teşkil edecek veriler elde edilmiştir. Daha sonra bu tane boyutlarının ve 850 mikrondan ince malzemenin belirli miktarlarda karıştırıldığı üç farklı Gates-Gaudin-Schuhmann (GGS) tane boyut dağılım modülüne (m=0,5; 0,7; 0,9) sahip numuneler elde edilmiştir. Bu numuneler de, belirli özgül kırılma enerjileri sağlayacak farklı yatak basınçları altında kırılmışlardır .

Bütün dar aralıklı tane boyutlarındaki ve farklı dağılım modüllerindeki numunelerle yapılan deneylerde kalsit numunelerinin kırılması sonucunda kuvarsa oranla daha çok ince tane elde edilmiştir. Ayrıca, deney sonuçlarına göre kırılma işlemine en çok direnç gösteren numuneler en geniş tane boyut dağılımına sahip olanlardır (m=0,5). Karışımın içerisinde bulunan ince tane miktarının diğer modüllere kıyasla çok

daha fazla olması sebebi ile artan direnç, harcanan enerji miktarını da arttırmaktadır. Diğer modüllerde de (m=0,7 ve m=0,9) kırılmaya karşı oluşan direnç fazla olmasına karşın, dar aralıklı tane boyutlarında elde edilen kırılma oranından daha yüksek kırılmalar elde edilmiştir. Bunların yanı sıra, numunelerin kırılma miktarları t-eğrileri (t_{50} and t_{10}) kullanılarak da karşılaştırılmıştır. Sonuç olarak, özellikle daha yumuşak olan kalsit minerali için m=0,9 modülü harcanılan enerji ve kırılma oranı açısından daha olumlu sonuçlar vermiştir.

Anahtar Kelimeler: Sıkıştırılmış Yataklarda Kırılma, Kırılma Enerjisi

TO MY FAMILY

ACKNOWLEDGEMENT

I would like to express my deepest gratitude to my supervisor Prof. Dr. Çetin Hoşten for his guidance, patience and advices throughout this research.

I would like to acknowledge the help of Doç.Dr.Levent Tutluoğlu and his guidance in the rock mechanics laboratory.

I want to thank to Natural and Applied Science Institute of METU for the financial support given for the project of BAP-2006-03-05-03.

I would like to thank to Cemil Acar, Arman Koçal, Tahsin Işıksal, Aytekin Aslan and Hakan Uysal for their help during laboratory work.

Thanks to my roommate Mehtap Gülsün Kılıç and my friends Seda Şalap and Savaş Özün. It was always nice to have their technical and moral support throughout this study.

I wish to express my special thanks to my mother Hilmiye Cimilli and my father Latif Cimilli and my grandparents for their patience, support and love in every moment throughout my education.

The acknowledgement would not be complete without the mention of my beloved fiancée, Emrah Mertyürek for patience and moral support he provided. Without his support and understanding I would never have completed this study.

TABLE OF CONTENTS

LIST OF TABLES

LIST OF FIGURES

xvi

CHAPTER 1

INTRODUCTION

1.1. General

Comminution is the most energy-intensive and energy-inefficient operation in mineral processing; however, the energy demand for comminution is continually rising because of a trend towards finer grinding due to the processing of low-grade ores and the liberation of finely disseminated ores.

Roller presses, also generally referred to high pressure grinding rolls (HPGR) or high pressure roll mills (HPRM), were developed in Germany by KHD and Polysius, on the principle of inter-particle comminution (Schönert, 1979 as cited in Mehra, 1998; Schönert, 1988) and first came on the market in 1986. Large scale continuous grinding in the particle bed mode is carried out in this relatively recently invented high pressure roll mills. The roller press technology established itself so quickly in the cement industry because of its two essential features: its energy efficiency and its suitability to upgrade existing ball mill systems up to 250 % of the original capacity (Seebach et. al., 1996 as cited in Holland et. al., 1997). So, the roller press technology has been well established for clinker grinding and originally applied in the cement industry treating relatively easily crushed materials. Since then, it has been applied to progressively harder, tougher and more abrasive materials. Evidence has emerged on the ability of high-pressure roll grinding in weakening a variety of materials, including tin ores (Clarke and Wills, 1989), cement clinker (Schwarz and Seebach, 1990), dolomite (Vázquez-Favela, 1995) and coal (Fuerstenau et al., 1995), among others.

In particle-bed comminution, energy is transferred directly to the mass, and breakage takes place by very high stresses generated locally at the contact points between particles in the tightly compressed bed. Also, comminution in the HPRM is the result of the high interparticle stresses generated when thick beds of particles compressed under high pressures as it moves down the gap between two pressurized rolls are compressed. However, it is difficult to attain a complete particle-bed mode of grinding in the HPRM. In some previous studies about particle-bed comminution, piston-die-press set-up was used for comminution which is illustrating the particle-bed mode of grinding and mostly narrow-range size fractions were used during experiments.

1.2 Objectives and Scope of the Thesis

In this thesis, quartz and calcite samples were comminuted in particle-bed mode by simulating the process with a piston-die-press batch operation in the laboratory. Beside narrow-size fractions, different size distributions having three different Gates-Gaudin-Schuhmann (GGS) size distribution moduli (m=0.5, 0.7, and 0.9) were comminuted and the effect of feed particle size distribution on particle bed comminution was investigated. Firstly, narrow size fractions were comminuted under different pressures to determine the baseline for energy utilization. Then these size fractions were proportionately mixed to produce feeds of three different size distributions having three different Gates-Gaudin-Schuhmann size distribution moduli and comminuted under different bed pressures of appropriate magnitudes to generate a reasonable range of specific breakage energy inputs. At the end of experiments, comparing the results of different particle size fractions; the influence of bed pressure and the effect of material hardness on particle bed comminution, breakage fraction, self-similarity, and energy absorption and energy utilization were investigated, which are fundamental discussion topics of particle bed comminution.

CHAPTER 2

LITERATURE SURVEY

In order to be efficient, the design of a grinding machine must follow some general principles. An efficient grinding device would involve the direct flow of particles to the breakage zone, slow compression loading of particles, and immediate removal of the broken fragments (Lo et al., 1993). As comminution is a high energy consuming process, each stage of the process must be as efficient as possible. The device that best fulfils the conditions listed above is a high-pressure roll mill (HPRM).

2.1 Operating Principle of HPRM

In the high pressure roll mill, thick beds of particles are compressed under high pressures, as shown in Figure 1. Complex stress fields exist in the particle bed under compression; compressive stresses and shear stresses, resulting from the relative motion of particles during compaction, are superimposed (Gutsche and Fuerstenau, 1999). Comminution in HPRM is the result of the high interparticle stresses generated when a bed of solids is compressed as it moves down the gap between two pressurized rolls. Such high interparticle stresses result in a much greater proportion of fines in comparison to conventional crushing.

In size reduction processes focus is primarily on the interrelated phenomena of energy absorption, energy utilization, reduction ratio, grind limit and size distributions of the comminuted product. In particle-bed comminution, unlike most conventional grinding mills, energy is transferred directly to the charge mass and breakage occurs by very high stresses generated locally at the contact points between the particles of the tightly compressed bed (Fuerstenau et al., 1991). The energy

utilization of ball mills is lower than in HPRMs, because of the ball mill's stochastic hit-and-miss collision process. For this reason, among others, significantly enhanced energy efficiency is realized when a confined bed of particles is comminuted under sufficiently high compressive loads.
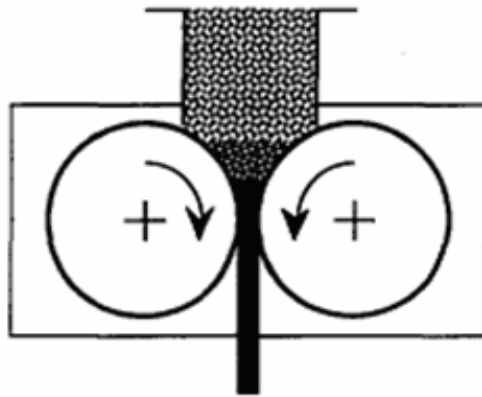
Figure 1: High pressure roll mill operating principle

2.2 Mill Performance

Strictly speaking, an ideal measure of the inherent grindability of a solid should be by definition independent of the feed size, product fineness, quantum of energy expended, particle-particle interaction and allied energy dissipation phenomena and the nature of the comminution equipment employed (Fuerstenau and Kapur, 1994). However, depending on the working principle employed; the nature of the material being ground and the extent of size reduction achieved, grinding mills can differ greatly in their performance, especially in the matter of energy utilization, which may be defined as the new surface generated in the comminuted particles per unit net grinding energy invested (Rumpf, 1973 and 1990 as cited in Fuerstenau and Kapur, 1994).

4

A straight-forward index of mill performance would be the ratio of the energy utilized in the test equipment and the energy utilized in a reference mode of comminution. Extensive studies have shown that the highest energy utilization is achieved when a single particle is loaded and crushed in slow compression (Schönert, 1986 as cited in Fuerstenau and Kapur, 1994). Earlier, using similar reasoning, Stairmand (1975, as cited in Fuerstenau and Kapur, 1994) proposed to compare mill performance against single-particle crushing data.

After single-particle breakage, the next most efficient method of comminution is particle-bed comminution (Schönert, 1988 and Fuerstenau and Kapur, 1995 as cited in Fuerstenau and Kapur, 2003). In this mode, comminution occurs primarily by very high localized interparticle stresses generated within the particle bed. No separate carrier is employed for the transport of energy to the solids, unlike in tumbling mills. Particle bed comminution is carried out continuously in a device comprised of two counter-rotating rolls. As the feed particles pass through the roll gap, the particle bed is compressed and the coarser particles undergo an isostatic-like compression by the fine particles in which the coarser ones are embedded. Energy is lost in the high-pressure roll mill due to friction between the particles as they pass through the roll gap and due to the ineffectiveness of the isostatic loading phenomenon.

2.3 Parameters Affecting the Breakage in HPRM

2.3.1 Particle Size

In the literature, comminution in the HPRM and subsequent ball milling has been observed to produce significant energy savings in comparison to ball milling alone. This has been partially attributed to the weakening resulting from compression of the bed of particles in the HPRM (Tavares, 2005). It is found that coarse particles are

damaged preferentially and weakening is more significant at higher pressures (and specific energy inputs) in the HPRM if compared to the products of conventional crushing equipment.

Tavares (2005) stated that, at sizes larger than about 1.5 mm, statistically significant differences exist between the fracture energies of the products of the hammer mill and the HPRM. About 35% less energy, on the average, is required to fracture particles from the HPRM product if compared to hammer-milled material. On the other hand, at sizes below 1.5 mm the differences in the fracture energies are no longer statistically significant. The greater effect of weakening at coarser sizes in the HPRM may be explained by the fact that a coarse particle, before being stabilized by neighboring particles as the result of the unfavorable stress field in its surroundings which can prevent its fracture, suffers a long history of stresses in multiple directions as it moves down toward the gap between the rolls. This longer exposure to the stress fields makes a coarse particle more amenable to damage than finer ones during comminution in high pressure grinding mills.

2.3.2 Influence of Position in the Particle Bed

Particle weakening was found to occur irrespective of the position of the particle within the bed (Tavares, 2005). Differences between the various portions of the bed were found to be insignificant, showing that damage in the HPRM takes place independent of lateral position. Approximately isostatic stress field existing within the confined bed is likely to produce the uniform weakening of the material. This determinate and relatively uniform loading of the material in the HPRM compression zone leads to efficiency in energy savings, whereas the loading in crushers and mills is random and highly variable, and therefore inefficient.

2.3.3 Influence of Energy Input on Breakage

It is commonly observed in particle bed compression that, as energy input is increased beyond a critical level, the breakage rates of the material decrease markedly, until breakage comes to a halt (Hanisch and Schubert, 1982 & Schönert and Flügel, 1980 as cited in Tavares, 2005). At that point, energy is mainly consumed in compaction of the bed. Considering this situation, it appears that the reduction in breakage rates at higher pressures may be compensated by an increase in the amount of damage induced in the material. An optimum energy level must therefore be established which considers not only the size distribution of the HPRM product but also its amenability to subsequent grinding stages.

2.3.4 Mechanics of Inter-Particle Breakage

At higher loads and degree of compaction, fine particles begin to transmit force, and distribute the force flux over the surface of large particles. The increasingly even distribution of stress on the particle surface stabilizes coarse particles. At high degrees of compaction a near isostatic stress field exists on the surface of large particles, and breakage of these particles ceases (Gutsche and Fuerstenau 1999). The increase of fracture strength resulting from the compaction of the particle bed and the associated granulometric stabilization has been coined retardation by Fuerstenau et al. Figure 2 taken from the paper of Gutsche and Fuerstenau (1999) illustrates the retardation of grinding kinetics of coarse particles in the presence of fine particles. The breakage fraction of the coarse 6x8 mesh constituent is plotted as a function of the fraction of fines in the feed. The breakage fraction, that is the ratio of the mass of broken particles to the total mass of the feed, is a modified fracture probability for irregular shaped particles. The general trend is that the breakage fraction decreases with the amount of fines in the feed. The energy per surface area, or the exerted stress, is lower in embedded coarse particles that have a large number of force transmitting neighbors. Thus, the stabilization of coarse particles by fines is the result

of the distribution of the force flux on the surface of coarse particles. Embedded coarse particles experience increasingly an even distribution of stress on their surface, which eventually becomes isostatic. The stabilization of the coarse size is a function of the size of the fine component; the smaller the fine component, the more rapid the decrease. The size effect disappears towards small fractions of fines in the feed, when the fine material mostly fills the voids between coarse particles and transmits only a small share of the total energy.

The retardation of grinding kinetics of coarse particles is accompanied by an acceleration of grinding kinetics of fine particles (Gutsche and Fuerstenau, 1999). Figure 3 shows the breakage fraction of 16x28 mesh limestone particles comminuted in the presence of 20% coarse 6x8 mesh particles as a function of bed pressure. The probability of fracture of 16x28 mesh limestone particles increases by about 10% when comminuted in the presence of coarse 6x8 mesh limestone particles. The fines in the admixture have only a few contact points that transmit force and thus experience much higher local stresses. As a consequence, their breakage fraction increases in the presence of coarse particles.
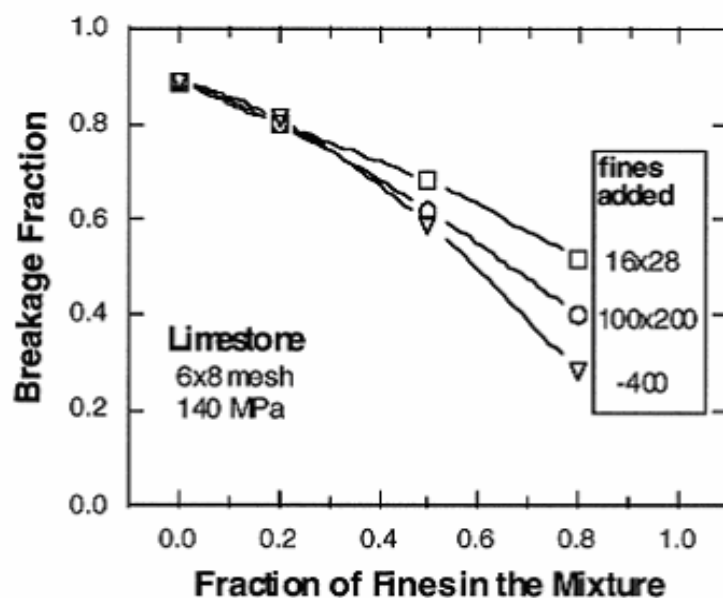
Figure 2: Breakage probability for 6x8 mesh limestone comminuted in the presence of fines (Gutsche and Fuerstenau, 1999)

8
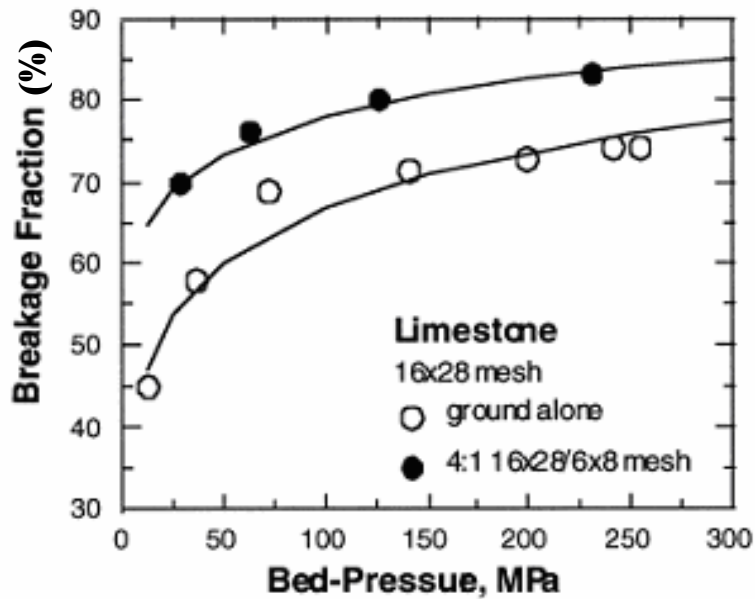
Figure 3: Breakage probability for 16x28 mesh limestone comminuted in the presence of 6x8 mesh coarse particles (Gutsche and Fuerstenau, 1999)

Fines are produced by stagewise size reduction, with coarse particles grinding finer particles and fine particles stabilizing coarse particles. Increasing the energy increases the portion of energy that flows into the production of fine particles.

Although the ball mill's energy transmission is less effective, its generation of -200 mesh particles at high energy inputs exceeds fines generation in the HPRM because increasing bed-compaction in the HPRM retards kinetics of size reduction and generation of -200 mesh particles. However, the HPRM's excess energy flows into overgrinding the -200 mesh product. Its energy utilization, that is the surface area created per energy invested, remains high (Gutsche and Fuerstenau, 1999).

If fines control size reduction of coarse particle and size reduction occurs stagewise from the largest particle size downward, adding fines to a coarse feed might reduce the production of fines from the coarse constituent of the feed. The idea is to add fines purposely to the mill feed in order to minimize the generation of difficult-to-

9

recover fines during size reduction of coarse particles. Fines in the feed absorb energy that would otherwise flow into the generation of unwanted fine particles resulting from size reduction of coarse particles. The relative production of fines decreased, but the kinetics of size reduction of the coarse particles also decreased.

2.3.5 Size Distributions and Energy Utilization

As illustrated in Figure 4 (Fuerstenau et al., 1996), the size distribution curves of quartz particles generated in particle-bed comminution are self-similar when plotted against a dimensionless size that has been scaled by the median size, X_{50}. This means that a unique size distribution is associated with any given median size, and the size spectrum is driven forward on its trajectory by reduction in the median size only. As such, this scalar is a valid and consistent measure of the product fineness and moreover, its variation with energy input is also a valid and meaningful energy-size reduction relationship (Kapur, 1987 as cited in Fuerstenau et. al., 1996).

It was pointed out by Fuerstenau et al. (1990) that, as shown in Figure 5 and 6 for galena and dolomite, the size distribution of ground material formed when particles are crushed singly are self-preserving when the particle size x is rescaled by a suitable scaling factor, median size.
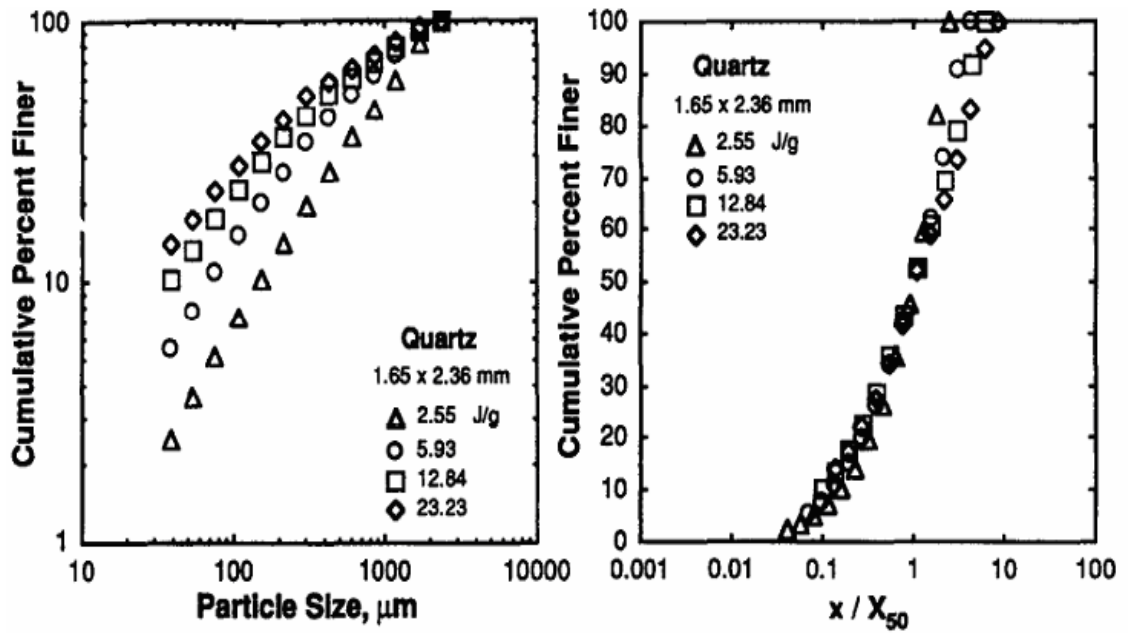
Figure 4: Self-similar size distribution of quartz comminuted in piston-die-press (Fuerstenau et. al., 1996)
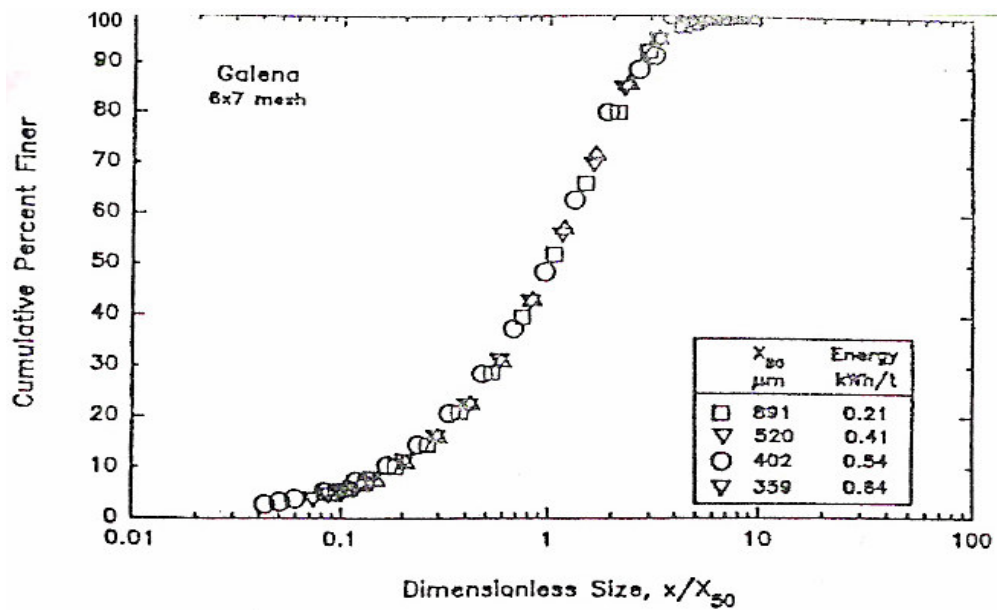
Figure 5: Self-similar size distribution of galena comminuted in the single-particle mode (Fuerstenau and Kapur, 1994)

11
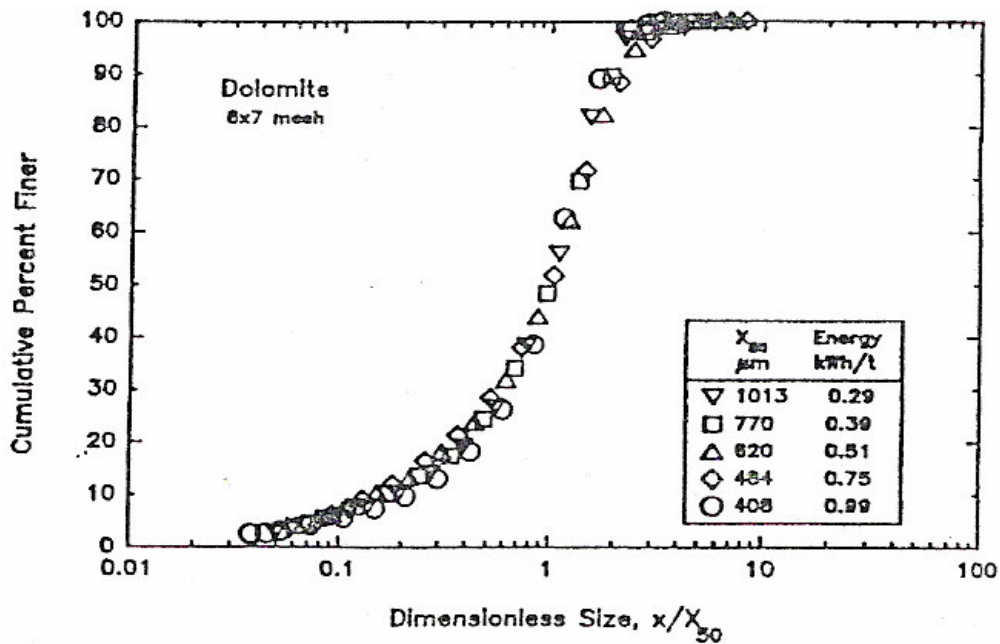
Figure 6: Self-similar size distribution of dolomite comminuted in the single-particle mode (Fuerstenau and Kapur, 1994)

A well-known property of self-similar distributions is that the percentile and mean sizes are interchangeable scaling factor and, in particular, median size is inversely proportional to specific surface area (Kapur, 1972 as cited in Fuerstenau and Kapur, 1994).

$$X_f / X_{50} = j E_m + e \quad \text{……………………………………………..…..……….....} \quad (1)$$

This equation relates a dimensionless reduction ratio defined as X_f / X_{50} with energy expended (E_m) in an exceptionally convenient manner for measurement, analysis and comparison. The reciprocal of the slope j, which has the units of kWh / ton (the same in the Bond index) is an appropriate measure of the inherent resistance to grindability of solid, because it is free of particle-interference effects, the nature of the grinding mill, the quantum energy invested and the extent of size reduction achieved, that is, the reduction ratio in single-particle breakage.

12

Figure 7 illustrates the reduction ratio X_f/X_{50} vs. E_m curves when 8x10 mesh dolomite is ground dry in a laboratory size batch ball mill (Herbst and Fuerstenau, 1968 as cited in Fuerstenau and Kapur, 1994); in a single pass laboratory scale, high pressure roll mill (Fuerstenau et. al. 1991 as cited in Fuerstenau and Kapur, 1994); and in the single-particle breakage mode in a rigidly mounted roll mill. Because linear energy –reduction ratio relationship exist in the latter two cases, the ratio of the two slopes provides a convenient and unambiguous index of the high pressure roll mill performance. This evaluation is meaningful in the sense that it is based on a comparison to single-particle breakage data, which is the most energy efficient mode of size reduction presently known. The three slopes are in the approximate ratios of 1:0.44:0.21; that is, the performance index of the ball mill is 21%.
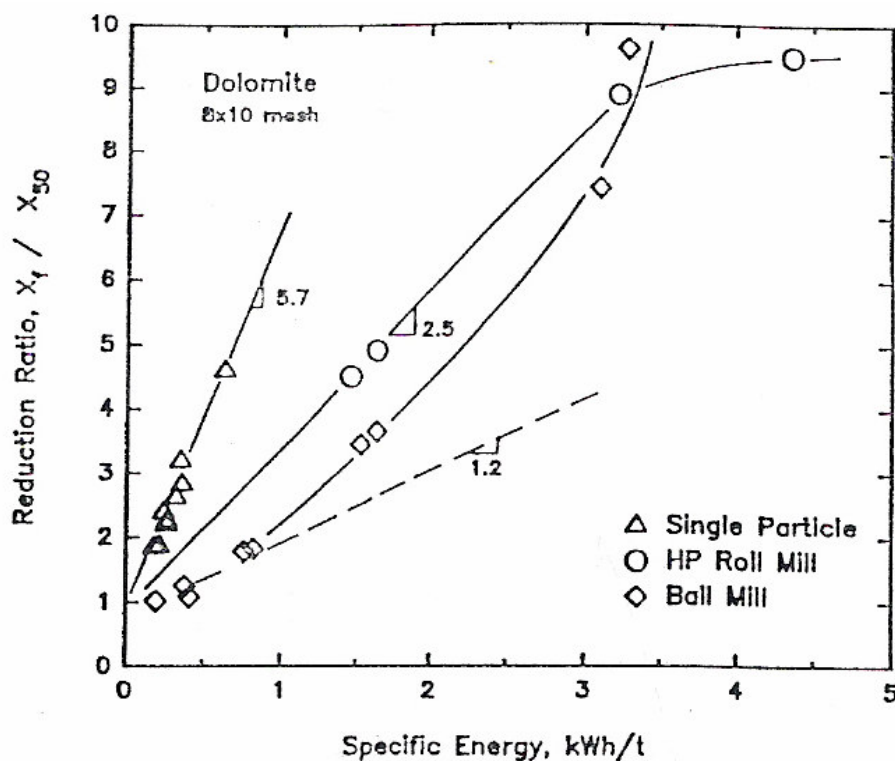
Figure 7: Reduction ratio as a function of specific grinding energy when 8x10 mesh dolomite is comminuted dry in the single particle mode, a high pressure roll mill and in a ball mill (Fuerstenau and Kapur, 1994)

13

Moreover, a characteristic feature of the high pressure roll mill is that beyond a point its performance drops rapidly. Figure 7 shows the rather abrupt bending over of the high pressure roll mill curve which results in virtual cessation of any meaningful size reduction in a single pass through the mill. On the other hand, the ball mill curve, after a slow start, raises steeply, eventually crossing over the high pressure roll mill curve. Even though at this stage the ball mill begins to exhibit a higher grinding efficiency than the high pressure roll mill (Fuerstenau and Kapur, 1994).

This does not mean that the process efficiency of a ball mill comminution circuit is necessarily better than that of the pressurized roll mill circuit. By operating the circuit below the crossover point, that is, at less than about 3.3 kWh/ton energy input per cycle followed by screening off the fines and recycling the oversize with make-up new feed, it is almost always possible to achieve significant energy savings in a high pressure roll mill circuit over the ball mill–based circuit.

To conclude, it will be seen that the high pressure roll mill circuit is always more energy efficient than the ball mill circuit, as long as the specific energy consumption per cycle does not exceed a certain limiting value (about 3.3 kWh/ton in this instance). It should be pointed out that, depending on the material ground and the fineness required, most high pressure roll mills in the industry operate in the range of 1 to 5 kWh/ton per pass (Schwechten and Milburn, 1990 as cited in Fuerstenau and Kapur, 1994).

CHAPTER 3

EXPERIMENTAL STUDIES

3.1 Preparation of Samples

Quartz and calcite samples, having relative hardness indices of 7 and 3 on the Mohs scale, were obtained from Kaltun Madencilik (Aydın) and Gülmer Madencilik (Bilecik), respectively and comminuted in a piston-die-press. Quartz and calcite were chosen on purpose to express the difference between hardness and their effect on the results of the experiments.

Quartz and calcite were stage-crushed (jaw & roll crusher) and dry screened to produce 3.35 x 2.36, 2.36 x 1.7, 1.7 x 1.18, 1.18 x 0.85, and minus 0.85mm size fractions. First, these narrow size fractions (excluding minus 0.85mm fraction) were comminuted under different pressures to determine the baseline for energy utilization and other characteristics. Then, these size fractions and minus 0.85mm size fraction were proportionately mixed to produce feeds of three different size distributions having three different Gates-Gaudin-Schuhmann (GGS) size distribution moduli (m=0.5, 0.7, and 0.9) and comminuted under different bed pressures of appropriate magnitudes to generate a reasonable range of specific breakage energy inputs. GGS distribution modulus (m) is a parameter of Gates-Gaudin-Schuhmann distribution function which is given in Equation 2. Detailed information about these distributed size fractions is given in Appendix A.

$$W(d) = \left(\frac{d}{d_{\max}}\right)^m \quad \text{... (2)}$$

where

$W(d)$: weight fraction (percentage divided by 100) of the particles finer than size d,

$\quad 0 <= W <= 1.0$

$d_{\max}$: GGS size modulus (maximum particle size in the distribution)

m : GGS distribution modulus, a measure of the spread of particle sizes.

3.2 Piston-Die-Press

Quartz and calcite samples were comminuted in a piston-die-press set-up as illustrated in Figure 8, under defined conditions that eliminated geometrical effects of the particle bed. SAE-1040 steel was used for the die-piston which has a Rockwell Hardness of C-30 and yield strength of 696MPa. The influence of bed pressure, material hardness and feed size on energy absorption, energy utilization and product size distributions were investigated.

The batch process in a piston-die-press set-up has some advantages over the continuous process in a high-pressure roll mill. Considerably less feed sample is required in a die-piston than what is needed for a laboratory-scale pressurized roll mill. The rate at which the bed is compressed in the former case can be fixed at a pre-assigned value or varied according to a pre-loaded program, whereas it is quite variable and inflexible in the latter case since it is determined in first instance by the geometry and speed of the rolls. It is also far more convenient to comminute appropriately "designed" beds of hard-soft solids or coarse-fine mixtures in a die-piston arrangement, in order to isolate and study interparticle interactions and particulate environment effects in the compressed bed. In general, much higher grinding pressures can be attained in a die-piston press than with the high-pressure

16

roll mill. In conclusion, the die-piston press provides a convenient and versatile tool for the study and analysis of the absorption, dissipation and utilization of grinding energy, size spectra of the ground product and virtual cessation of further size reduction at high pressures (Fuerstenau et. al., 1996).
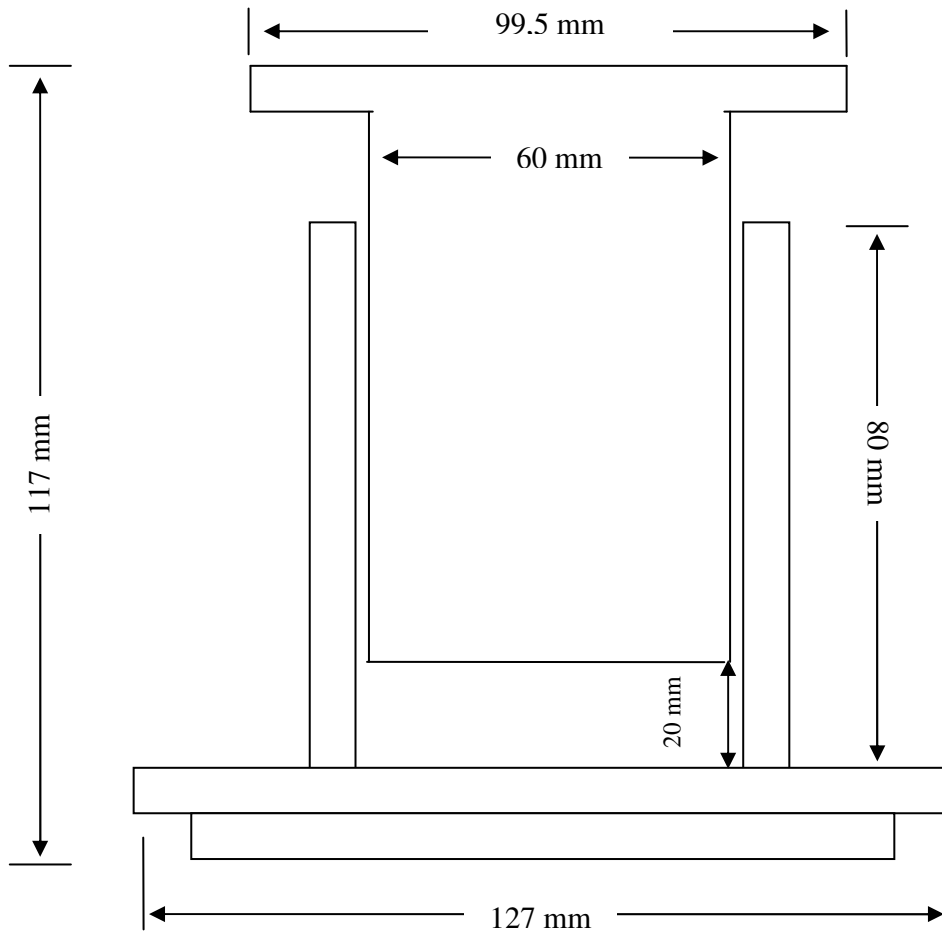
Figure 8: Illustration of the die-piston

Although a number of investigators have studied particle-bed comminution in the piston-die-press, undoubtedly the most detailed and significant work in this area was done by Schönert and coworkers. According to these authors, the container effect is eliminated if the following inequalities are satisfied between the die diameter D, initial bed height h, and the maximum feed size X_{max} (Aziz and Schönert 1980 & Schönert et al., 1990 as cited in Fuerstenau et al., 1996):

$$D / X_{max} > 10.............\ (3) \quad ; \quad h / X_{max} > 6...............\ (4) \quad ; \quad h / D < 1/3..............\ (5)$$

According to these equations, the thickness of the particle bed in the die-piston press was set to 20mm. The amounts of the samples were changed to fix this thickness (Table 1).

Table 1: Amounts of samples for each narrow-range size fraction and distributed size fractions for comminution in piston-die-press

QUARTZ		CALCITE	
Size	**Weight**	**Size**	**Weight**
-3.35+2.36 mm	75g	-3.35+2.36 mm	75g
-2.36+1.7 mm	80g	-2.36+1.7 mm	80g
-1.7+1.18 mm	80g	-1.7+1.18 mm	80g
-1.18+0.85 mm	80g	-1.18+0.85 mm	80g
(GGS) m=0.5	95g	(GGS) m=0.5	95g
(GGS) m=0.7	95g	(GGS) m=0.7	95g
(GGS) m=0.9	95g	(GGS) m=0.9	95g

Experiments were designed to investigate the influence of bed pressure, feed size and material hardness on size reduction in compression-loaded particle beds. Comminution tests were carried out in a piston-die press with steel die of 60

18

mm diameter and loaded with MTS Rock Mechanics Test System in the rock mechanics laboratory at the first step of the experiments. 75, 150, 200, 250, 300, 350, 400 kN forces were applied to quartz with MTS. According to the results obtained from this machine and also from papers investigated, it was decided to load the samples under higher forces to make the differences between product particle size distribution curves more evident (Figures D.3 and D.4). In order to supply the requirements for the experiments, Tinius Olsen Compression Testing Machine was used instead of MTS with new force values of 300, 400, 600, 800 and 1000 kN. As experiments were proceeding it was decided to re-adjust the values of force for the calcite samples. Due to the softness of calcite, the die-piston stuck at 1000 kN force; consequently, 1000kN force was not applied to calcite samples.

3.3 Experimental Procedure

The experimental procedure involved filling the die with sample, tapping (once or twice depending on sample) and measuring the initial bed height. The sample was then compression-loaded to a pre-selected bed pressure at a rate of 1-1.8 MPa/s. At the end of the compaction cycle, the compressed bed was fragmented manually and mixed with water in glass beakers to assure dispersion. The resulting aggregates were then wet screened at 38 microns to remove the fine sized product. Later, the +38 micron material was dried and sieved using standard sieve series. Force-displacement data from the press were logged digitally and numerically integrated with the help of MATLAB software program to obtain the work of compression. Figures 9 and 10 are force–displacement graphs of m=0.5 quartz and calcite samples at different force values, respectively. The forward travel in the graphs became negative during the elastic expansion of the material and the die-piston, so the elastic expansion was excluded when calculating the area under the compression curve. Subsequently, the work of compression was used to find expended specific energies of samples of each size by dividing them to the weight of samples in grams. According to those calculations, specific energy versus pressure graphs of each sample were drawn.

Particle size distribution graphs for different sizes of samples were drawn according to the results of sieve analyses. Median sizes, X_{50}, were calculated in MATLAB software program by fitting cubic splines to sieve analyses data.
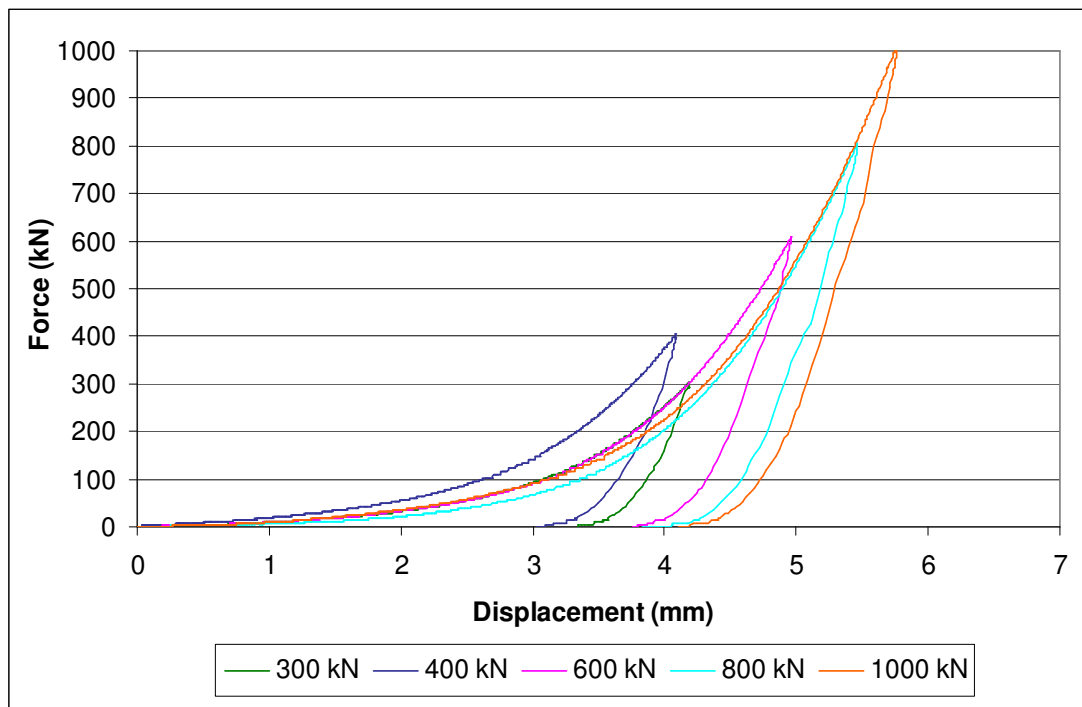
Figure 9: Force versus Displacement graph of m=0.5 quartz sample
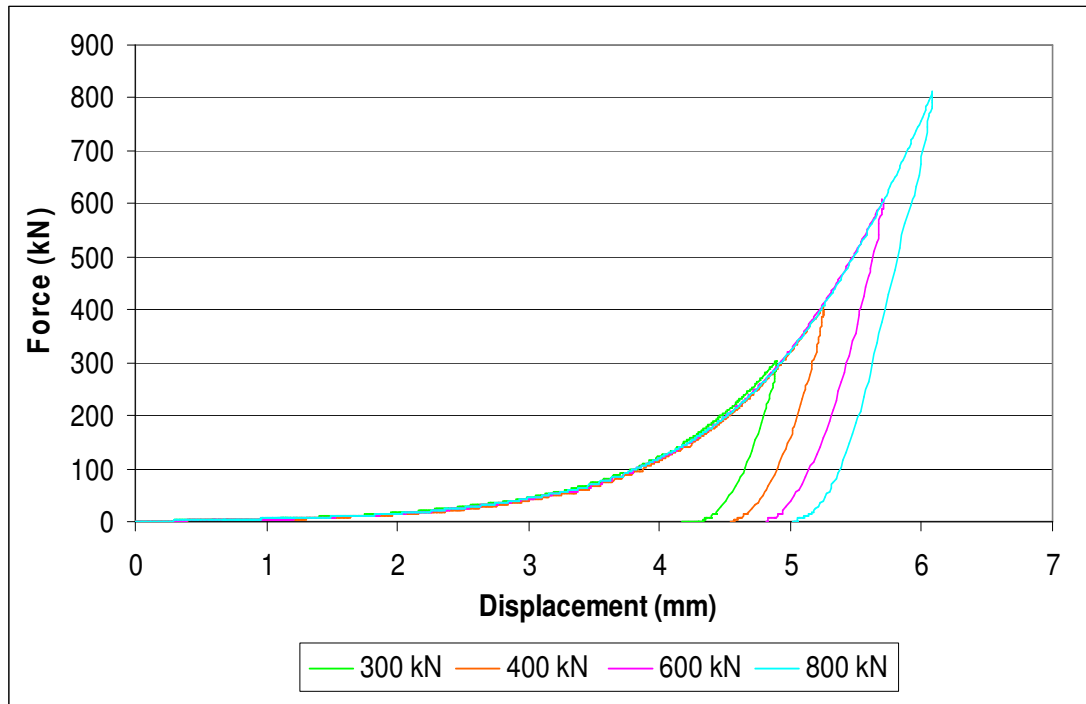
Figure 10: Force versus Displacement graph of m=0.5 calcite sample

For quartz samples of different sizes, 40 experiments; and for calcite samples, 28 experiments were conducted. Beside those 68 experiments, 24 experiments were performed to control the repeatability of the experiments. The specific energies and the particle size distributions were controlled in the repeated experiments According to the results of these experiments, it is concluded that the experiments were highly repeatable. The values of specific energy varied in a range of ±0.5 of the first measurements; however, in the particle size distribution graphs the differences between the curves were extremely small that it was actually difficult to distinguish the differences and specify the amount of variance between samples (Appendix F).

CHAPTER 4

RESULTS AND DISCUSSION

4.1 Product Particle Size Distribution and Self-Similarity

Figures D.1-D.5 in Appendix D present cumulative undersize values of the narrow-range size fractions of quartz samples for different applied pressure values. The amount of fines increases as the pressure applied on the particles increases. Although the differences between curves at different pressures are very similar for different particle sizes, the differences between the curves decrease with decreasing particle size when the experimental results were carefully examined. The maximum difference between the highest and the lowest pressure values results in at most 5-6% change in cumulative undersize of the finest screen size in the plots. In Figures D.6-D.8, product size distributions from the breakage of size-distributed feeds are given for different applied pressures together with the feed size distributions. As the separation between the feed size distribution curve and any product size distribution curve increases with increasing pressure, the amount of fines also increases. In Figure D.8, the largest separation can be seen, probably due to the presence of higher amounts of coarse particles in the feed having distribution modulus of 0.9 when compared with the feeds having the moduli of 0.5 and 0.7. Therefore, the presence of coarse particles accelerates the production of fine particles. The degree of size reduction achieved at the end of comminution was computed for all feed particle size distributions and discussed later in Section 4.6.

Figures D.10-D.13 present the product size distributions of calcite feeds. As calcite is not as hard as quartz, particle size distribution curves have different characteristic shapes especially under 800µm as shown in Figures D.1 and D.10 for quartz and

calcite; detailed graphs are given in Appendix D. The maximum difference in cumulative undersize between the highest and the lowest pressures results in similar values with quartz. Also, same with quartz samples the amount of fines increases as the pressure applied on the particles increases. On the other hand, calcite samples results in higher amounts of fines than those of quartz at all narrow-range size fractions. In Figures D.14-D.16, product size distributions from the breakage of size-distributed feeds are given for different applied pressure together with the feed size distributions. Again it can be said that, as the separation between the feed size distribution curve and any product size distribution curve increases with increasing pressure, the amount of fines increases (Figure D.16). If particle size distribution graphs of quartz and calcite are compared for distribution moduli of m=0.5, m=0.7 and m=0.9, it can be observed that finer products were obtained with calcite samples as exemplified by the test results for feeds of quartz and calcite having distribution modulus of 0.5, shown in Figure C.18.
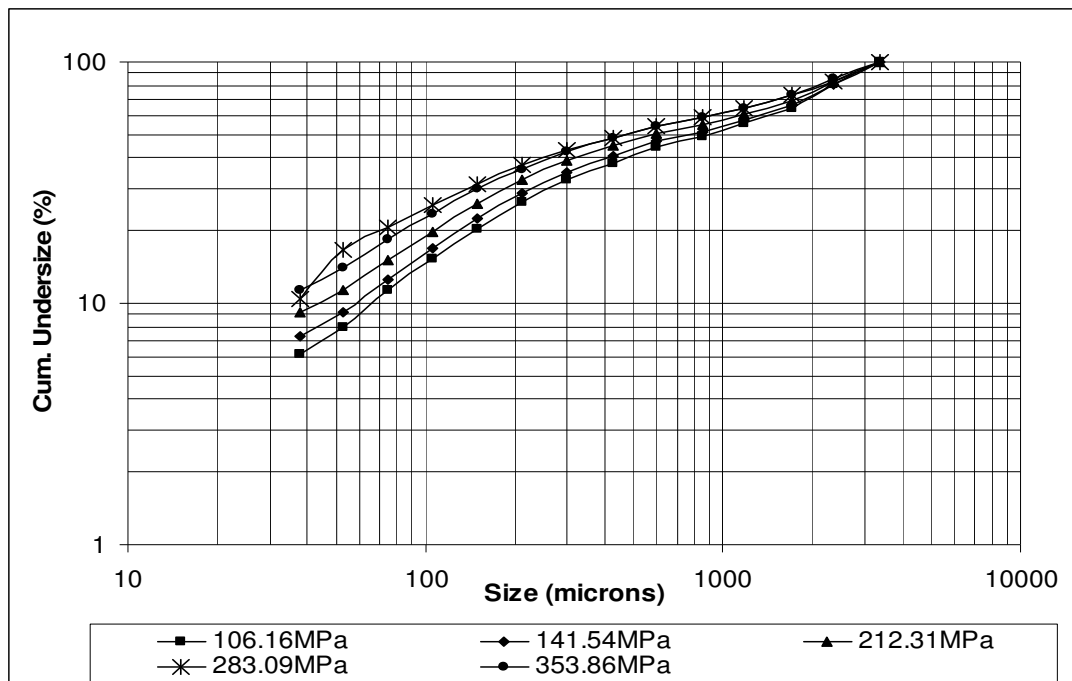
Figure 11: Product particle size distribution graph of -3.35+2.36mm quartz sample
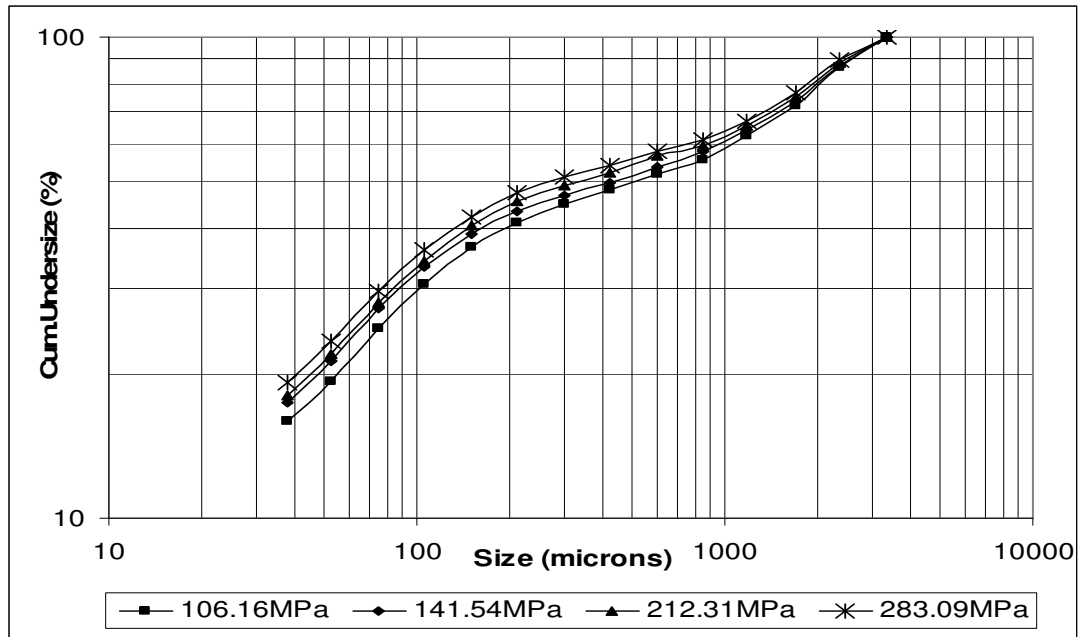
Figure 12: Product particle size distribution graph of -3.35+2.36mm calcite sample

Figures 13-26 show self-similar size distribution of different particle sizes of quartz and calcite samples that were comminuted in the piston-die-press. The piston-die-press product size distribution is normalisable leading to self-similar grinding curves when the particle size X is rescaled by a suitable scaling factor, median size X_{50}. Subsequently, Fuerstenau et. al. (1993) reported that this self-similarity is maintained regardless of variations in feed size distribution. Indeed, for a given material, one master curve appears appropriate to describe the entire product size distribution function. In the experiments, to a large extent self-similarity appears to be preserved. However, some deviations from self-similarity were observed at coarse end of product size distributions. On the other hand, self-similarity was not preserved for -3.35+2.36mm and -2.36+1.7mm narrow-size calcite samples In addition, at low specific comminution energies self-similarity may not be preserved. Self-similarity curves of low specific comminution energies have larger percentages of coarser material at the coarse end probably due to insufficient amount of breakage motion. So it can be concluded that the shape of the size distribution curves can change somewhat with specific comminution energy.

24
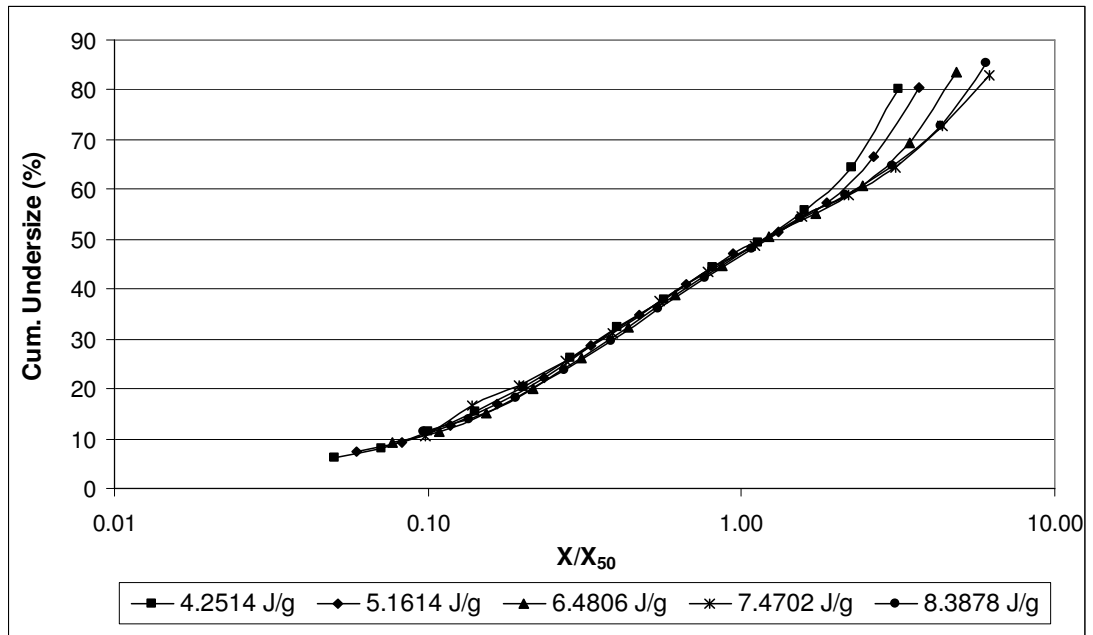
Figure 13: Self-similar size distributions of -3.35+2.36mm quartz sample comminuted in piston-die-press
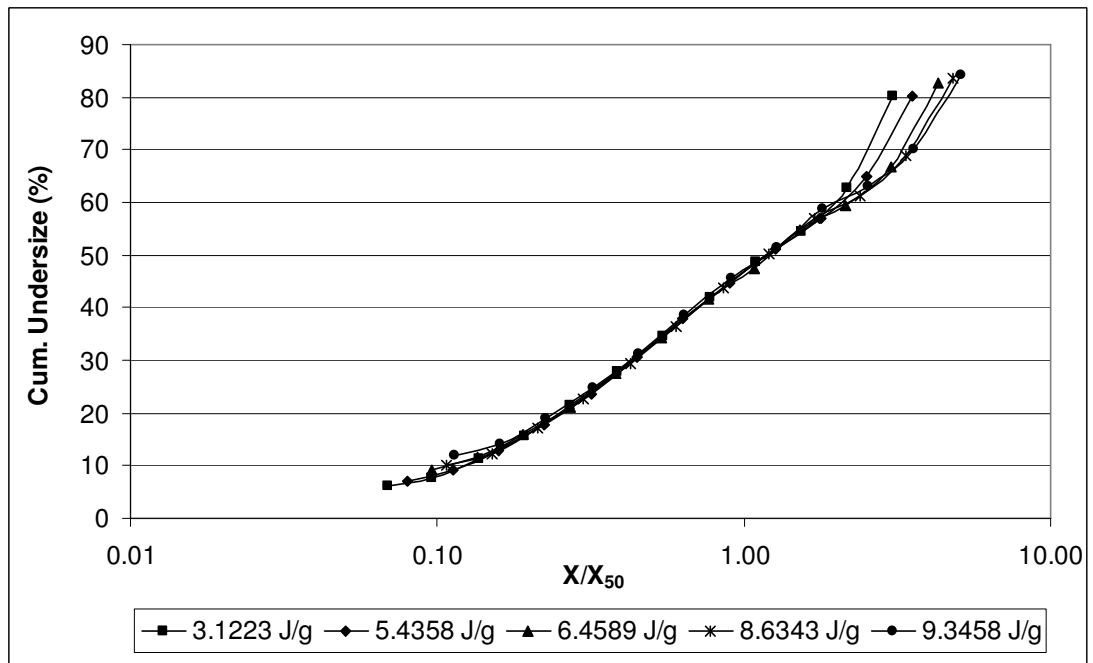
Figure 14: Self-similar size distributions of -2.36+1.7mm quartz sample comminuted in piston-die-press
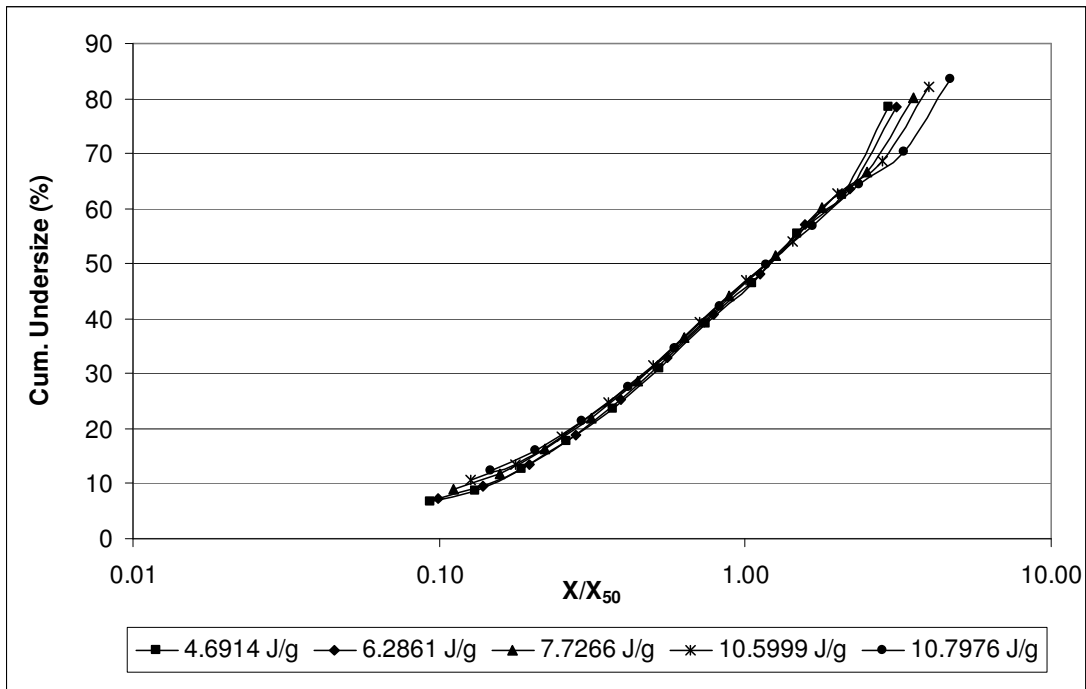
Figure 15: Self-similar size distributions of -1.7+1.18mm quartz sample comminuted in piston-die-press
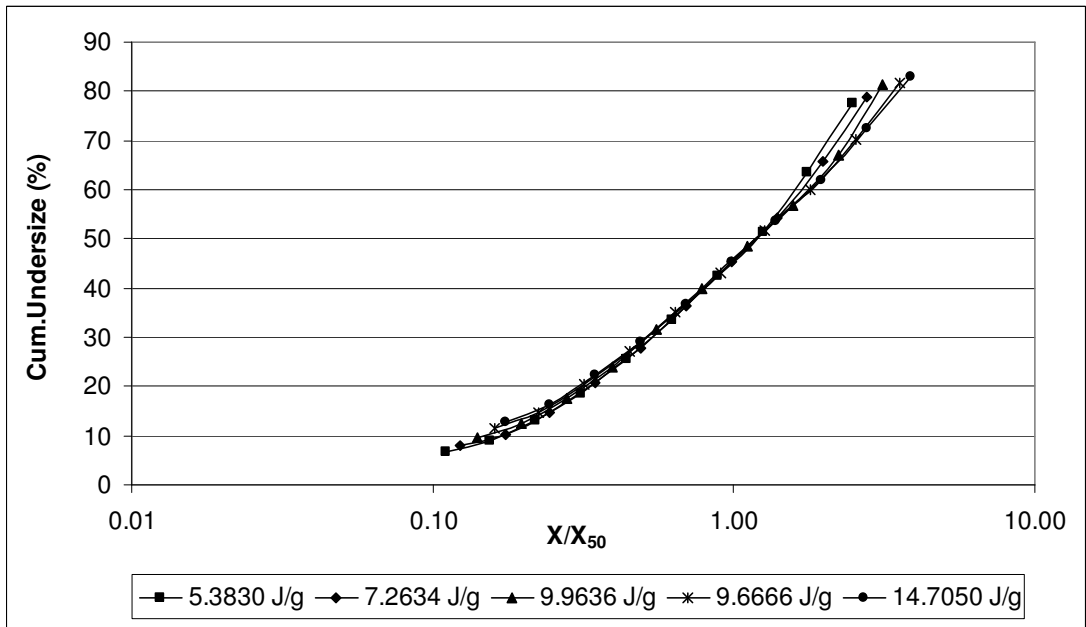
Figure 16: Self-similar size distributions of -1.18+0.85mm quartz sample comminuted in piston-die-press
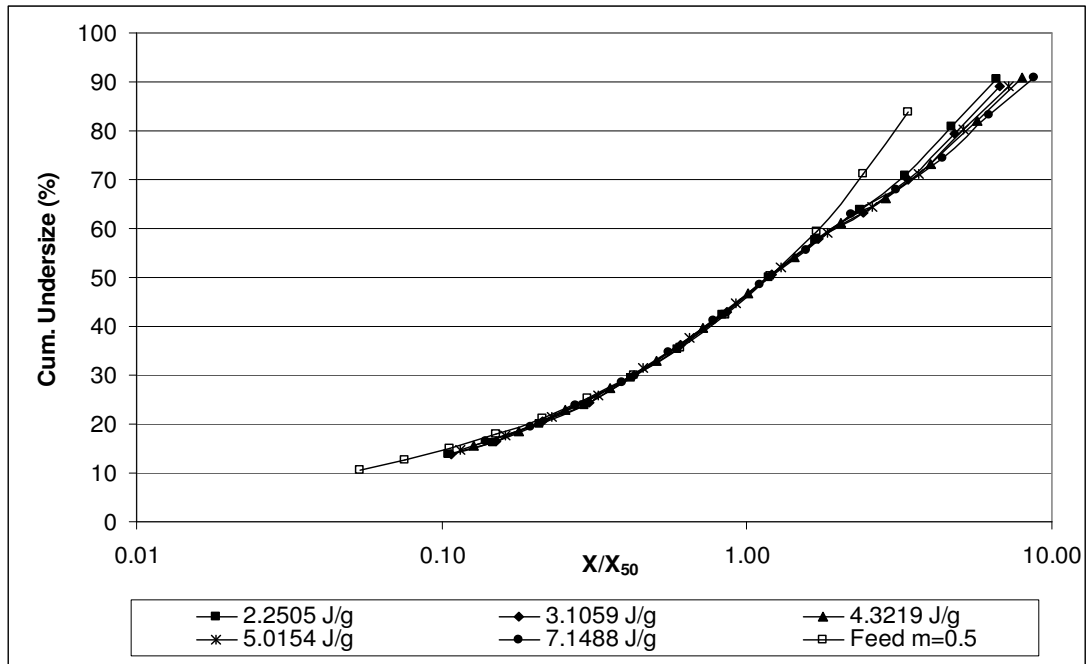
Figure 17: Self-similar size distributions of m=0.5 quartz sample comminuted in piston-die-press
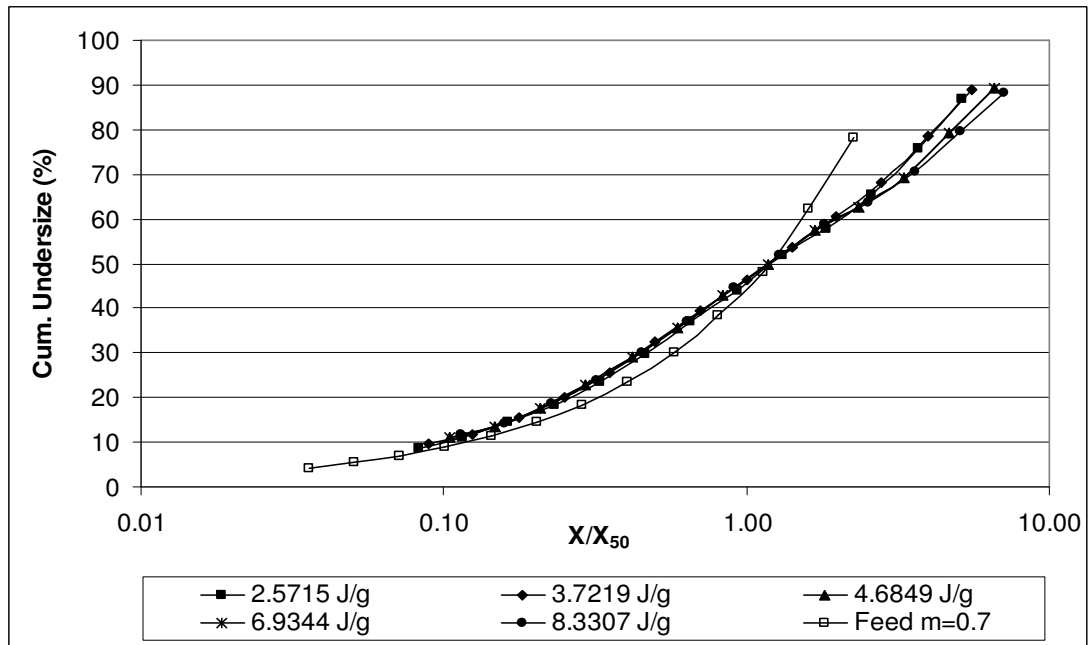
Figure 18: Self-similar size distributions of m=0.7 quartz sample comminuted in piston-die-press
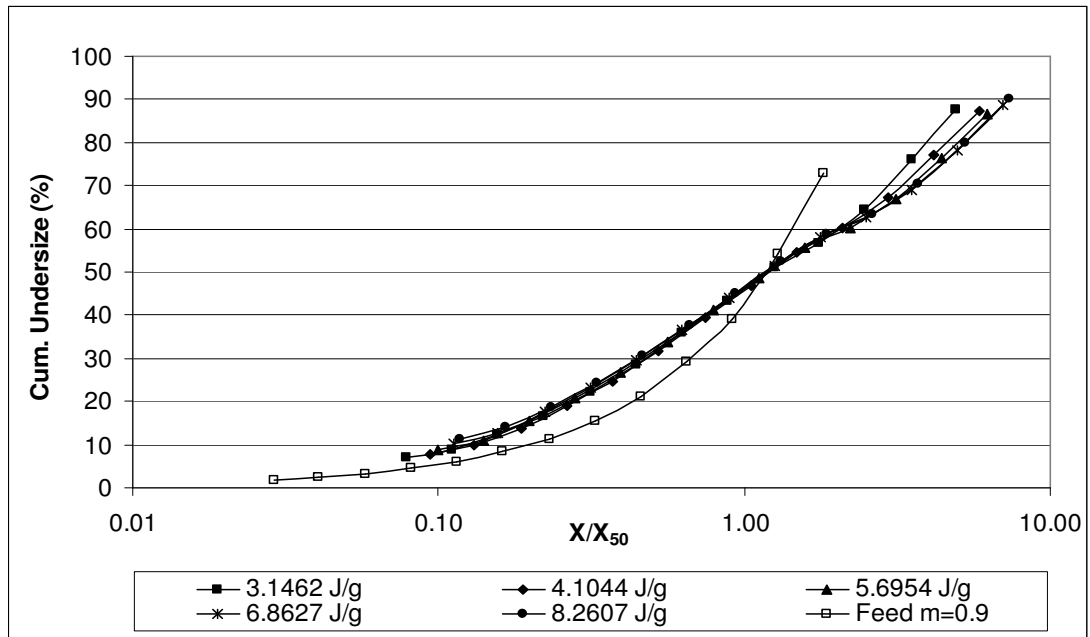
Figure 19: Self-similar size distributions of m=0.9 quartz sample comminuted in piston-die-press
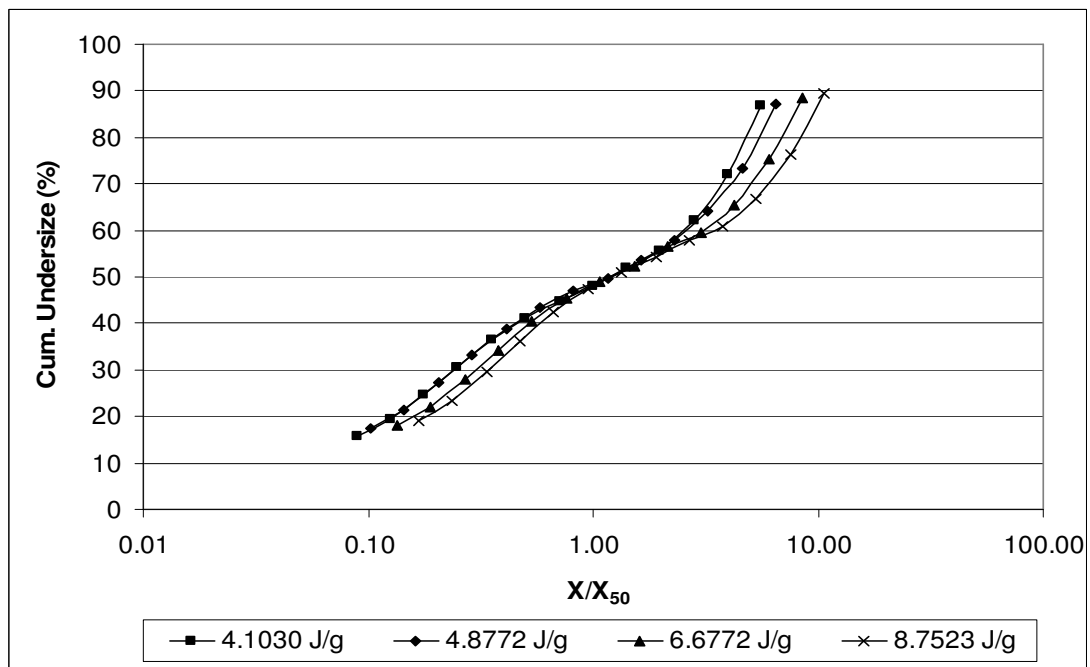
Figure 20: Self-similar size distributions of -3.35+2.36mm calcite sample comminuted in piston-die-press
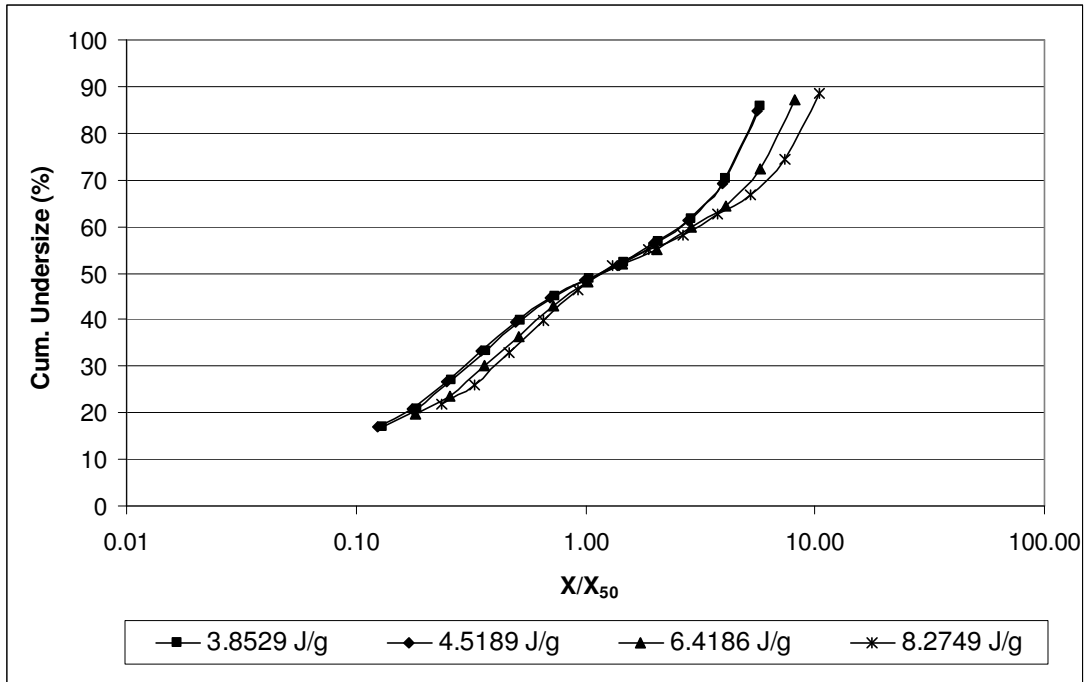
Figure 21: Self-similar size distributions of -2.36+1.7mm calcite sample comminuted in piston-die-press
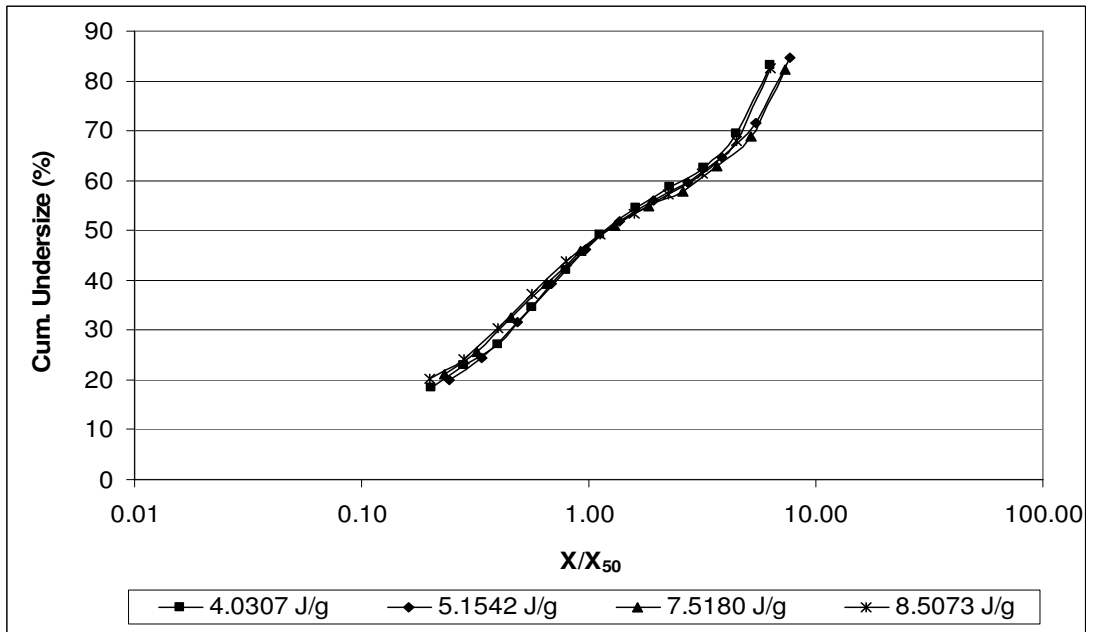
Figure 22: Self-similar size distributions of -1.7+1.18mm calcite sample comminuted in piston-die-press
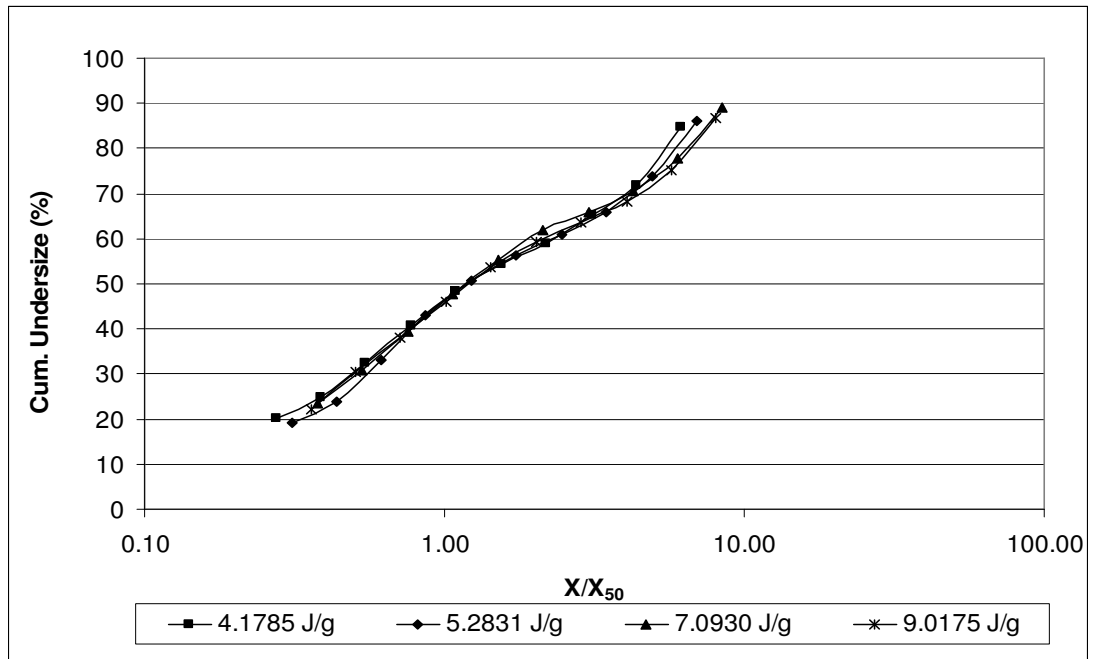
Figure 23: Self-similar size distributions of -1.18+0.85mm calcite sample comminuted in piston-die-press
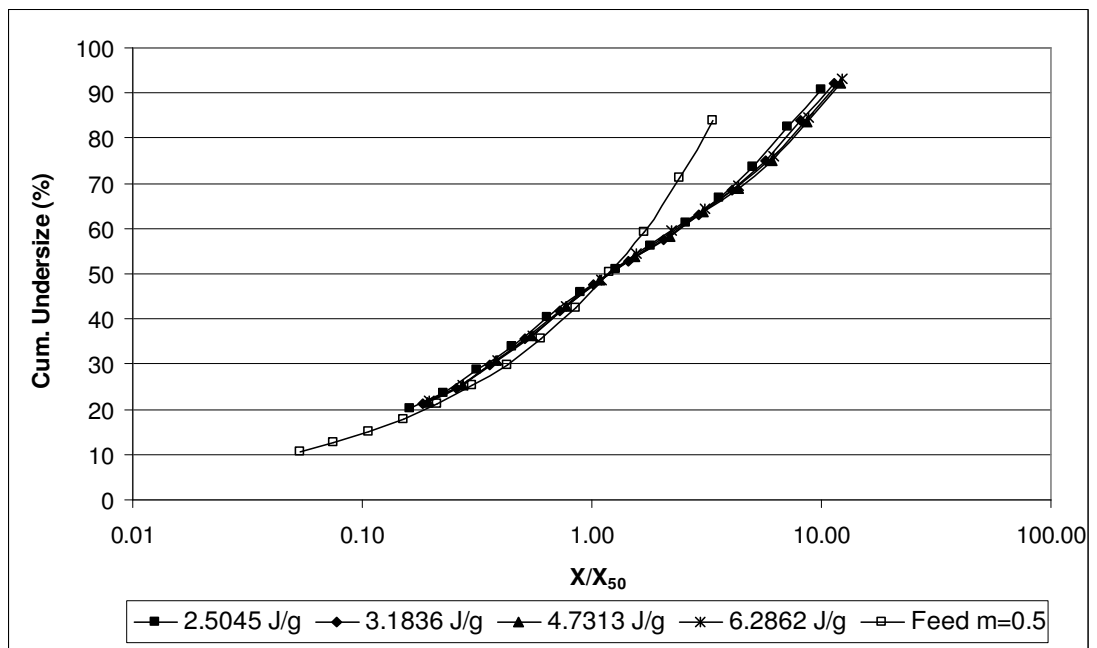
Figure 24: Self-similar size distributions of m=0.5 calcite sample comminuted in piston-die-press

30
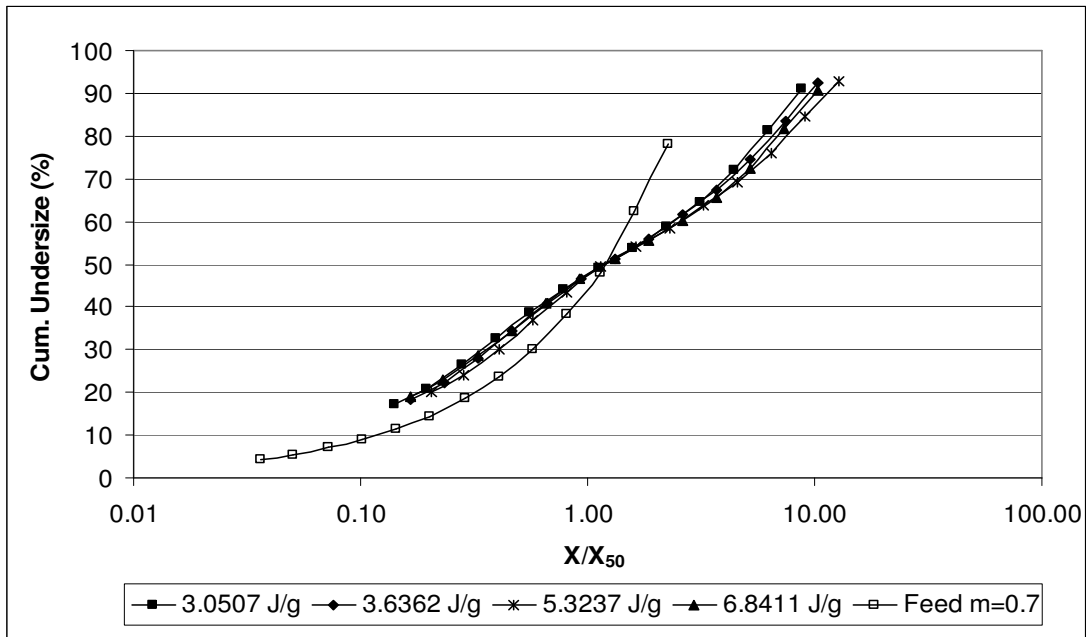
Figure 25: Self-similar size distributions of m=0.7 calcite sample comminuted in piston-die-press
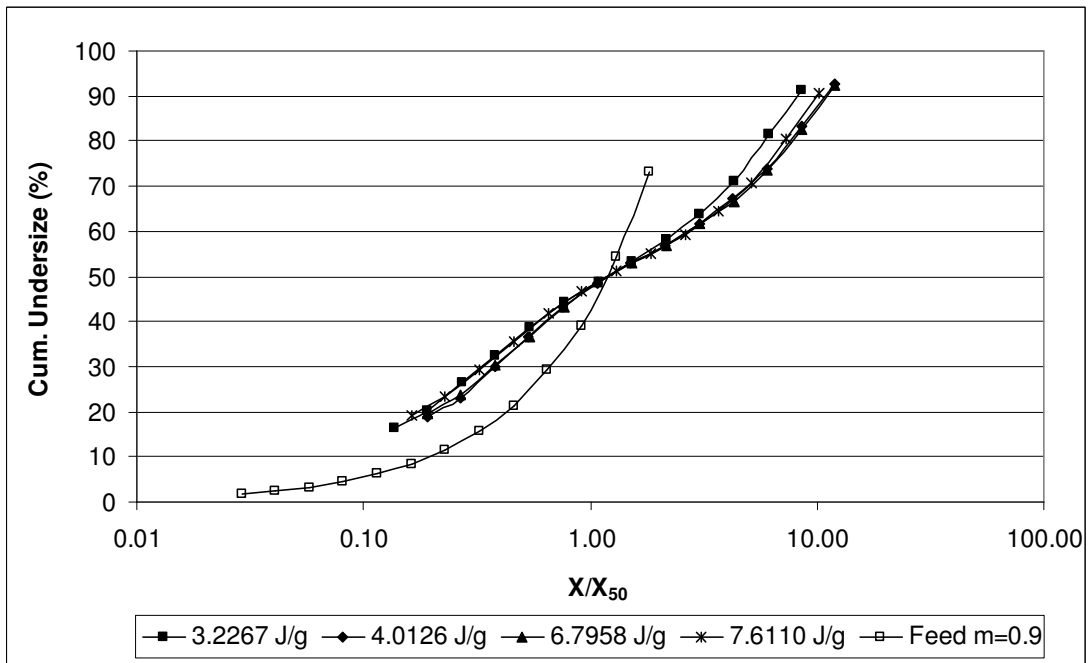
Figure 26: Self-similar size distributions of m=0.9 calcite sample comminuted in piston-die-press

31

4.2 Specific Energy Absorption of Quartz and Calcite Beds

In Figure 27, specific energy absorbed by calcite is higher than that of quartz for -3.35+2.36mm particle size only at the highest applied pressure. Although the same pressures (same forces) were exerted on the die-piston for quartz and calcite, displacement values differ from each other and calcite samples give higher displacement values. Compaction and elasticity characteristics of calcite, which is softer than quartz, should be the reason for these outcomes. Conversely, below 2.36mm particle size quartz bed absorbs higher amounts of specific energy and the amount increases with decreasing particle size (Figures 29 and 30). This means that lower amounts of pressure can be applied on calcite samples which also results in an approximately the same amount of breakage with quartz samples, by expending lower specific energies for coarse particle sizes. In Figure 28, it can be easily seen that both calcite and quartz have similar specific energy profiles at all pressures.

Force-displacement graphs of samples are given in Appendix C for all narrow-range particle sizes and particle size distributions at four different forces. Breakage behavior of the samples is not only influenced by the hardness, both plastic and elastic parameters have to be taken into account. The forward travel in the graphs becomes negative during the elastic expansion of the particle bed and the die-piston (maximum strain at highest pressure, 0.14mm). Area under this negative travel gives the elastic expansion and A2 expressions in Appendix C gives the amounts of elastic expansion areas. The elastic recovery of quartz is about 13% in the unloading curve; however, calcite has an elastic recovery of 10% at -2.36+1.7mm particle size under 600kN force. Also similar results were obtained at all narrow-range particle sizes and distributions for all applied forces. According to those values, mostly quartz bed behaves slightly more elastic than calcite bed during comminution in piston-die press. Since quartz is slightly more elastic than calcite, it demands higher loads than calcite until particle breakage is induced. Consequently quartz bed needs higher amounts of specific energy inputs for sufficient comminution. Beside slight difference in elastic behavior, calcite has significantly lower hardness than quartz. As

calcite is much softer than quartz good grindability was expected and achieved at the end of the experiments.

Elastic behavior of particle beds are influenced both from the elastic behavior of individual particles and stiffness of the beds. The reciprocal of the slope 'j' in Equation 1, which has the units of kWh/ton, is an appropriate measure of the inherent resistance to grindability of solid and the index is approximately 0.167 for quartz and 0.135 for calcite at 3.00mm feed size (Fuerstenau and Kapur, 1994).
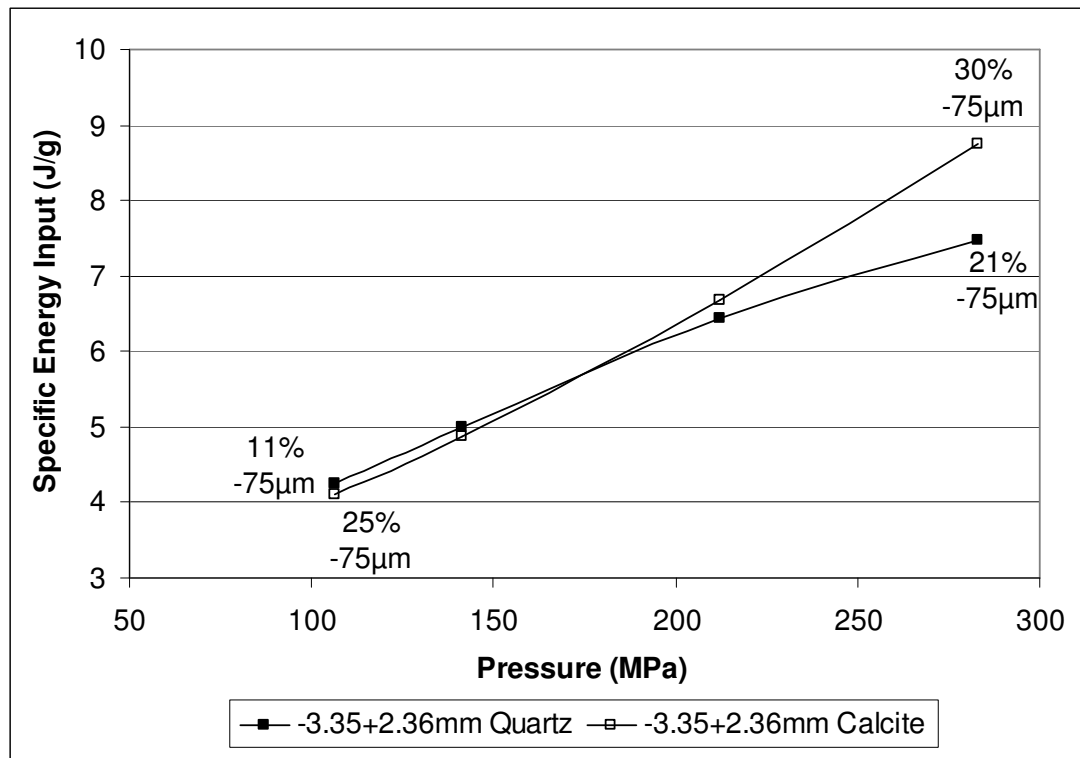
Figure 27: Specific energy comparison of -3.35 +2.36mm quartz and calcite samples at specified pressures
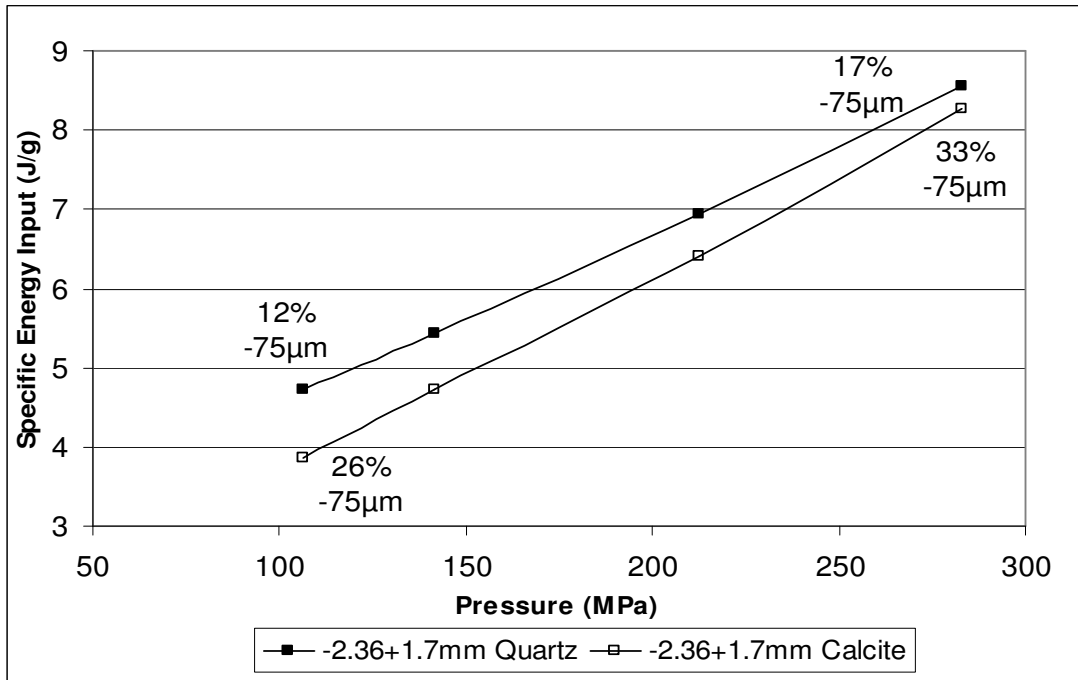
Figure 28: Specific energy comparison of -2.36 +1.7mm quartz and calcite samples at specified pressures
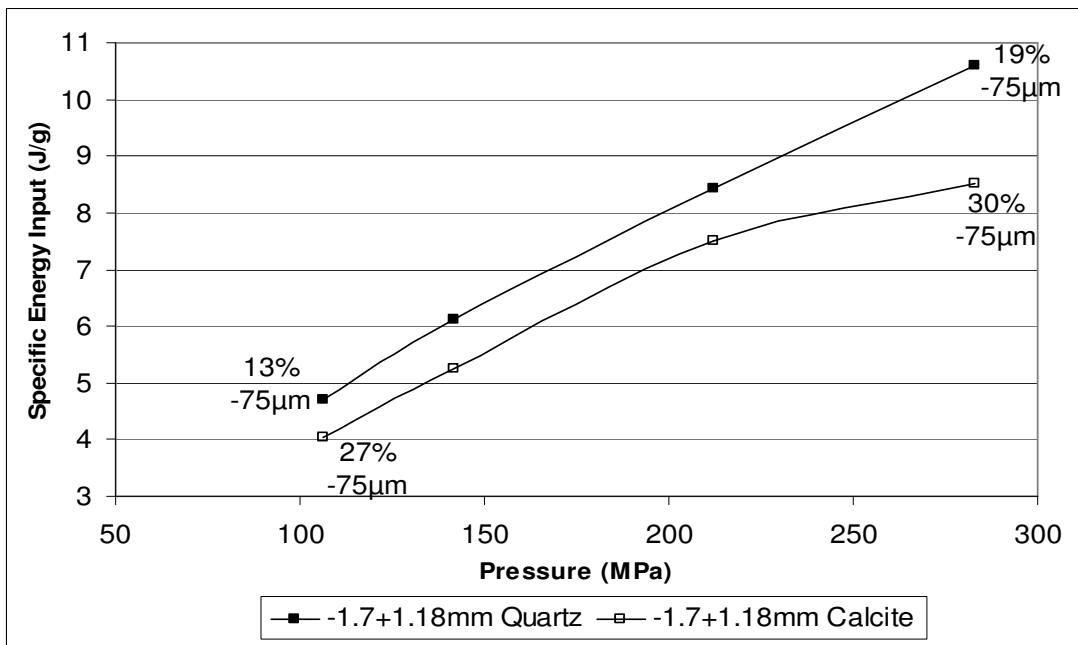
Figure 29: Specific energy comparison of -1.7 +1.18mm quartz and calcite samples at specified pressures
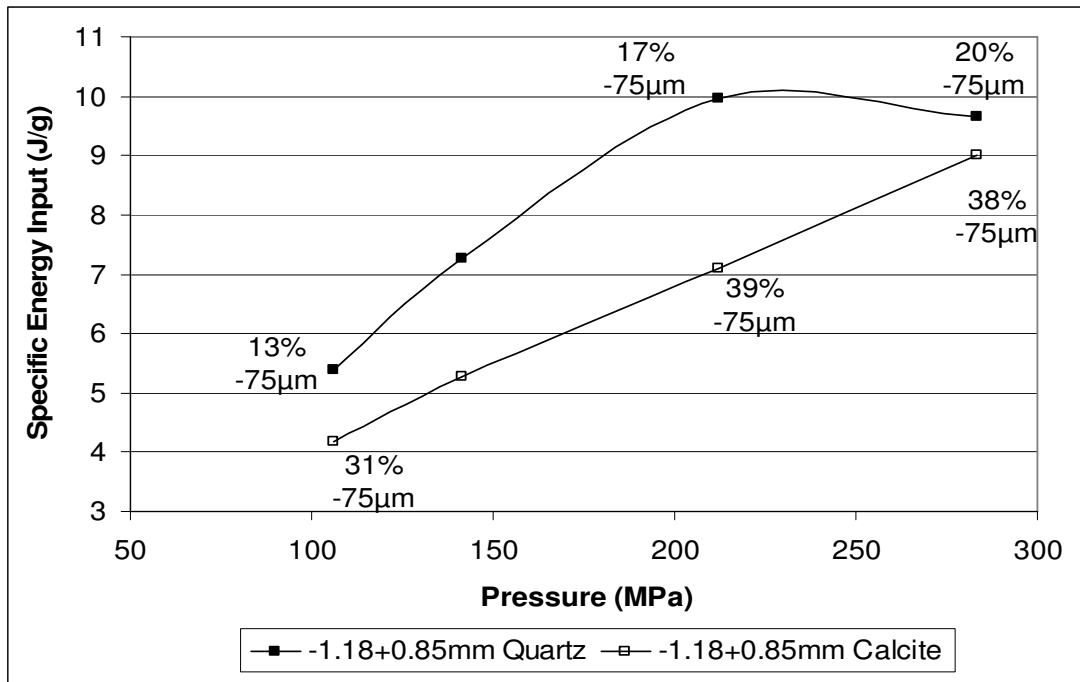
Figure 30: Specific energy comparison of -1.18 +0.85mm quartz and calcite samples at specified pressures

In the case of the distributed feed particle size samples, again calcite consumes higher amounts of specific energy as the pressure increases (Figure 31) for the widest size distribution (distribution modulus = 0.5). On the other hand, for the two coarser feed size distributions (distribution moduli of 0.7 and 0.9), quartz and calcite have similar specific energy absorption values except the difference at the highest pressure in Figure 32 (Figures 32 and 33). However, the amounts of fines obtained at the end of the experiments differ from each other significantly. In Figures 27-33 percentage of particles under 75µm are given at the lowest and highest pressures. At all particle sizes and distributions the amounts of fines under 75µm are always higher for calcite samples. The differences in the percentages between the highest and lowest pressures are always higher for calcite samples at all narrow-range particle sizes except -1.7+1.18mm particle size. However, the differences are slightly higher for quartz samples at distributed sizes. As a result it can be concluded that the amount of breakage is always higher for calcite samples.
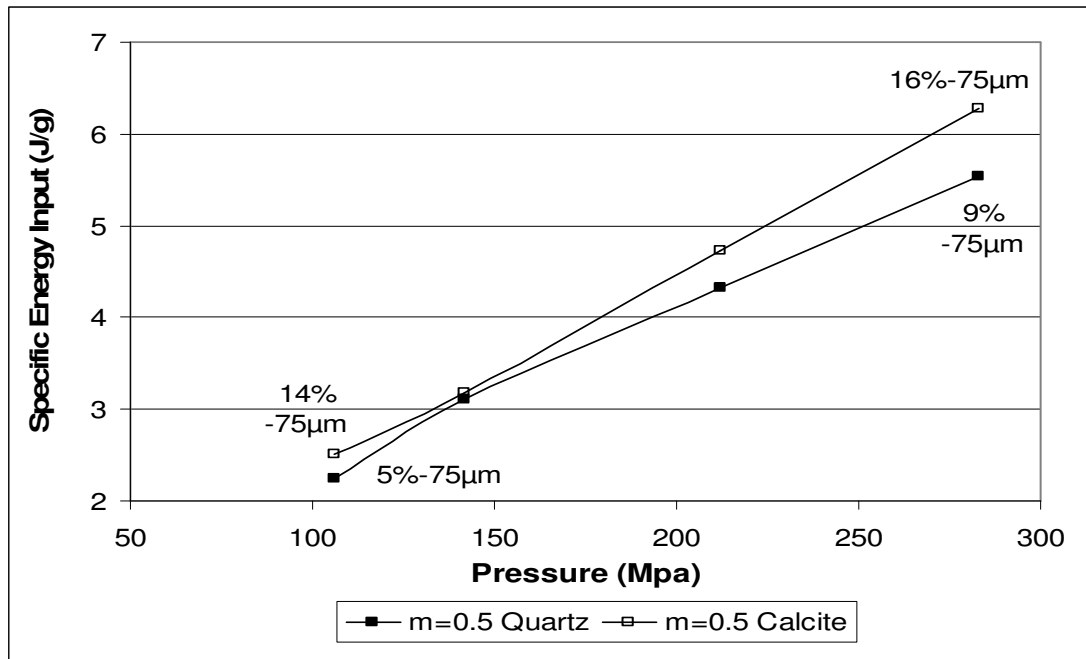
Figure 31: Specific energy comparison of m=0.5 quartz and calcite samples at specified pressures
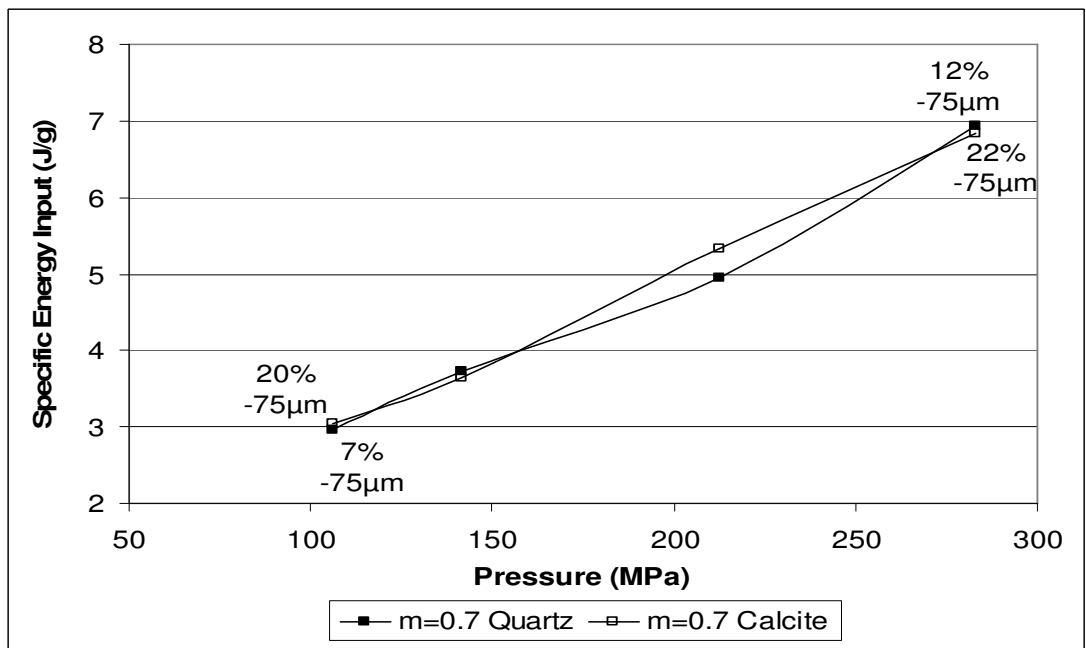
Figure 32: Specific energy comparison of m=0.7 quartz and calcite samples at specified pressures
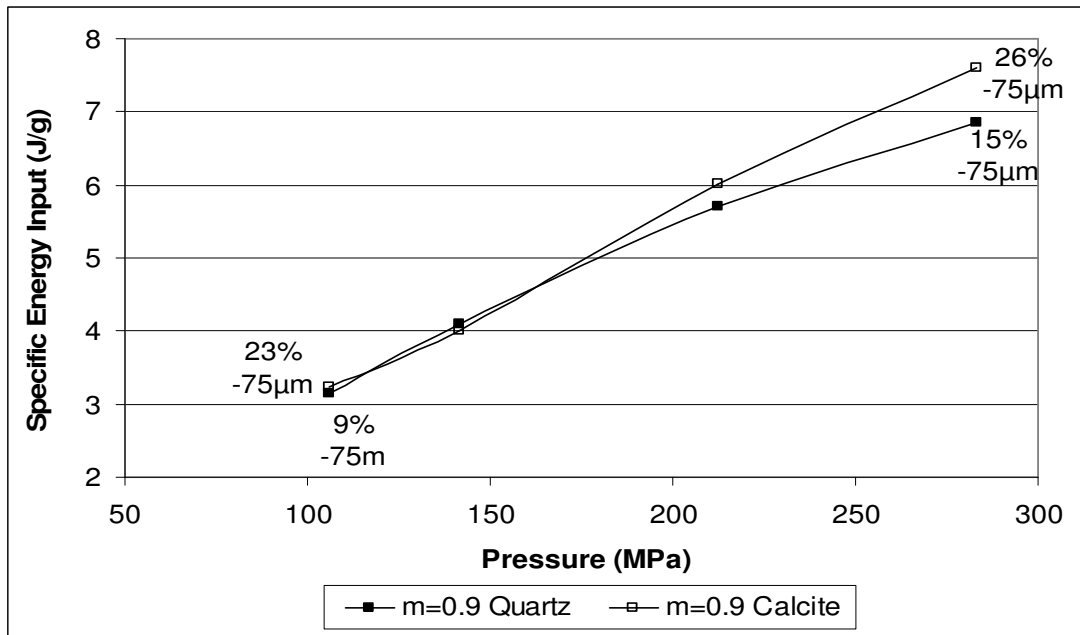
Figure 33: Specific energy comparison of m=0.9 quartz and calcite samples at specified pressures

In Figures 34 and 35, specific energy versus pressure graphs for different sizes of quartz sample are illustrated. In Figure 34, except the point of 300MPa pressure for -1.18+0.85mm size fraction it can be concluded that specific energy absorption increases with decreasing particle size, verifying the fact that finer particles are more resistant to comminution than coarser ones. The peculiar behaviour of the -1.18+0.85m size fraction at 300MPa could not be due to experimental error since it was verified by a number of repeat tests. In Figure 35, distributed feed particle size samples are illustrated and it is seen that the specific energy expended increases in the following order: m=0.5; m=0.7 and m=0.9. Distribution modulus of 0.9 has the highest values of specific energy, its reduction ratios are the highest among others (Reduction ratio concept will be discussed in Section 4.4).
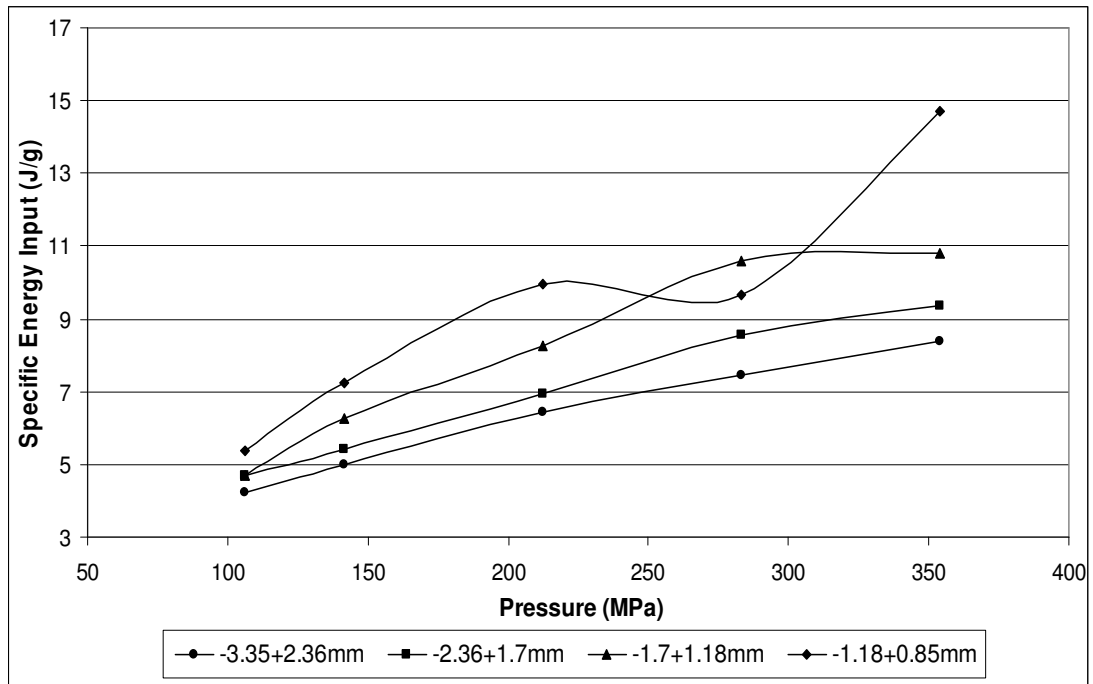
Figure 34: Specific Energy versus Pressure for different sizes of quartz sample
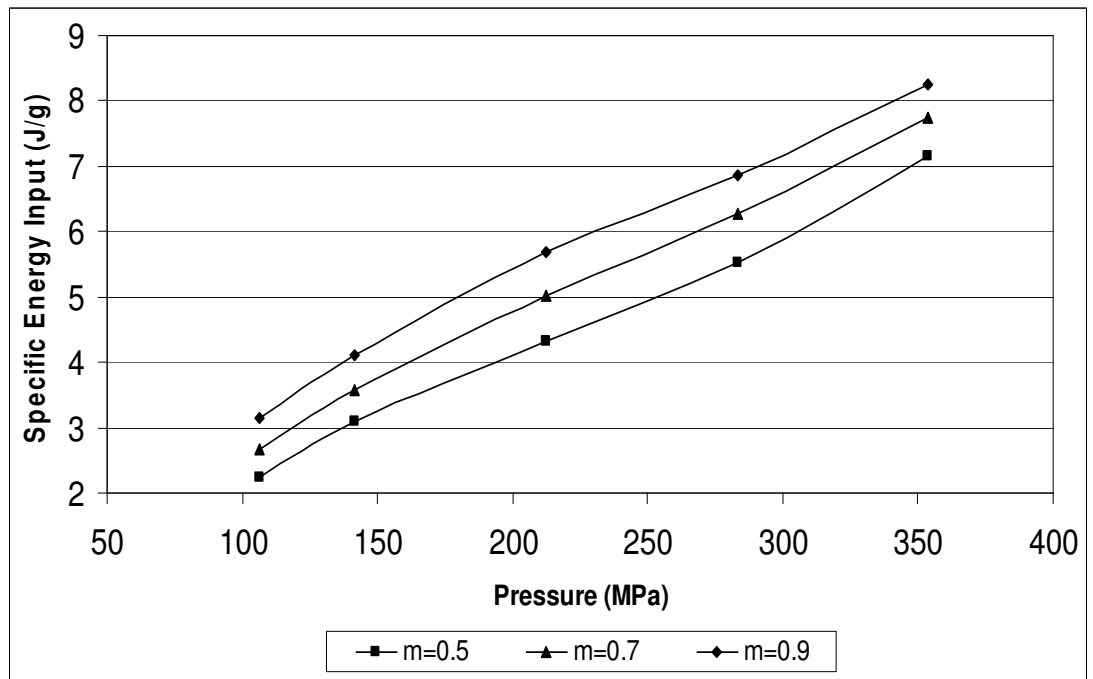
Figure 35: Specific Energy versus Pressure for m=0.5 m=0.7 and m=0.9 values of quartz sample

In Figures 36 and 37, specific energy versus pressure graphs for different sizes of calcite sample are illustrated. Specific energy absorption does not show a definite trend with respect to particle sizes of calcite samples in narrow-range particle sizes (Figure 36). However, it can be concluded that calcite generally consumed lower amounts of specific energy than quartz at specified pressures in the graphs. For distributed feed particle size samples the results obtained from graphs are very similar to those of quartz (Figure 37).
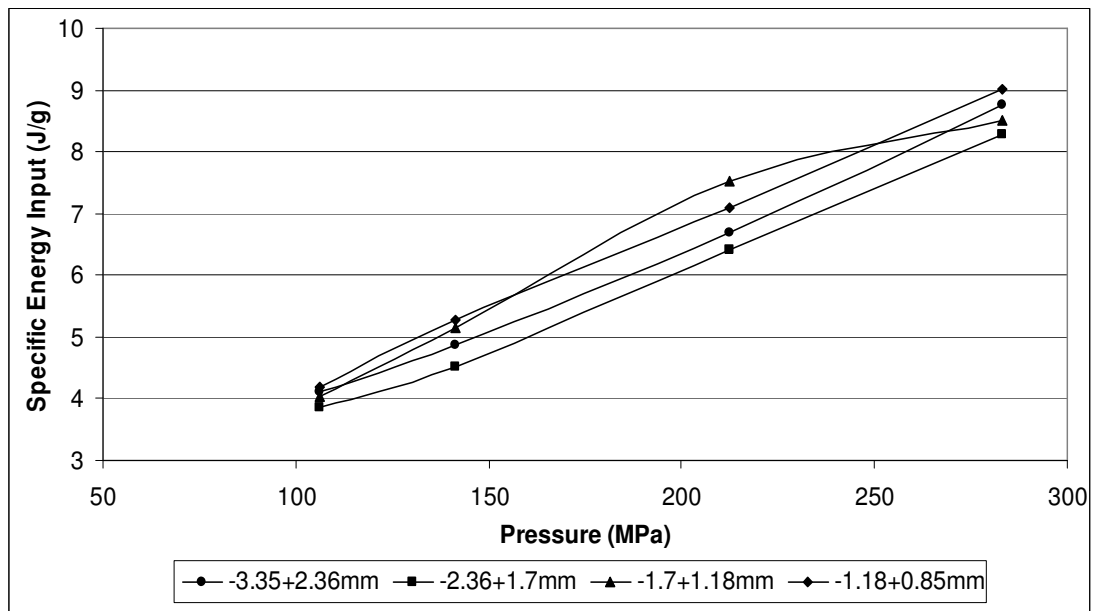
Figure 36: Specific Energy versus Pressure for different sizes of calcite sample
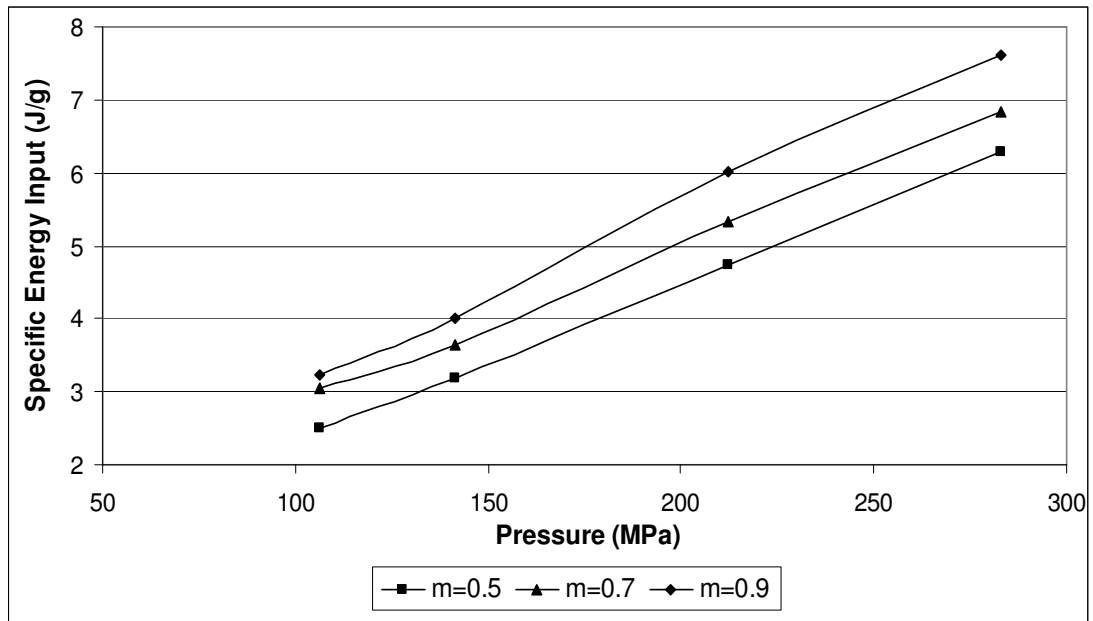
Figure 37: Specific Energy versus Pressure for m=0.5; m=0.7 and m=0.9 values of calcite sample

4.3 Solid Fraction

The compressibility of soft mineral (calcite) in terms of the solid fraction is significantly greater than that of hard material (quartz). At 280 MPa pressure, for -3.35+2.36mm particle size, calcite can be compacted to about 80 percent of solids content as against 73 percent for quartz, despite the fact that the energy absorption by the harder materials is considerably more (Figure 38). For all narrow-range particle sizes and particle size distributed samples, calcite has higher solid fraction values than quartz except -1.7+1.18mm particle size (Figures 38-44). In Figure 40, till 200MPa pressure -1.7+1.18mm quartz samples are more compact than calcite samples.
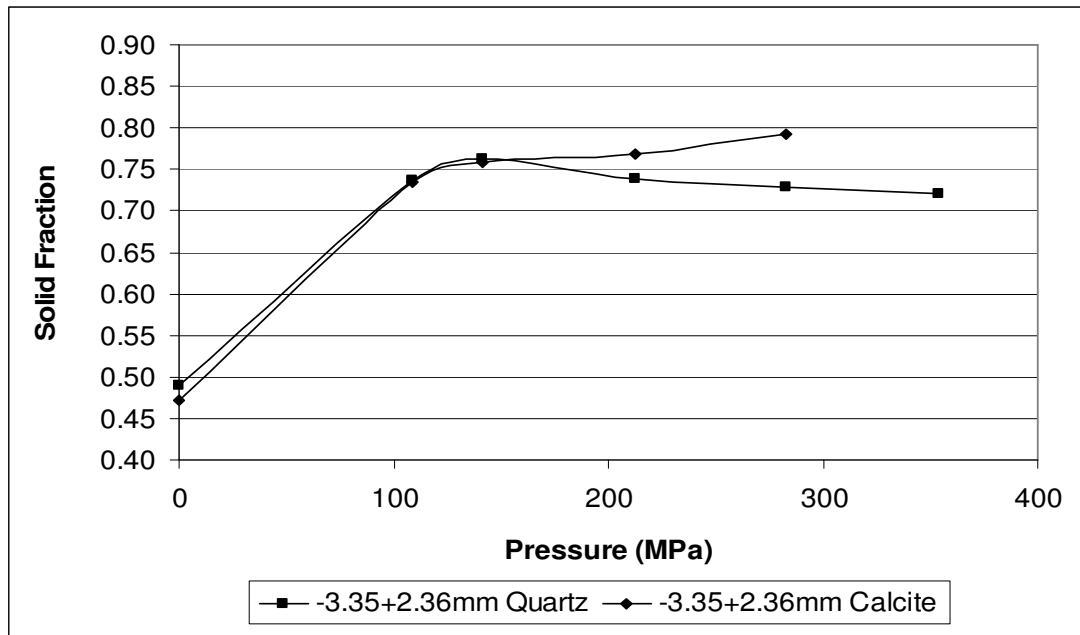
Figure 38: Solid fraction as a function of pressure applied in the particle bed comminution of quartz and calcite
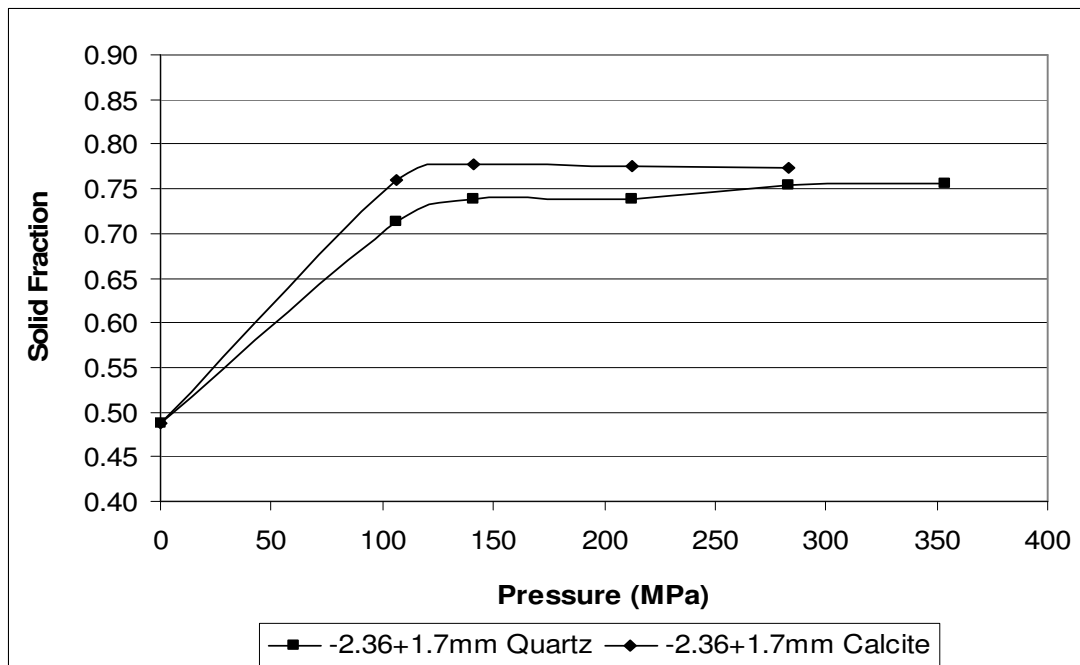
Figure 39: Solid fraction as a function of pressure applied in the particle bed comminution of quartz and calcite
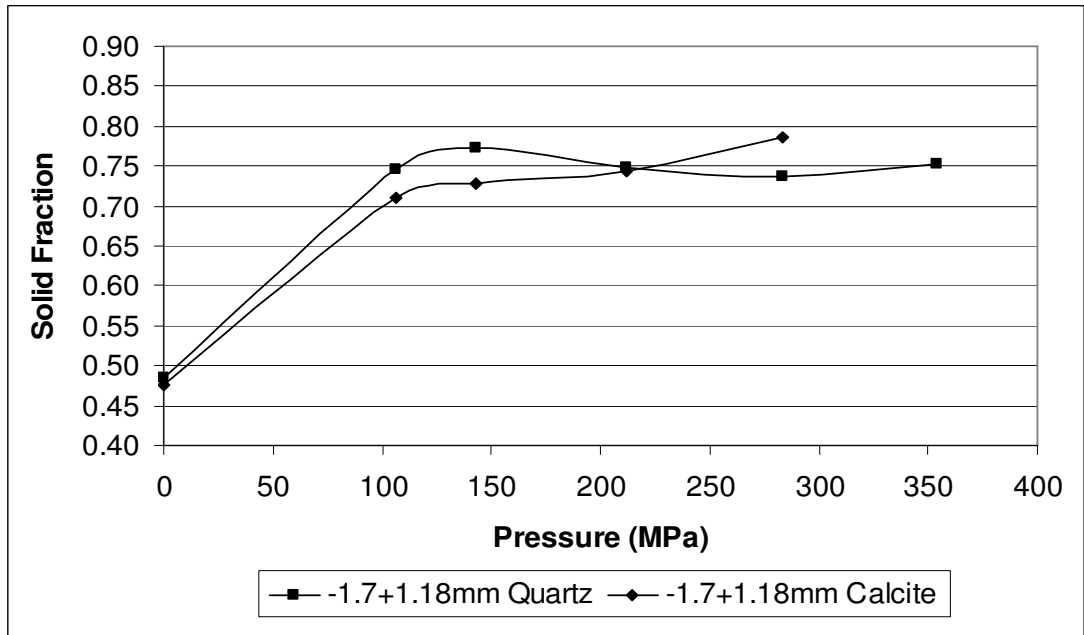
Figure 40: Solid fraction as a function of pressure applied in the particle bed comminution of quartz and calcite
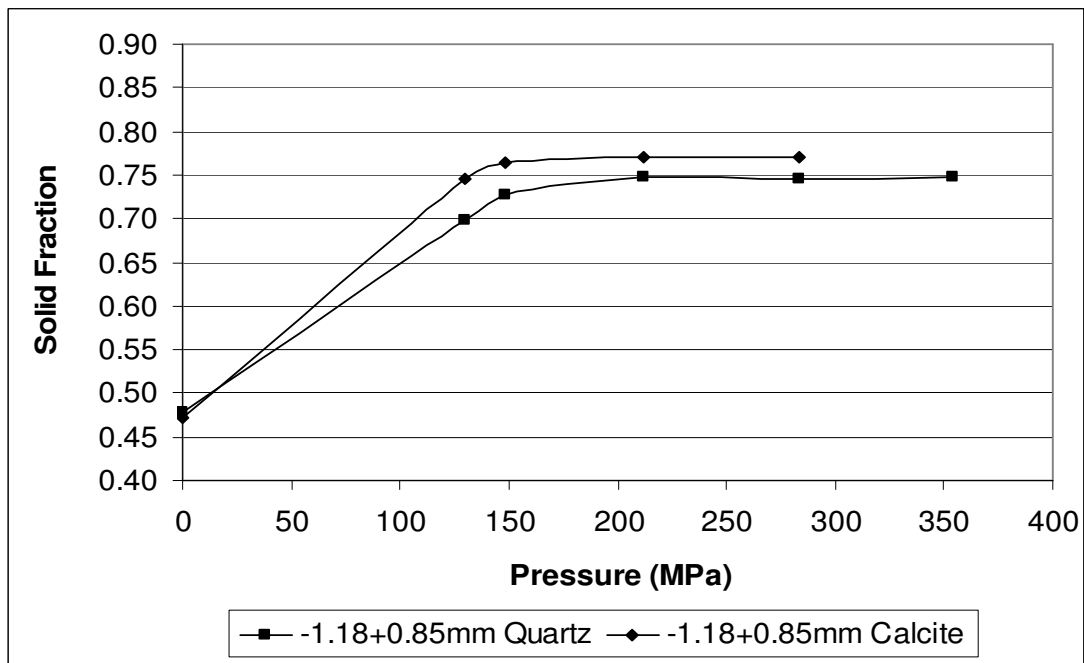
Figure 41: Solid fraction as a function of pressure applied in the particle bed comminution of quartz and calcite
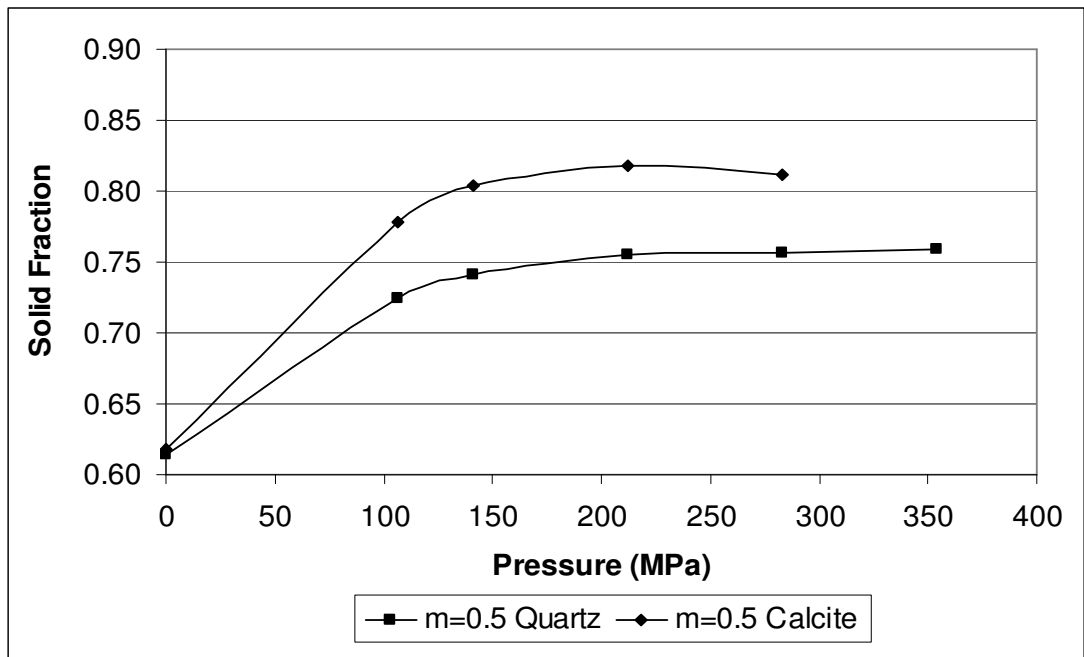
Figure 42: Solid fraction as a function of pressure applied in the particle bed comminution of quartz and calcite
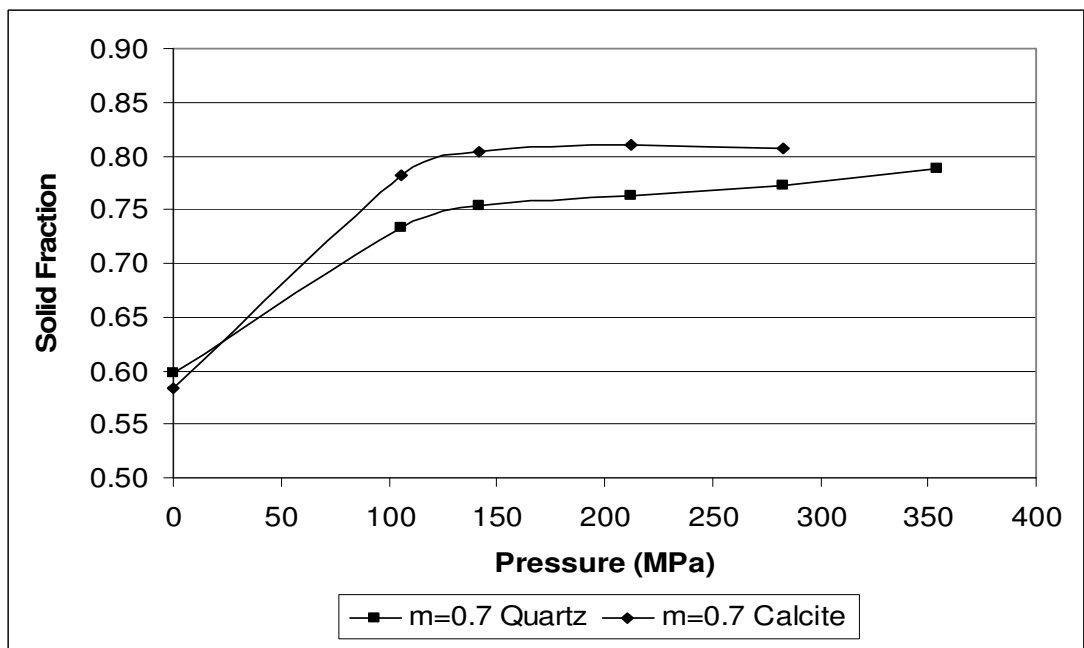
Figure 43: Solid fraction as a function of pressure applied in the particle bed comminution of quartz and calcite
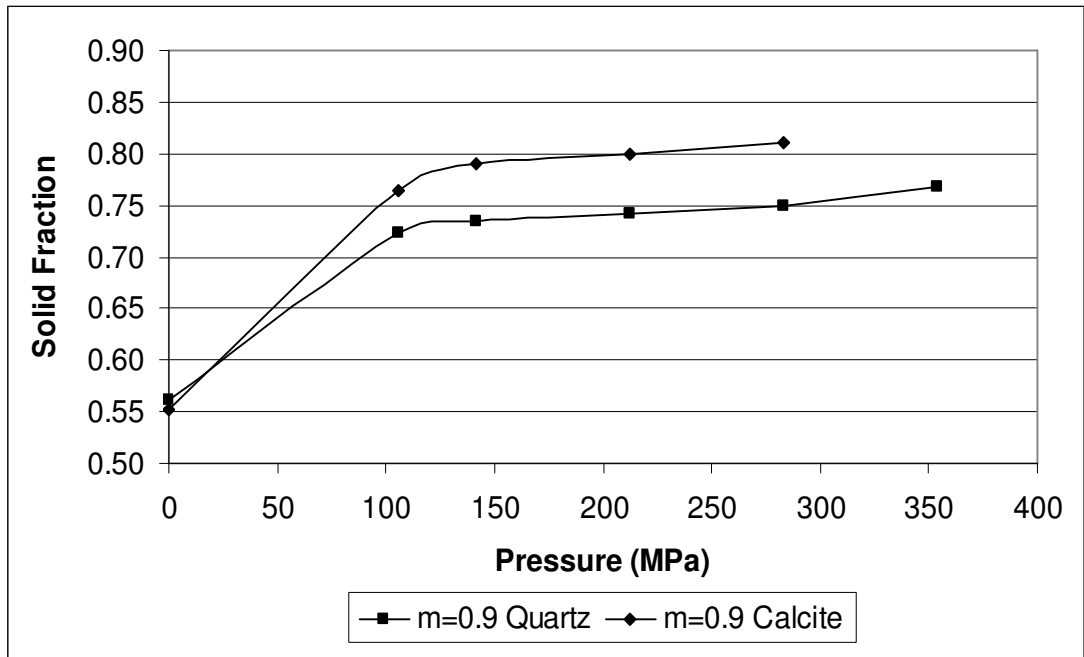
Figure 44: Solid fraction as a function of pressure applied in the particle bed comminution of quartz and calcite
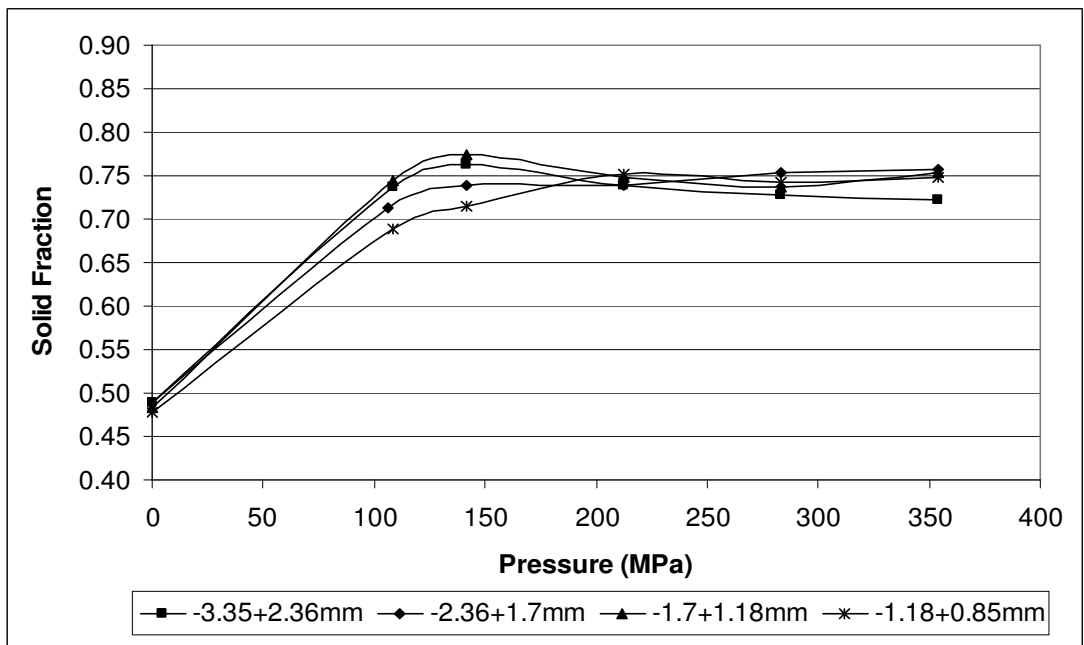
Figure 45: Solid fraction as a function of pressure applied in the particle bed comminution of quartz at different size ranges
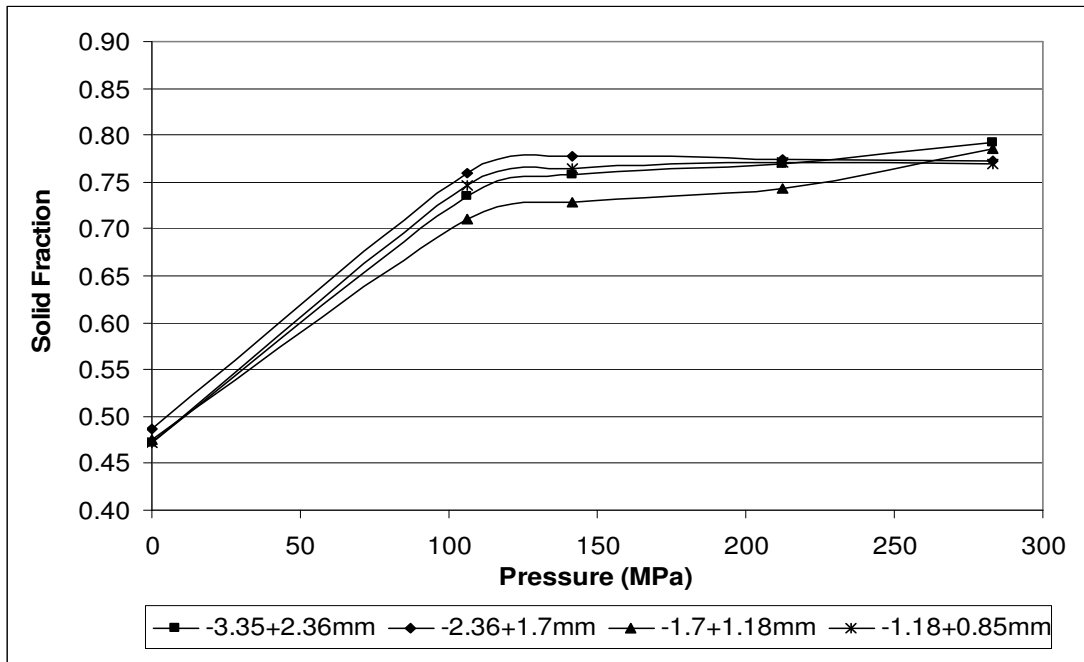
Figure 46: Solid fraction as a function of pressure applied in the particle bed comminution of calcite at different size ranges
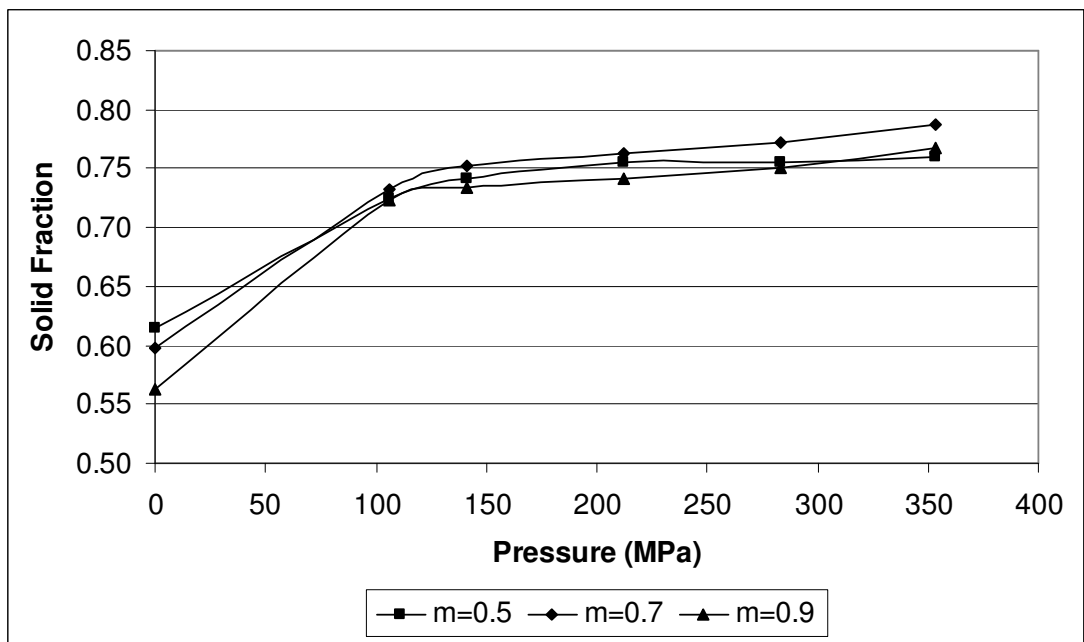
Figure 47: Solid fraction as a function of pressure applied in the particle bed comminution of quartz at different GGS distribution moduli
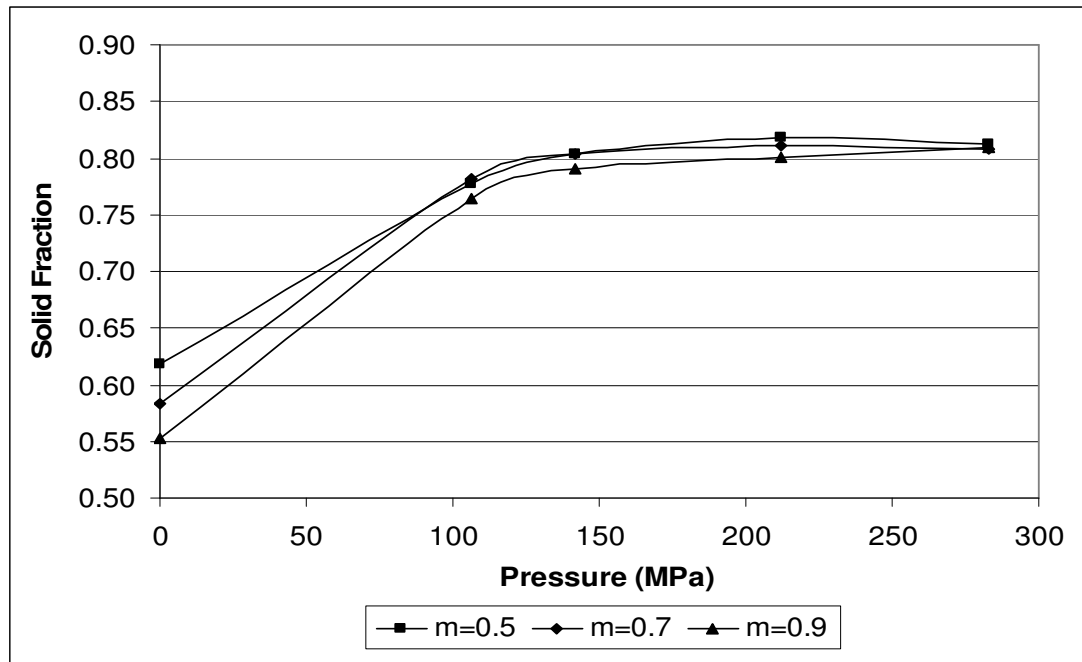
Figure 48: Solid fraction as a function of pressure applied in the particle bed comminution of calcite at different GGS distribution moduli

4.4 Reduction Ratio

A simple linear relationship was suggested by Fuerstenau et. al (1991) between the reduction ratio (X_f/X_{50}) and specific energy input (E_m) for single-particle breakage, in Equation 1. However, the important point to notice here is that the linear relationship between X_f/X_{50} and E_m in Eqn. 1 is valid over a limited range of reduction ratio only. Depending on the material, feed size and loading rate, the straight line plots begin to deviate from anywhere beyond a reduction ratio of about five. The straight line formations in Figures 49-57 show deviations in some parts, especially at high specific energies. The probable reasons of this condition are agglomeration, aggregation and interfragment friction effects that are formed in the piston-die-press, which are enhanced at higher specific energies (Fuerstenau and Kapur, 1994). Removal of the broken fragments during the experiment is not

46

possible for the piston-die-press as the loading machine is working till the wanted pressure is applied to the particles. So, this situation can probably lead to excess pressure application on the particles and cause the undesired effect described before. For calcite samples, reduction ratios larger than five can also cause deviations in some parts.

Norgate and Weller (1994, as cited in Lim et. al., 1996) proposed that a power law relationship is more appropriate when a larger range of specific energies is investigated. The power law equation is given below:

$$X_{50f} / X_{50p} = aE^b + 1 \quad .... (6)$$

where a and b are constants. Both relationships are applied to quartz and calcite samples. In general, both linear and power law relationships provide excellent fits with quartz samples through the experimental data. However, the linear relationship is not suitable for -3.35+.236mm quartz sample and for calcite samples feed particle size of -1.7+1.18 and -1.18+0.85mm and particle size distributions of m=0.5, m=0.7 and m=0.9.
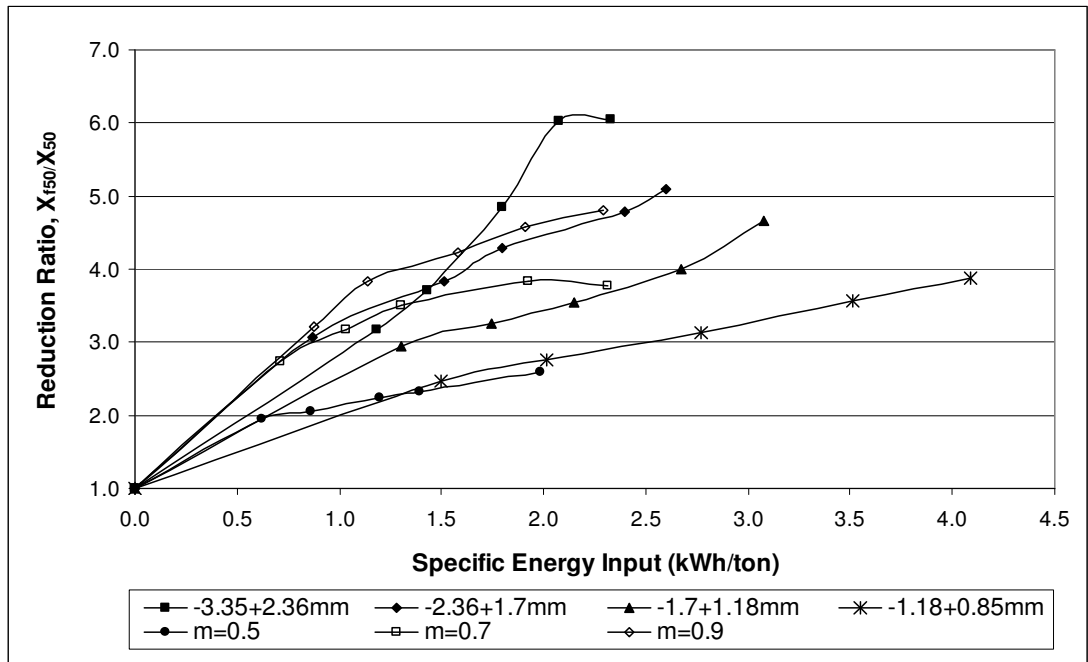
Figure 49: Reduction ratio as a function of specific energy input for different sizes of quartz samples comminuted in the piston-die-press
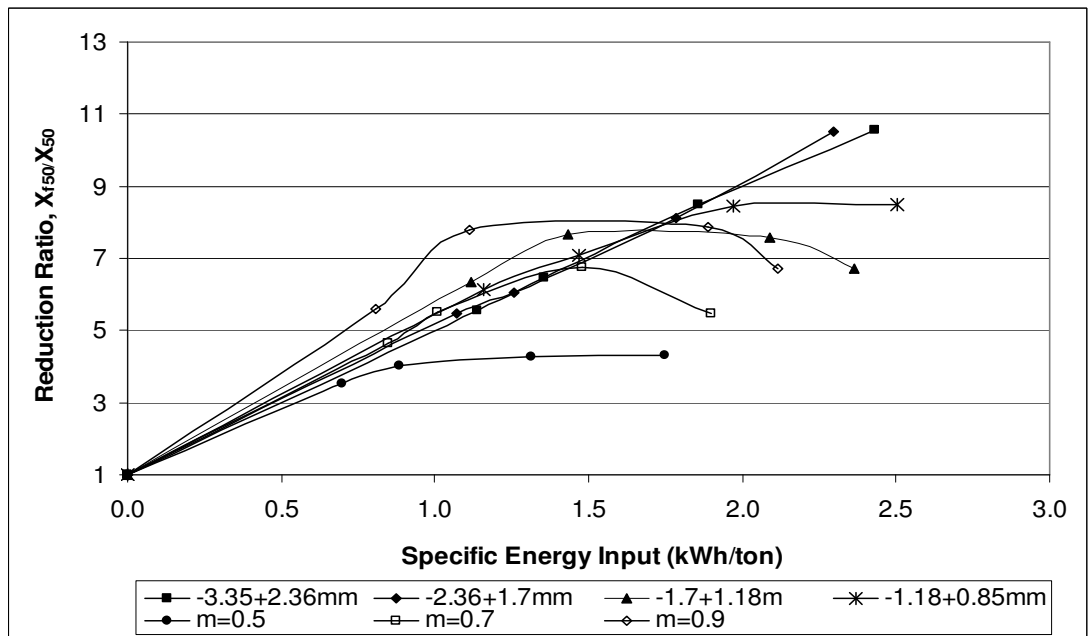
Figure 50: Reduction ratio as a function of specific energy input for different sizes of calcite samples comminuted in the piston-die-press

Distribution modulus of m=0.9 has higher reduction ratios when compared with narrow-size samples for quartz. Also, m=0.7 has higher reduction ratios than -1.7+1.18mm and -1.18+0.85mm narrow-range size fractions (Figure 49). Experimental results showed that the feed material having the widest size distribution (distribution modulus = 0.5) has lower reduction ratios when compared with other distribution moduli, due to the presence of higher amounts of fines in the mixture. For calcite sample, it can be concluded that only m=0.9 gives higher amounts of reduction ratio below 1.6 kWh/ton specific energy level when compared with narrow-range size fraction samples (Figure 50).
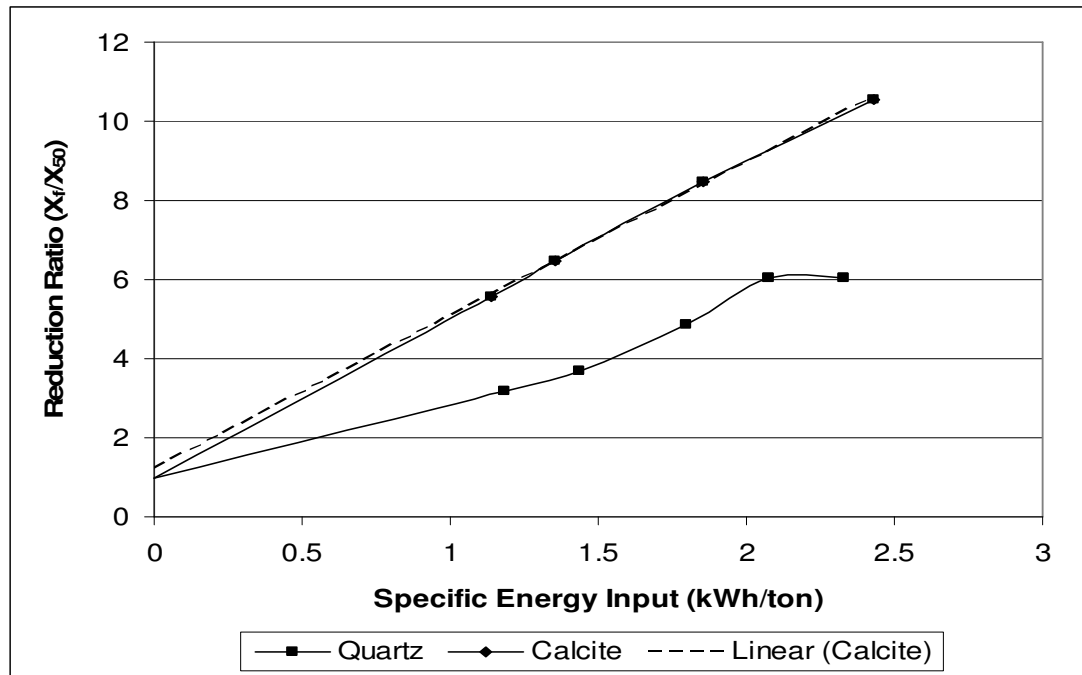
Figure 51: Reduction ratio as a function of specific energy input for -3.35+2.36mm quartz and calcite samples comminuted in the piston-die-press
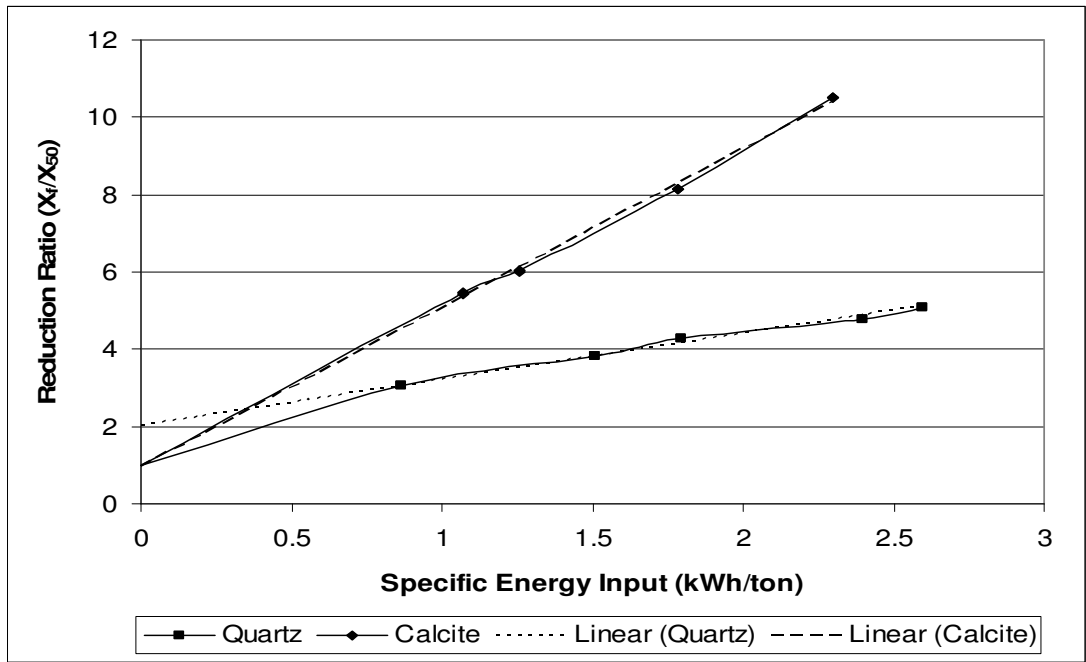
Figure 52: Reduction ratio as a function of specific energy input for -2.36+1.7mm quartz and calcite samples comminuted in the piston-die-press
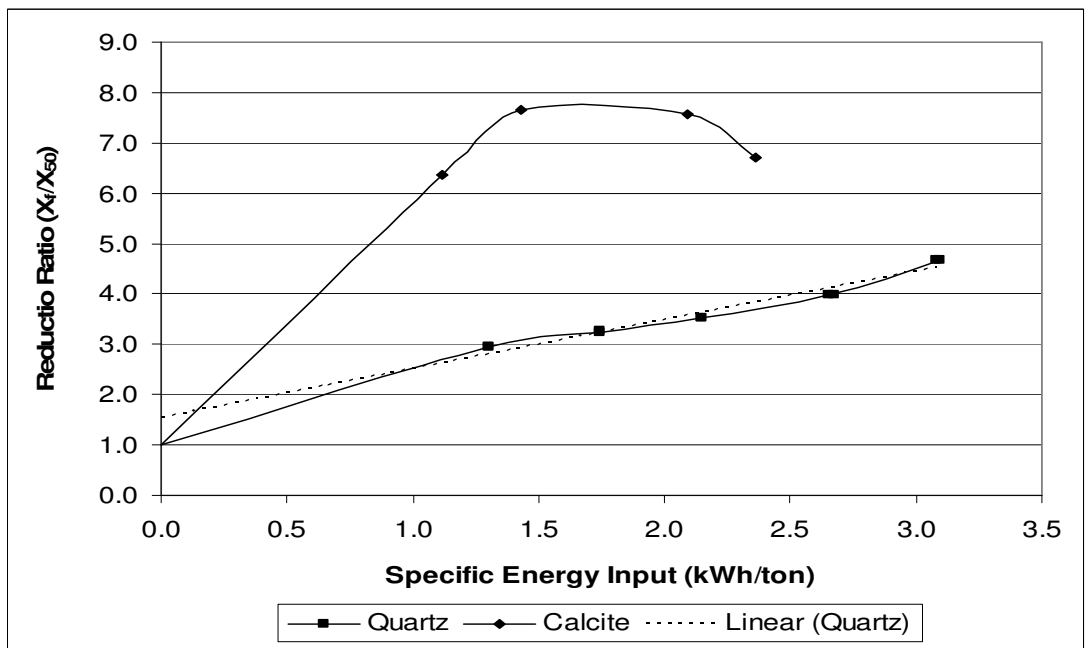
Figure 53: Reduction ratio as a function of specific energy input for -1.7+1.18mm quartz and calcite samples comminuted in the piston-die-press
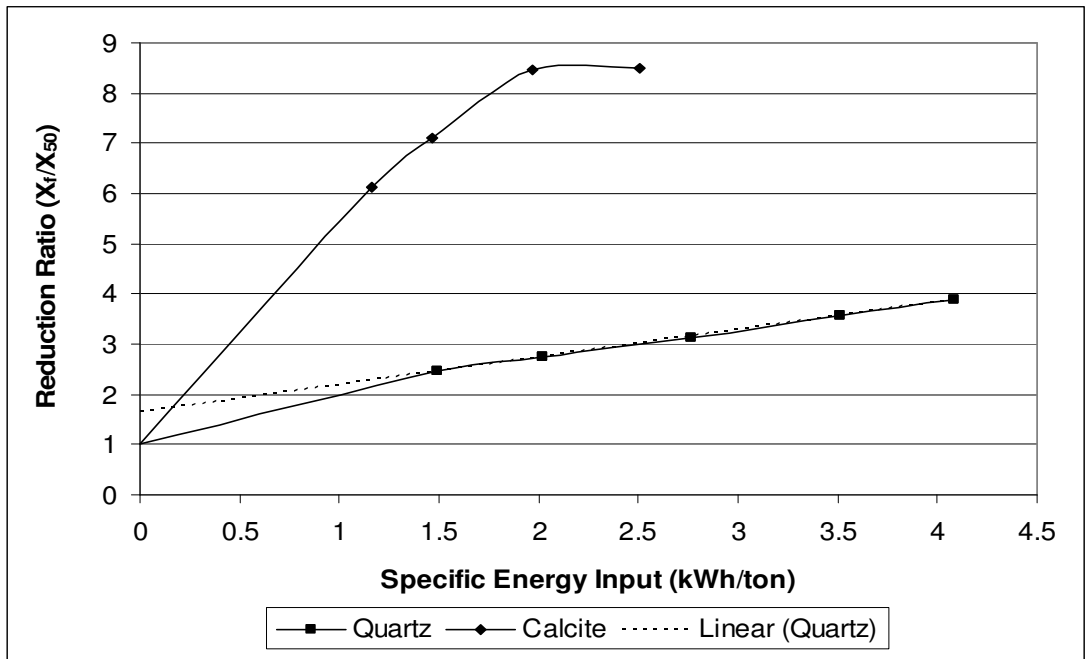
Figure 54: Reduction ratio as a function of specific energy input for -1.18+0.85mm quartz and calcite samples comminuted in the piston-die-press
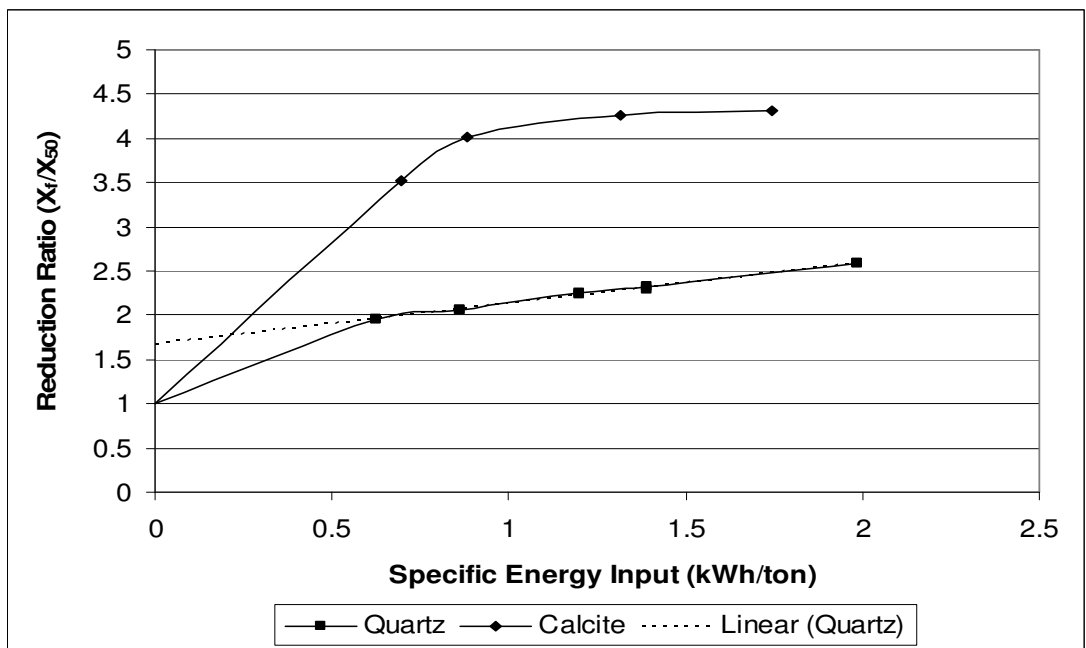
Figure 55: Reduction ratio as a function of specific energy input for m=0.5 quartz and calcite samples comminuted in the piston-die-press
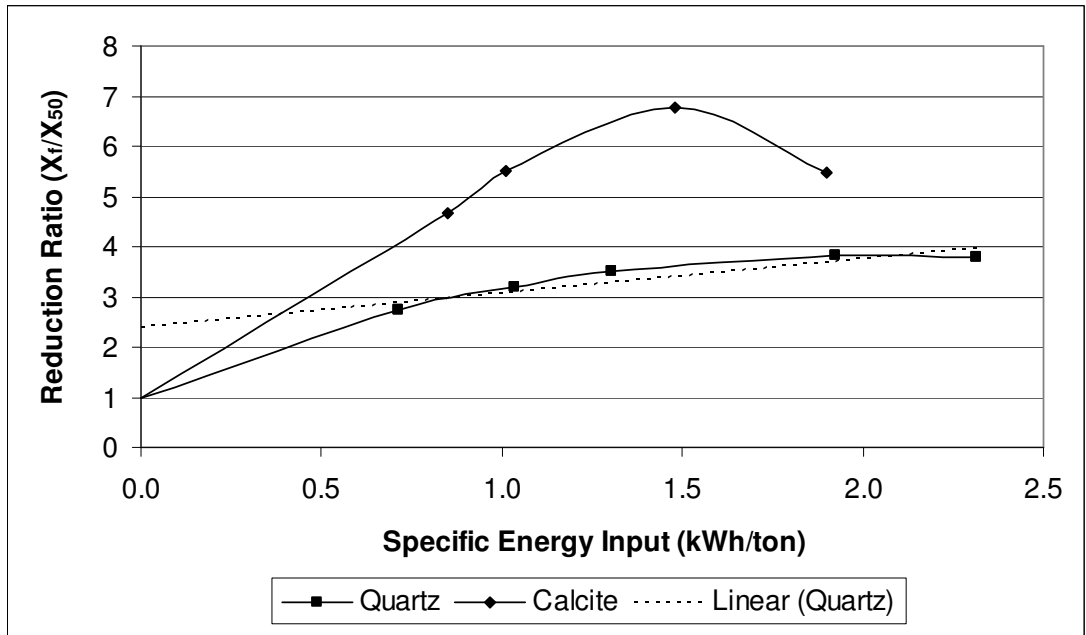
Figure 56: Reduction ratio as a function of specific energy input for m=0.7 quartz and calcite samples comminuted in the piston-die-press
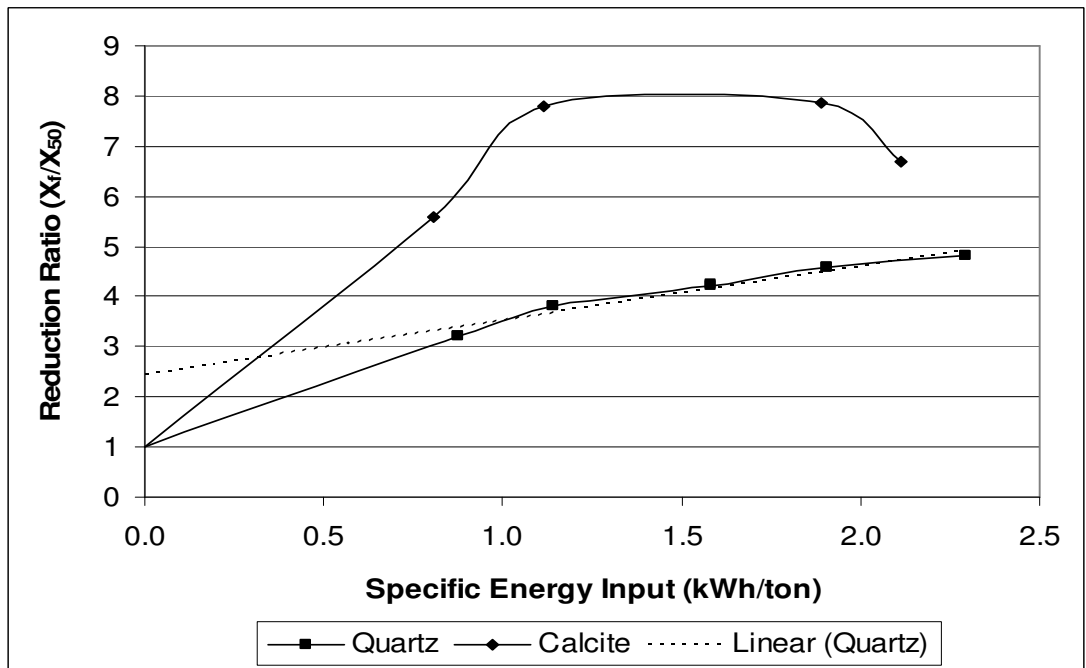
Figure 57: Reduction ratio as a function of specific energy input for m=0.9 quartz and calcite samples comminuted in the piston-die-press

When Figures 51-57 are examined it can be concluded that, calcite has higher reduction ratios at all particle sizes and distributions when compared with quartz. But, for -1.7+1.18mm particle size (Figure 53) and samples of m=0.7 and m=0.9 distribution moduli; reduction ratios of calcite started to decrease at higher specific energies (Figure 56 and 57). So, increasing specific energy over that point is not efficient for comminution purposes.

4.5 Size Fractions in the Product

Figure 58 shows the size fraction of -3.35+2.36mm quartz particles contained in size-distributed feeds comminuted at specified pressures. According to the graphs, it can be concluded that, although the feed having distribution modulus of 0.9 have the highest initial amount of -3.35+2.36mm particles; final mass fraction of this size particles at 353.86 MPa pressure is approximately the same with those of the other two size-distributed feeds. As the fraction of coarse particles reaches approximately 9-10%, breakage of the quartz particles ceases.
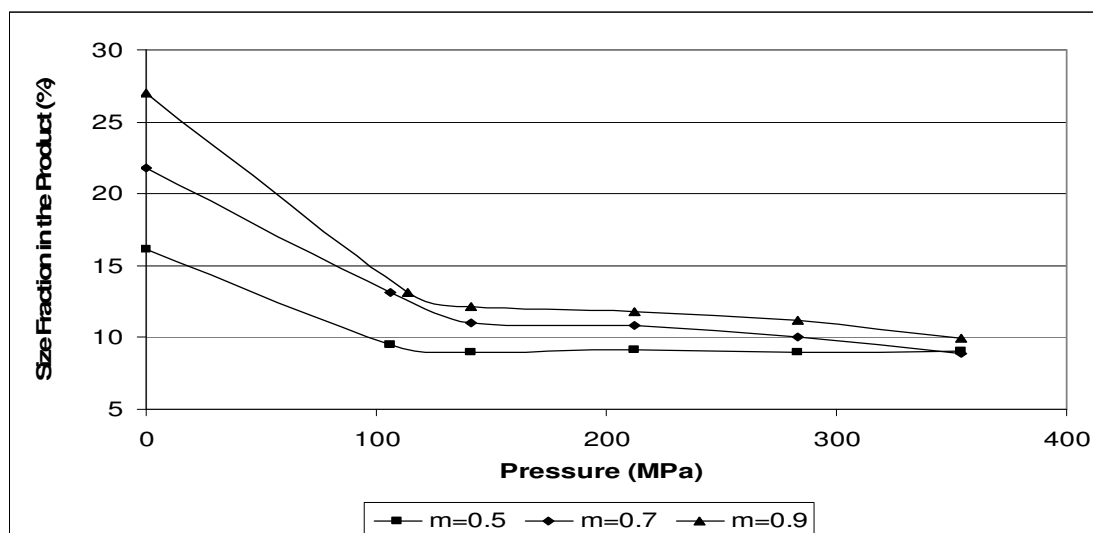
Figure 58: Size fraction of -3.35+2.36mm quartz sample in m=0.5, m=0.7 and m=0.9 distribution moduli at specified pressures

53

For calcite sample, m=0.7 and m=0.9 distribution moduli have very similar size fractions for -3.35+2.36mm particle size (Figure 59). Although m=0.7 and m=0.9 have higher fractions initially, the final scene is similar which means that the amount of breakage is higher at m=0.7 and m=0.9, respectively. As the fraction of coarse particles reaches approximately 7-8%, breakage of the calcite particles ceases. This means that coarser particles of calcite became finer than those of quartz.
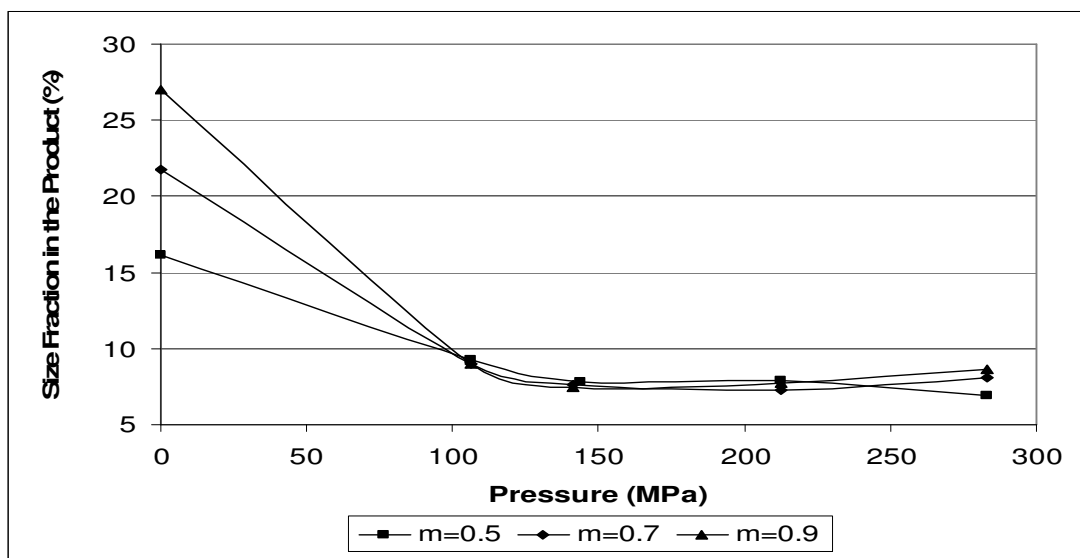
Figure 59: Size fraction of -3.35+2.36mm calcite sample in m=0.5, m=0.7 and m=0.9 distribution moduli at specified pressures
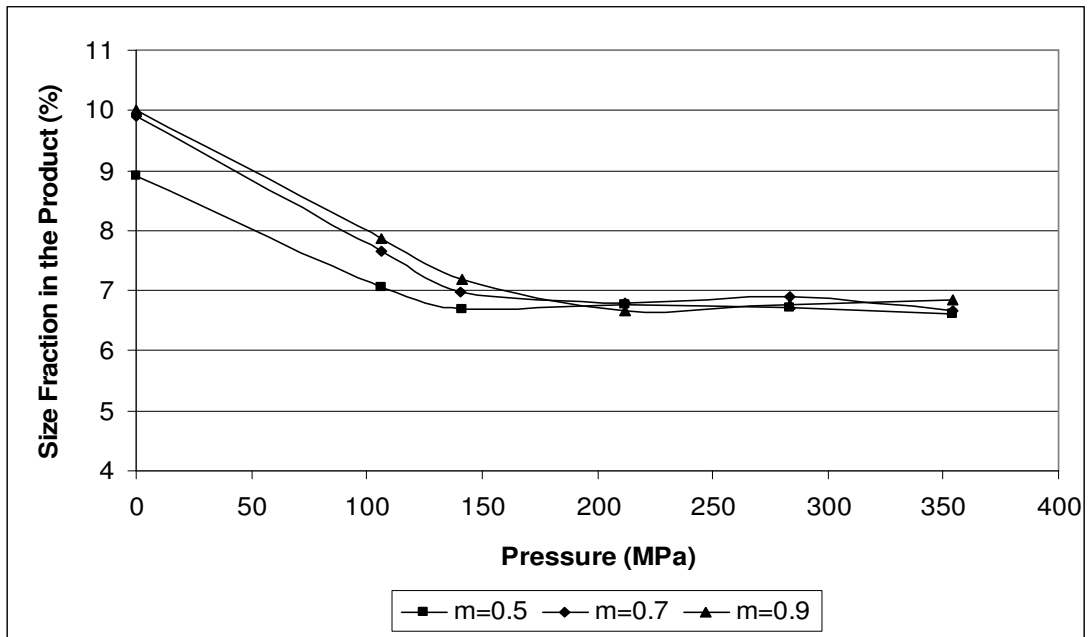
Figure 60: Size fraction of -1.18+0.85mm quartz sample in m=0.5, m=0.7 and m=0.9 distribution moduli at specified pressures
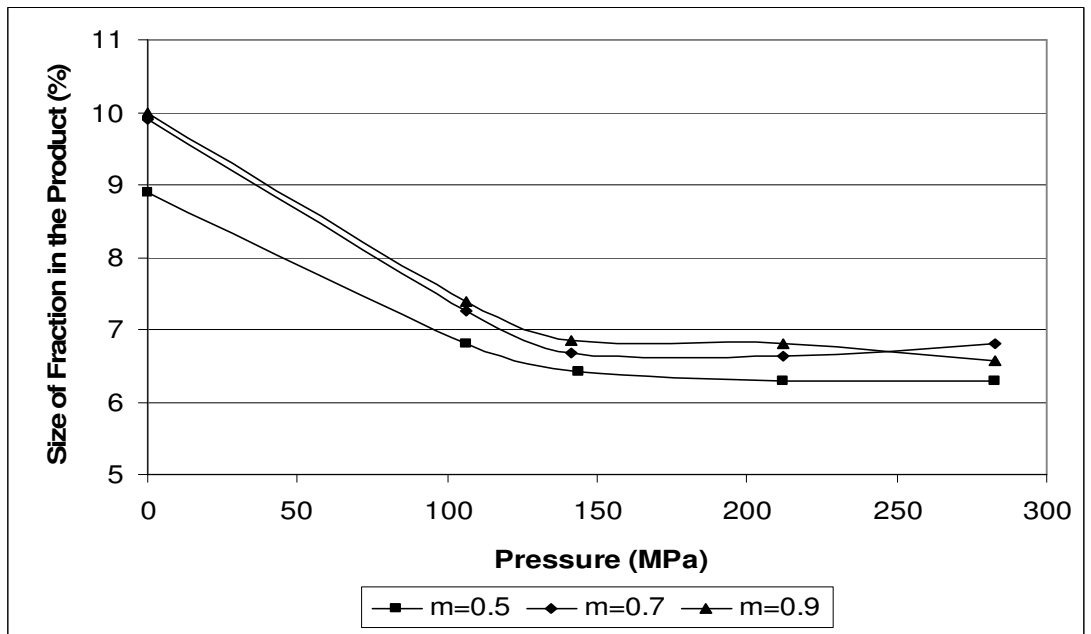
Figure 61: Size fraction of -1.18+0.85mm calcite sample in m=0.5, m=0.7 and m=0.9 distribution moduli at specified pressures

Figures 62 and 63 illustrate the size fraction of -425+300µm quartz and calcite particles contained in size-distributed feeds comminuted at specified pressures. Beside comminution of -425+300mm particles, quartz samples receive particles from coarser sizes and the breakage of these particles also takes place (Figure 62). However, in calcite samples breakage of this size fraction to finer sizes is more efficient when compared with quartz samples (Figure 63).

Figure 64 illustrates size fraction of -150+106µm quartz sample, and distribution modulus of m=0.9 has the highest fraction among others at high pressures. This situation indicates that at the end of breakage m=0.9 has the highest amount of -150+106µm size fraction, which implies that comminution is much more effective on this modulus for this size fraction. At the same particle size, calcite samples have similar fractions values for all distribution moduli (Figure 65).
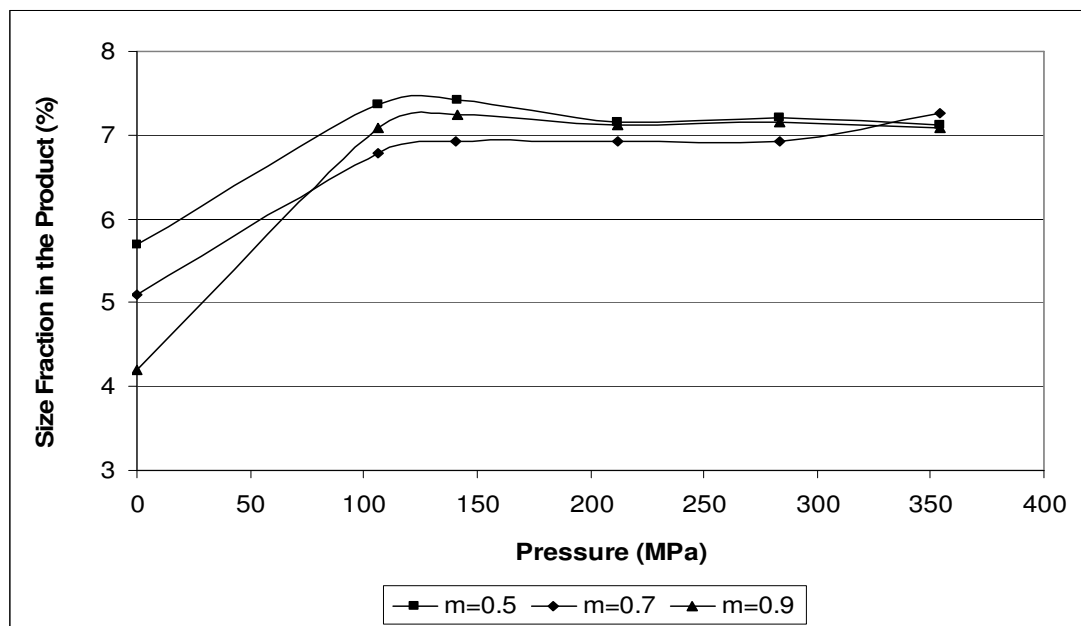
Figure 62: Size fraction of -425+300µm quartz sample in m=0.5, m=0.7 and m=0.9 distribution moduli at specified pressures
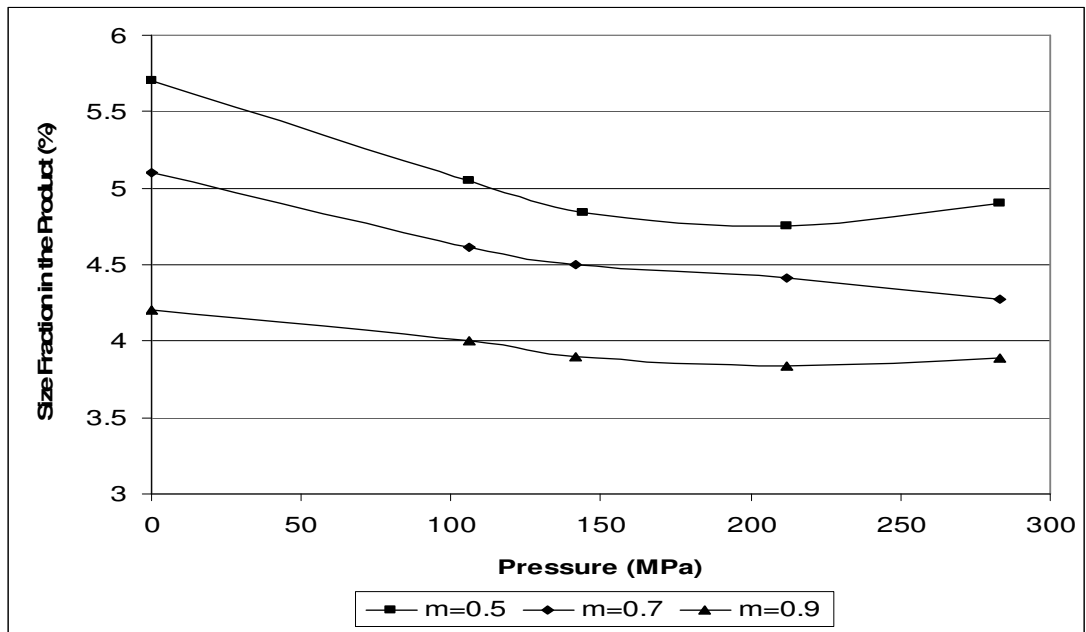
Figure 63: Size fraction of -425+300µm calcite sample in m=0.5, m=0.7 and m=0.9 distribution moduli at specified pressures
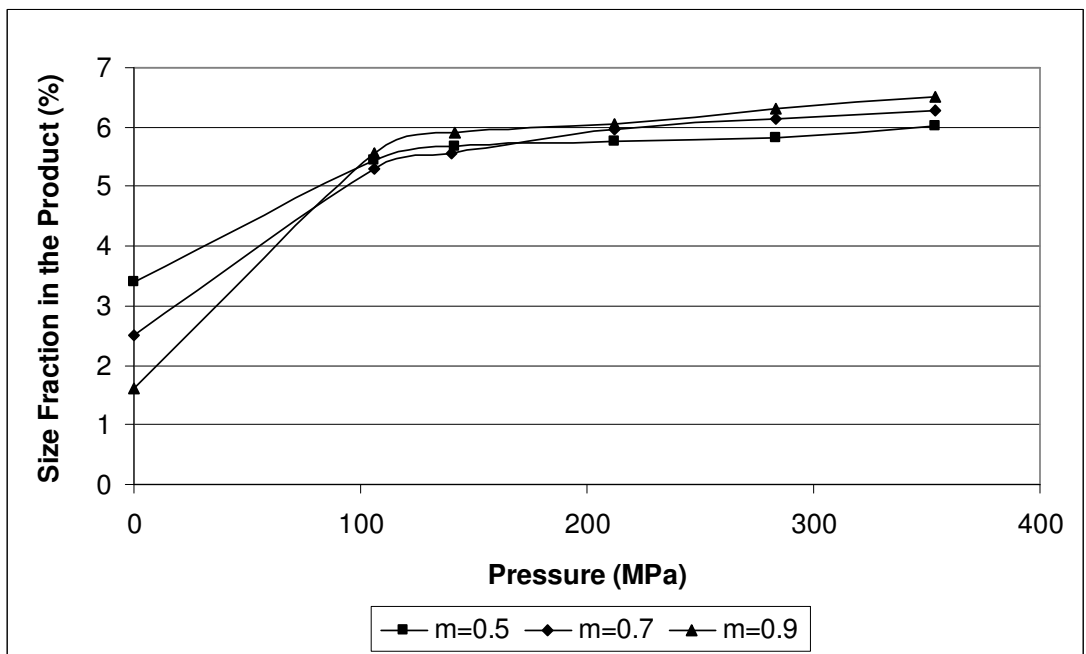
Figure 64: Size fraction of -150+106µm quartz sample in m=0.5, m=0.7 and m=0.9 distribution moduli at specified pressures
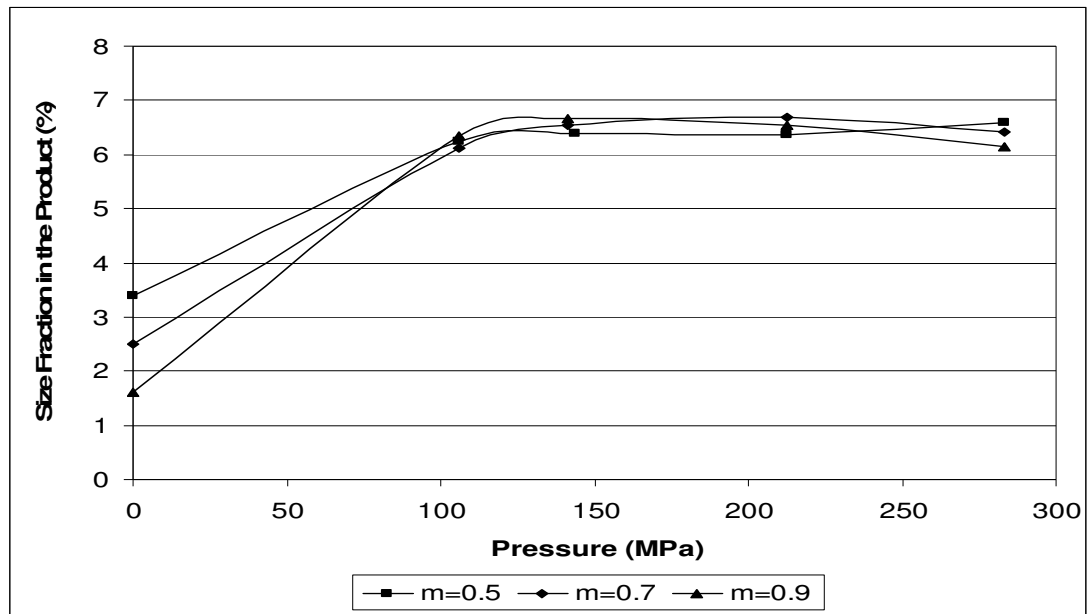
Figure 65: Size fraction of -150+106µm calcite sample in m=0.5, m=0.7 and m=0.9 distribution moduli at specified pressures

According to curves in Figure 66, the highest amount of -53+38µm size fraction is obtained from m=0.7 distribution modulus. However, by comparing the ratios of fractions in Table 2 it can be concluded that the amount of size reduction is higher in m=0.9 modulus, but the amount of -53+38µm size fraction in the mixture is not as much as in m=0.5 and m=0.7 moduli. Consequently, for the pressures greater than 260 MPa distribution modulus of 0.7 results in much finer sizes at the end of comminution and followed by m=0.5 and m=0.9 moduli for quartz samples.

In Figure 67, size fraction of -53+38µm calcite samples started to stabilize after 140MPa pressure for all distribution moduli. m=0.9 distribution modulus has the highest amount of -53+38µm size fraction, followed by m=0.7 and m=0.5, respectively; which means that breakage of m=0.9 modulus results in much finer sizes. m=0.9 distribution modulus has the lowest amount of fines at the beginning so that isostatic regime generated more slowly in comminution and breakage lasts

longer than other moduli. Furthermore, comparing the size fraction amounts of quartz and calcite it can be stated that breakage is more effective on calcite samples since the fraction amounts are higher than that of quartz at the end of comminution (Table 2).
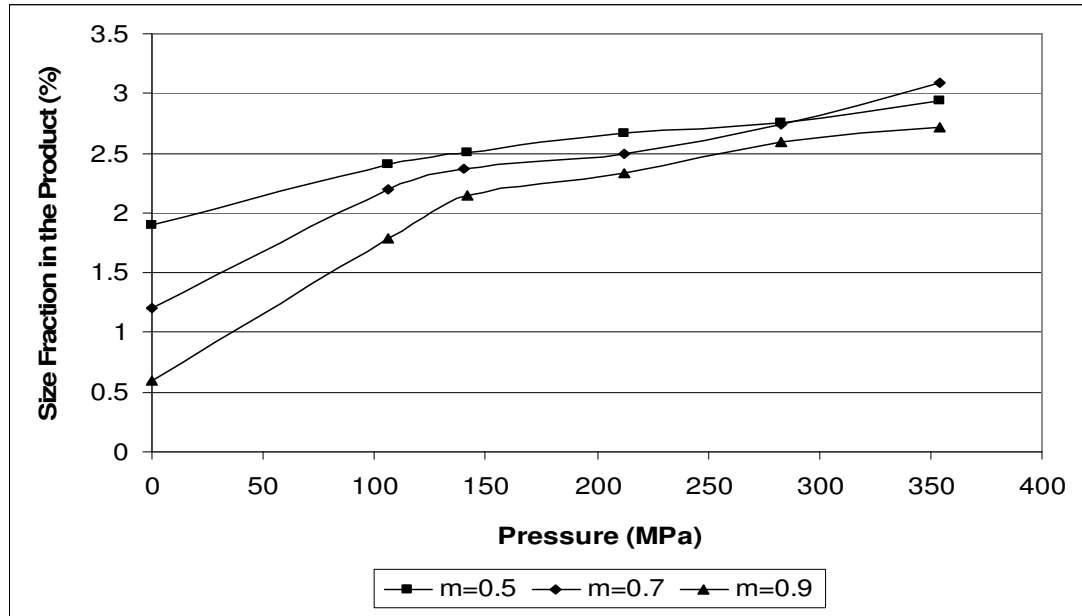
Figure 66: Size fraction of -53+38µm quartz sample in m=0.5, m=0.7 and m=0.9 distribution moduli at specified pressures

Table 2: Size fraction ratios of -53+38µm quartz samples in m=0.5, m=0.7 and m=0.9 distribution moduli at initial and final pressures

Distribution Modulus	Size Fraction at 0 MPa Pressure	Size Fraction at 353.86 MPa Pressure	Ratio
m=0.5	1.9	2.94	1.55
m=0.7	1.2	3.09	2.58
m=0.9	0.6	2.72	4.54
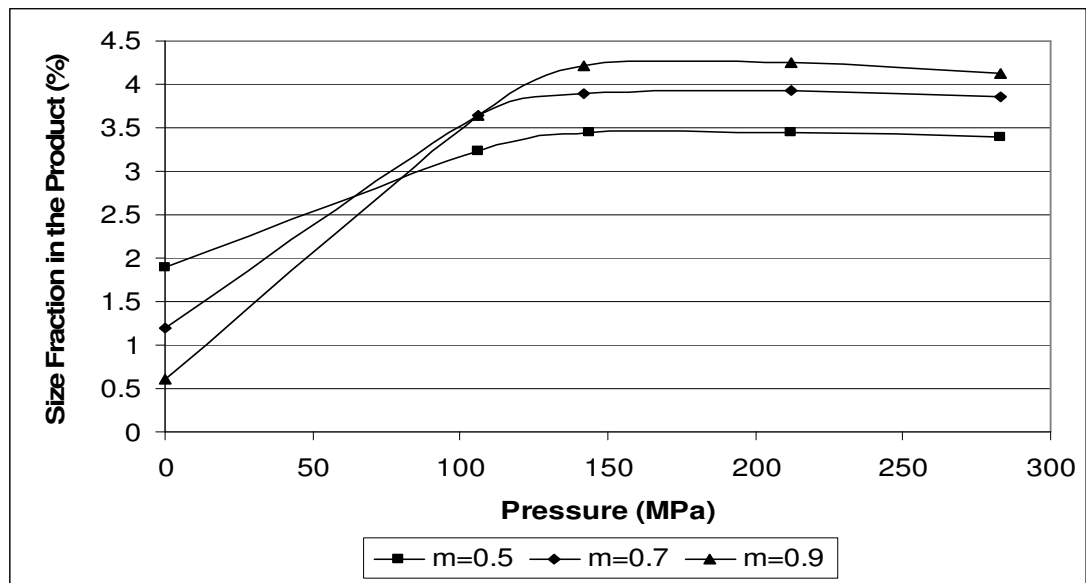
Figure 67: Size fraction of -53+38µm calcite sample in m=0.5, m=0.7 and m=0.9 distribution moduli at specified pressures

4.6 Size Reduction Curves

The curves in Figures 68-70 are called as the size reduction curves. The bisect line gives the no size-reduction condition. This line shows the original feed particle size distribution of quartz with values of m=0.5 m=0.7 and m=0.9 in three different graphs. For each specified feed particle size distribution, different bed pressure values were investigated to evaluate the amount of reduction achieved. The degree of size reduction can be computed by the area caught between the size reduction curve and the no size-reduction line. This area can be calculated by trapezoidal method of numerical integration method with the help of MATLAB computer program. According to Bazin and Hodouin (2004), it can be concluded that the larger the area the more size reduction is performed by piston-die-press. This means that as the amount of bed pressure increases the amount of the size reduction increases; however, at higher pressures the difference between the reduction amounts become

smaller, especially for m=0.5 illustrated in Figure 68. This is probably related to the presence of fine particles that act as a cushion, since the breakage fraction decreases in the presence of fine particles. When the amounts of fines are compared in different feed particle size distributions before comminution operation, m=0.5 has the highest amount among each other, so the cushion effect was more effective on those samples. In addition, as indicated in Table 3 the highest reduction ratio is obtained from m=0.9 samples of quartz and calcite, which have the smallest amount of fines at the beginning (Figure 70).
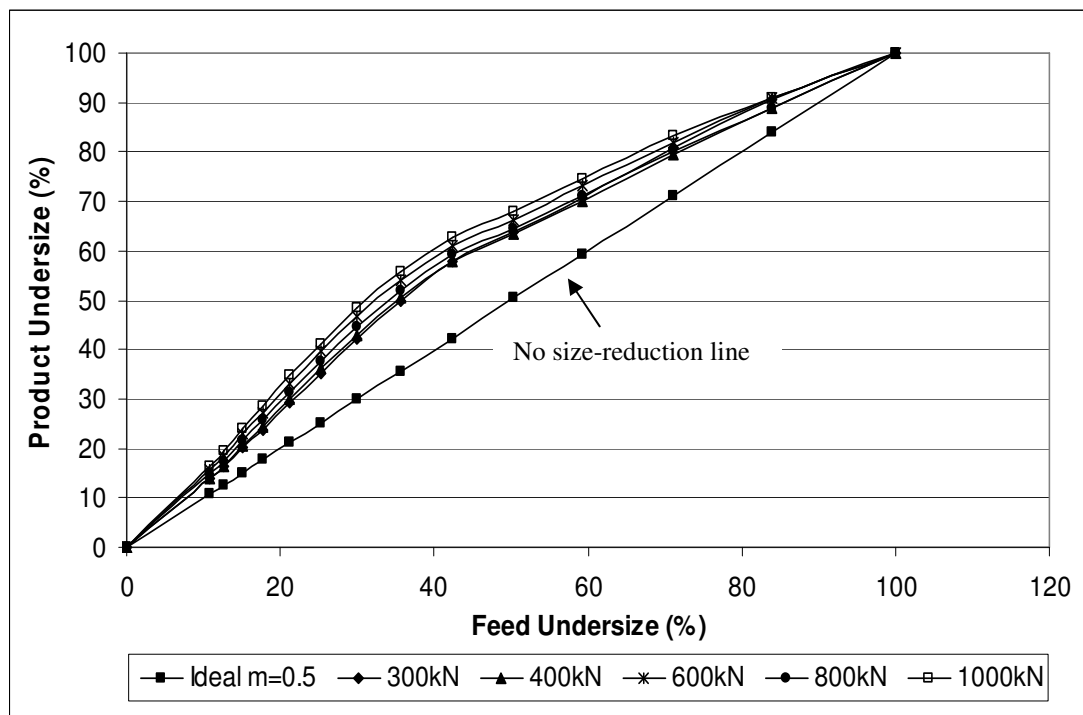
Figure 68: Size reduction curves for quartz sample of m=0.5
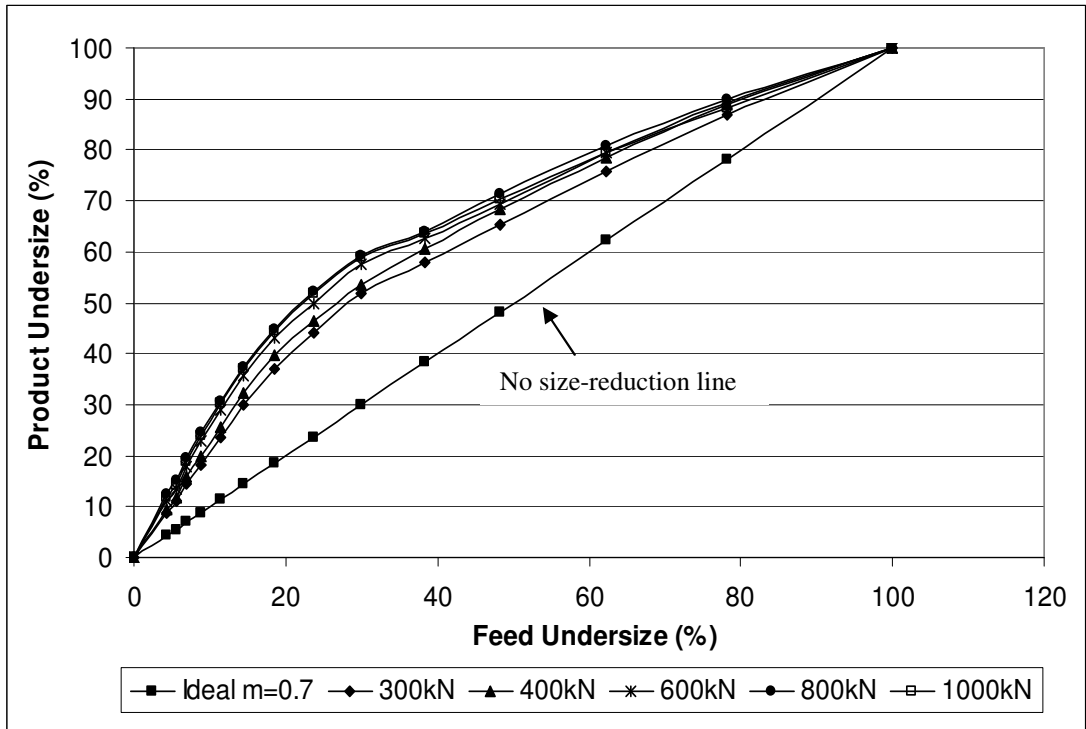
Figure 69: Size reduction curves for quartz sample of m=0.7
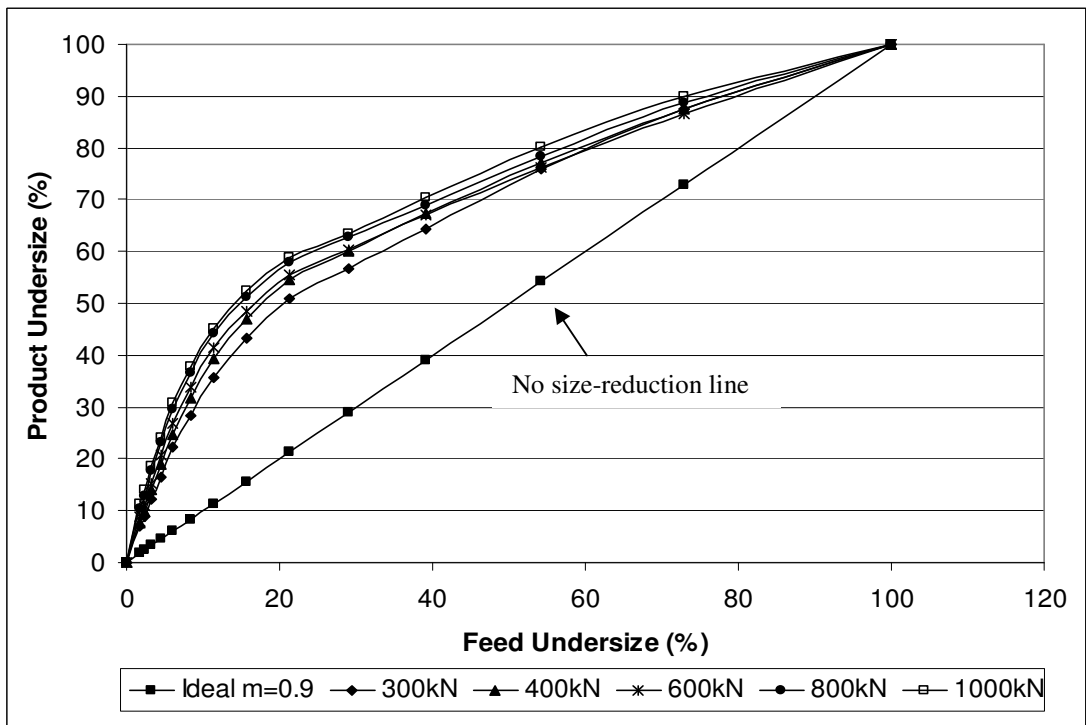
Figure 70: Size reduction curves for quartz sample of m=0.9

To compare the energy utilization of different distribution moduli during comminution in die-piston press, following figures are demonstrated for quartz and calcite samples with the help of Tables 3-6. In Tables 3-6, areas ($\%^2$) and reduction ratios of quartz and calcite samples were compared for m=0.5; m=0.7 and m=0.9 at four different forces. Distribution modulus of 0.9 have the highest size reduction area when compared with others, approximately at the same specific energy inputs for quartz samples (Figure 73). This means that this modulus results in higher amounts of breakage and utilizes energy in more efficient way than others due to its higher amounts of coarse particles in the mixture. In addition, calcite samples give similar results with quartz samples; however, size reduction areas are higher in calcite at all distribution moduli (Figure 74). As a consequence, the amount of breakage is higher in calcite samples at all distribution moduli and the breakage of calcite is more energy-efficient than quartz, approximately at the same specific energy inputs (Figures 75-77). Figures 71 and 72 show the comparison of size reduction curves of quartz and calcite at distribution modulus of 0.5 at 300kN and 800kN force, respectively.

Beside these figures, a table is given in Appendix G which gives the amounts of specific energy inputs for unit size reduction areas. This table shows the energy utilization of different distribution moduli and supports the results obtained from Figures 73-77. Specific energy input increases with increasing pressure both for quartz and calcite samples. In addition, specific energy input decreases in the following order; m=0.5, m=0.7 and m=0.9 at all pressures, due to decreasing amounts of fines in the mixtures (decreasing breakage strength). Same amounts of pressures results in different specific energy inputs for quartz and calcite samples. When compared with quartz, calcite absorbs lower amounts of specific energy at all distribution moduli for all pressures; which means that comminution of softer sample, calcite, is more efficient in terms of energy usage.
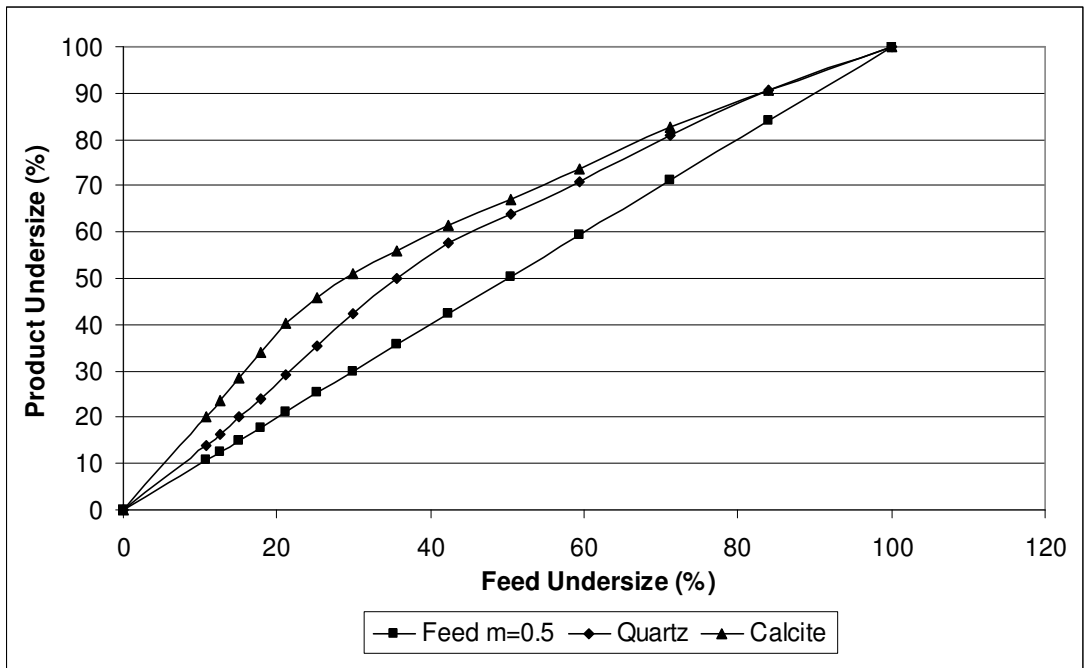
Figure 71: Comparison of size reduction curves of quartz and calcite at 300kN pressure in piston-die-press
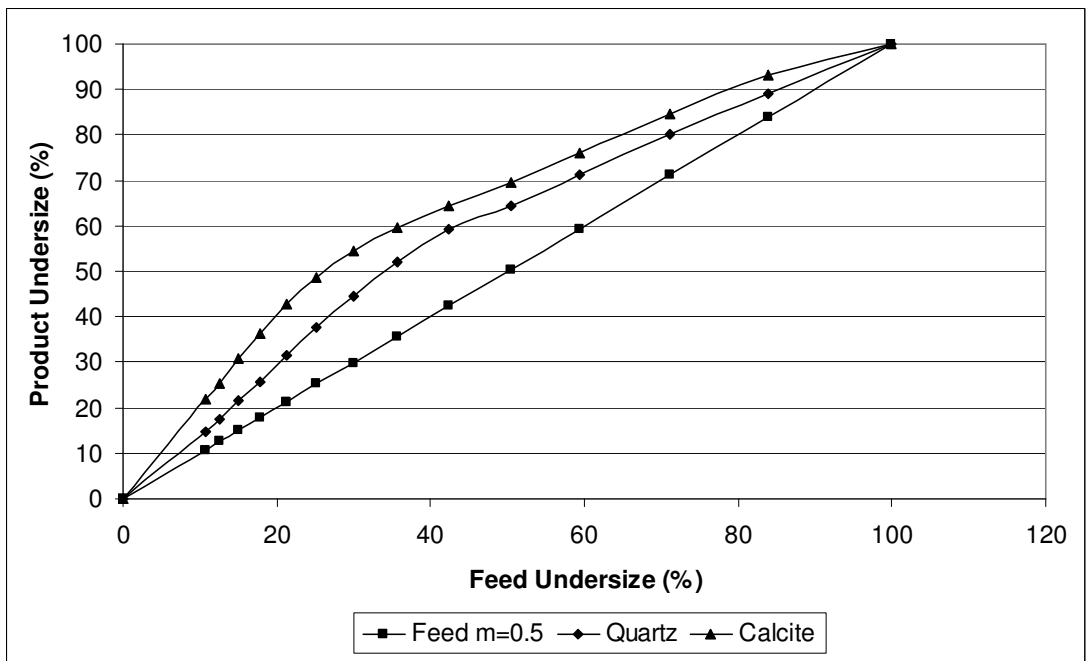
Figure 72: Comparison of size reduction curves of quartz and calcite at 800kN pressure in piston-die-press

64

Table 3: Size reduction areas for quartz and calcite samples at 300kN force in piston-die-press

Feed Particle Size Distribution	Area($\%^2$)		Reduction Ratio		Specific Energy Input (J/g)	
	Quartz	Calcite	Quartz	Calcite	Quartz	Calcite
m=0.5	847.87	1234.2	1.96	3.49	2.25	2.50
m=0.7	1252.1	1899.4	2.71	4.81	2.57	3.05
m=0.9	1812.9	2416.4	3.11	5.83	3.15	3.23

Table 4: Size reduction areas for quartz and calcite samples at 400kN force in piston-die-press

Feed Particle Size Distribution	Area($\%^2$)		Reduction Ratio		Specific Energy Input (J/g)	
	Quartz	Calcite	Quartz	Calcite	Quartz	Calcite
m=0.5	814.89	1360.3	1.99	3.8	3.11	3.18
m=0.7	1455.8	2082.6	2.98	5.33	3.72	3.64
m=0.9	1973.6	2627.2	3.71	7.99	4.10	4.01

Table 5: Size reduction areas for quartz and calcite samples at 600kN force in piston-die-press

Feed Particle Size Distribution	Area($\%^2$)		Reduction Ratio		Specific Energy Input (J/g)	
	Quartz	Calcite	Quartz	Calcite	Quartz	Calcite
m=0.5	1055.6	1386.2	2.20	4.49	4.32	4.73
m=0.7	1606.0	2217.5	2.94	6.78	4.68	5.32
m=0.9	1970.2	2597.5	3.95	7.99	5.70	6.80

Table 6: Size reduction areas for quartz and calcite samples at 800kN pressure in piston-die-press

Feed Particle Size Distribution	Area($\%^2$)		Reduction Ratio		Specific Energy Input (J/g)	
	Quartz	Calcite	Quartz	Calcite	Quartz	Calcite
m=0.5	899.21	1453.7	2.14	4.49	5.02	6.29
m=0.7	1735.0	1975.1	3.78	5.33	6.17	6.84
m=0.9	2166.4	2430.7	4.59	6.45	6.86	7.61
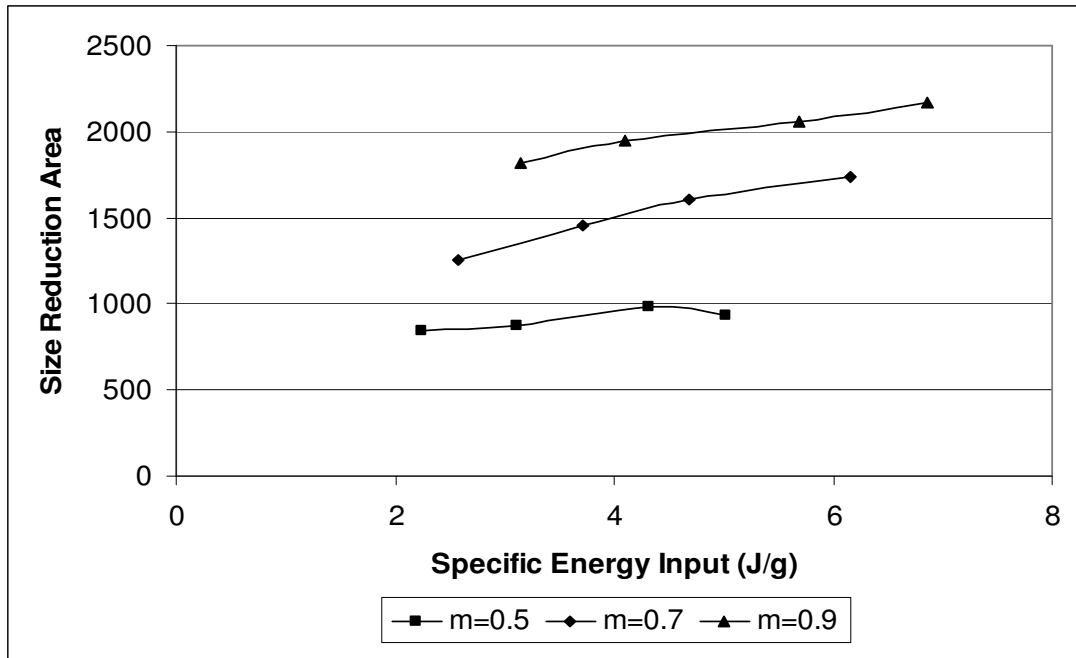
Figure 73: Size reduction areas of quartz as a function of specific energy inputs for different distribution moduli compared to evaluate the energy utilization of samples
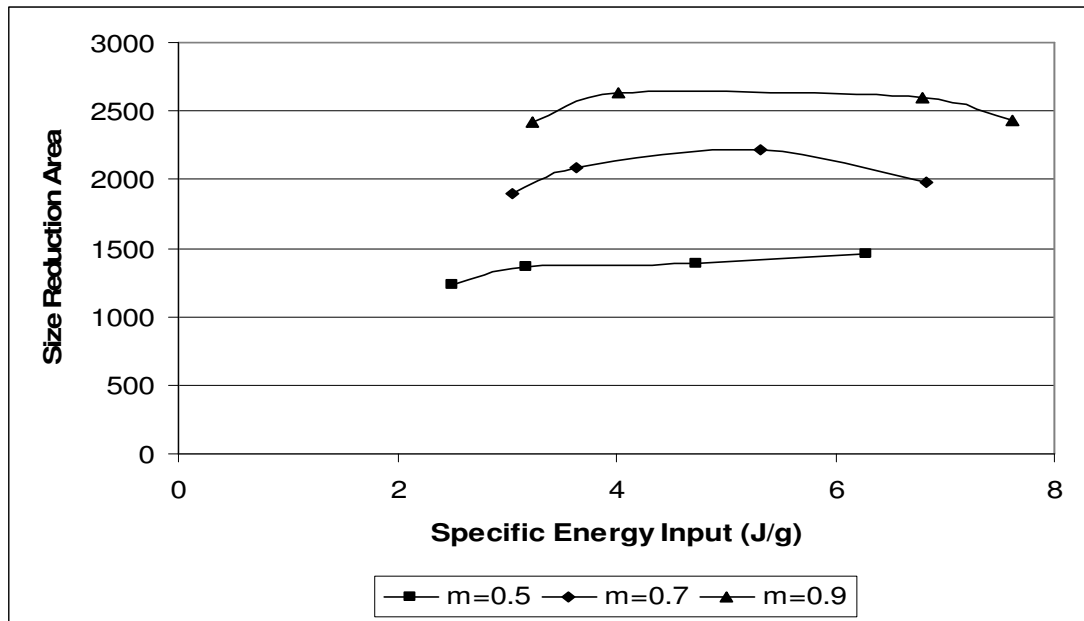
Figure 74: Size reduction areas of calcite as a function of specific energy inputs for different distribution moduli compared to evaluate the energy utilization of samples
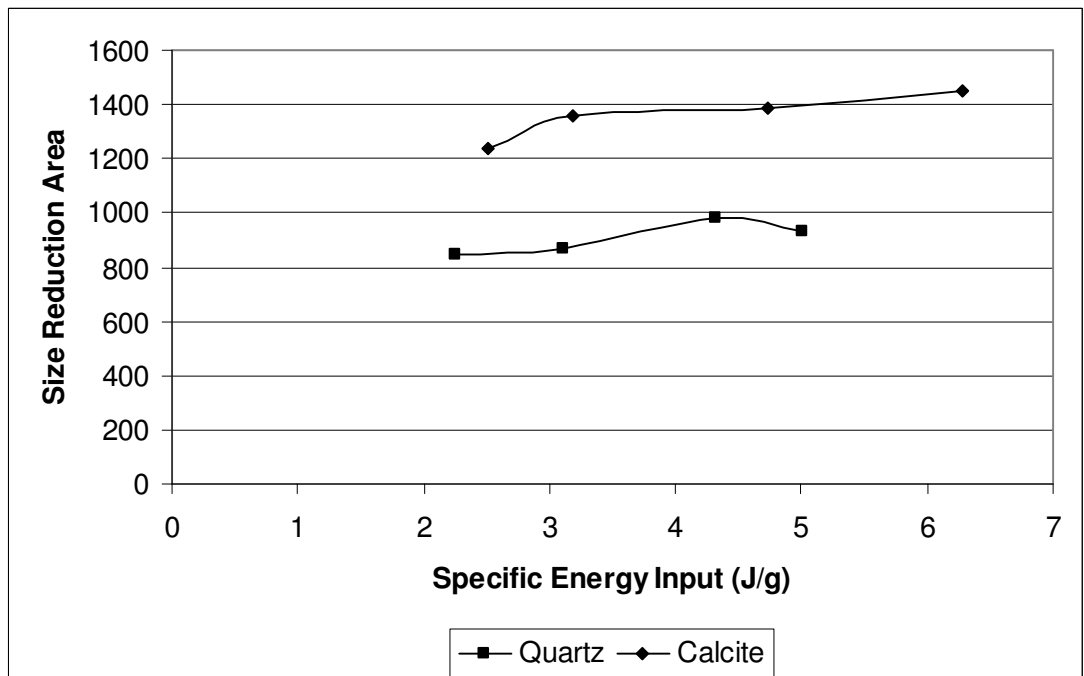
Figure 75: Comparison of size reduction areas for quartz and calcite samples having distribution moduli of 0.5 to evaluate the energy utilization
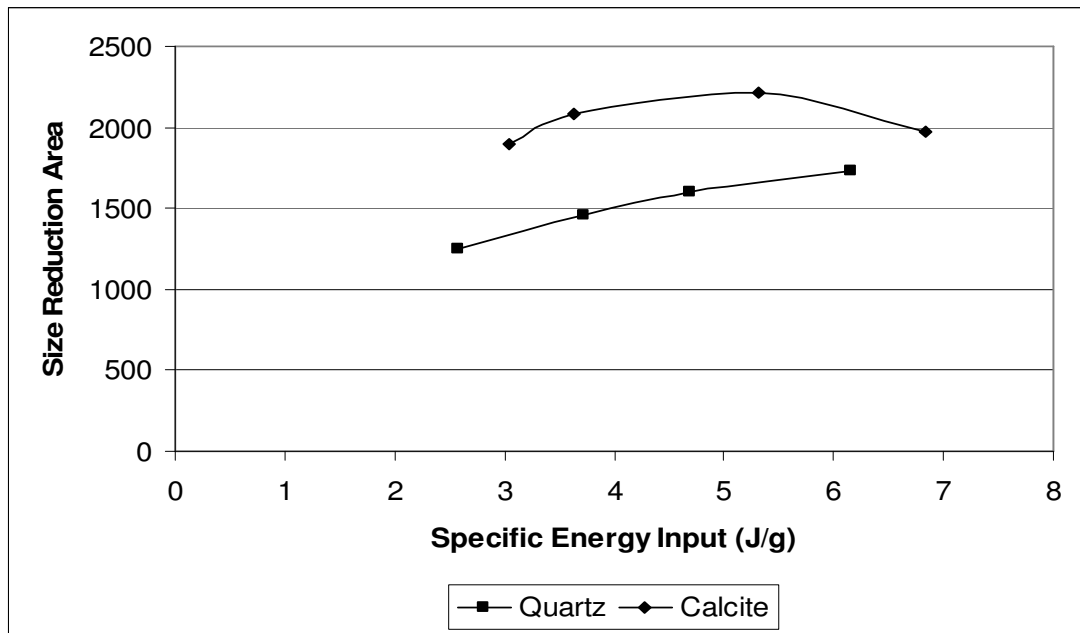
Figure 76: Comparison of size reduction areas for quartz and calcite samples having distribution moduli of 0.7 to evaluate the energy utilization
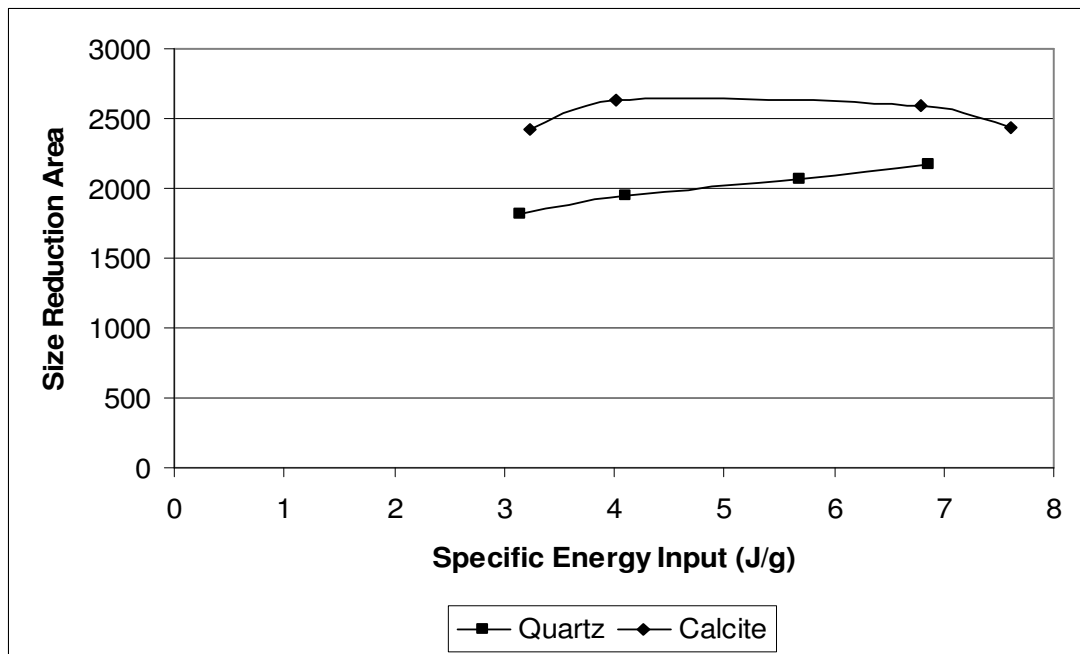
Figure 77: Comparison of size reduction areas for quartz and calcite samples having distribution moduli of 0.7 to evaluate the energy utilization

4.7 Resistance of Particulate Solids to Size Reduction

Bond (1961) stated that single-particle grindability index can be described as the resistance of solid to size reduction which can be measured by the specific energy required to overcome it. With the help of Equation1, the reciprocal of the slope "j" was calculated and the resistance of solid to size reduction in piston-die-press set-up was found. Although the breakage mechanism of piston-die-press is not single-particle breakage, the method is applied to see the differences in resistances for different size fractions and samples (quartz and calcite). Consequently, it is obvious that the resistance of quartz samples to size reduction is higher than that of calcite samples at different size ranges, due to its higher hardness value.

With the help of the data obtained from reduction ratio graphs, Figure 78 can be drawn and it can be concluded that the resistance of solid increases with decreasing particle size for all particle size ranges defined before.
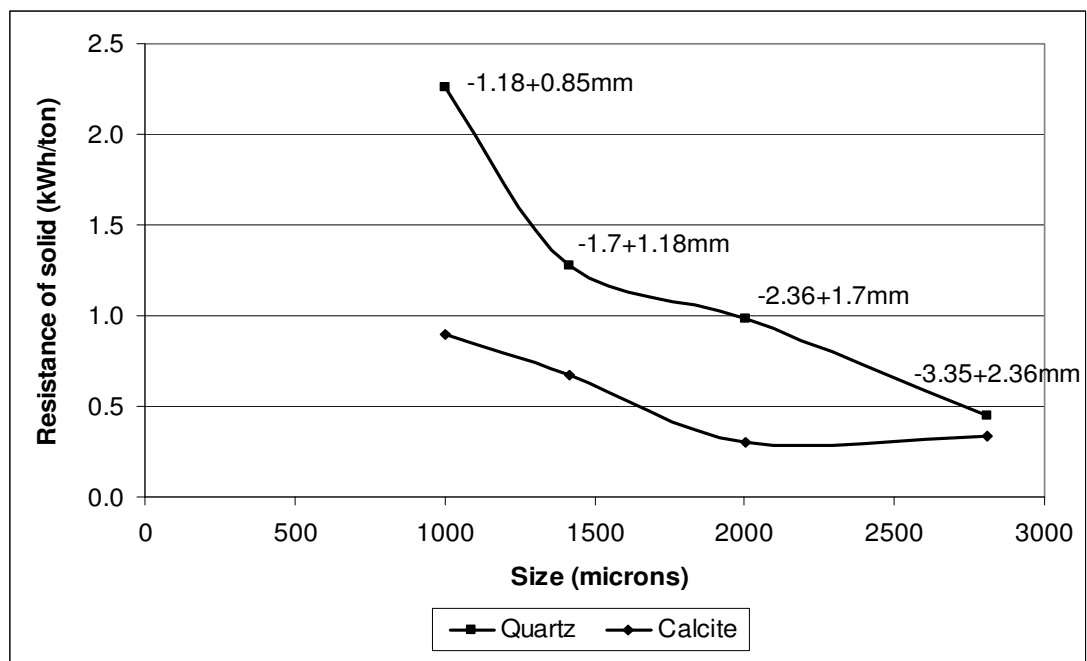
Figure 78: Resistances of narrow-range size fractions of quartz and calcite to size reduction in die-piston press.

4.8 t-curves

In order to describe the product size distribution of the breakage particles during single particle breakage tests, Sahoo et al. (2004) used t-curves which are the family of size distribution curves. The parameter t_{50} defined as the cumulative percentage passing of a characteristic size, which is $1/50^{th}$ of the geometric mean size of the particle. Similarly, the cumulative percentages passing of the parameters $t_{1.4}$, t_2, t_5, t_{10}, t_{25} and t_{100} are determined from the breakage products passing against the different range of sieve sizes. The parameters $t_{1.4}$ and t_2 represent the coarser region of the size distribution curves, while t_{100} describes the finer region. Hence the parameter t_{50} was suitable as global representation of the individual size distribution data and it was obtained from quartz and calcite samples with four different particle sizes and three different particle size distributed samples at five different particle bed pressures.

The size distribution parameter t_{50} has a linear relationship with the specific energy input as illustrated in Figure 79 and 80, for quartz and calcite. The amount of t_{50} is increasing with the increasing particle size, and this means that the production of fines is higher at coarser particle sizes in piston-die-press.
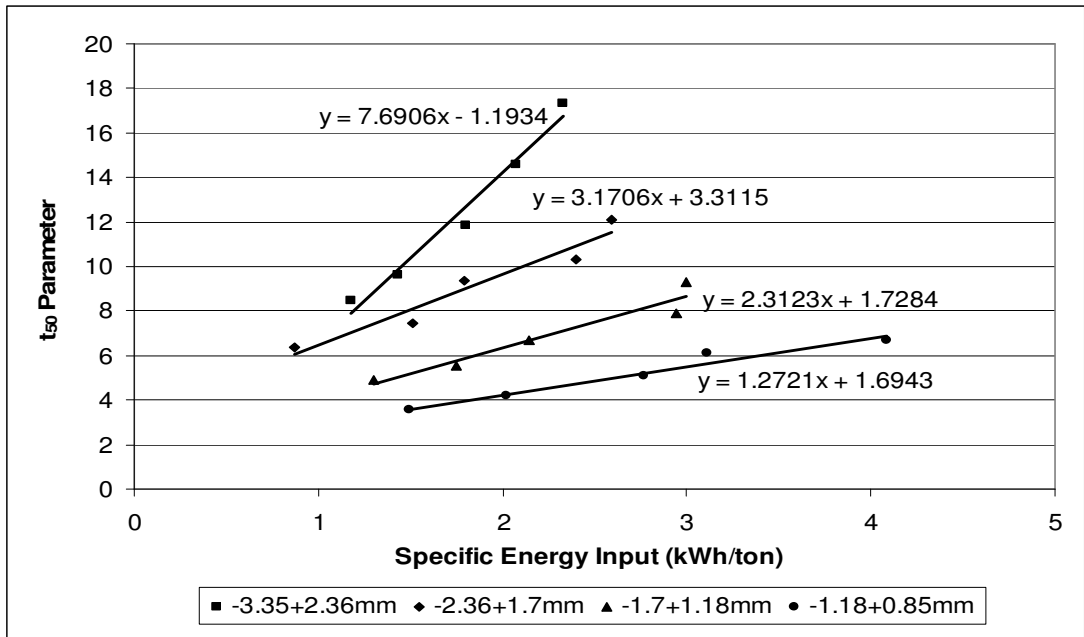
Figure 79: t_{50} parameter vs. specific energy input for different sizes of quartz samples
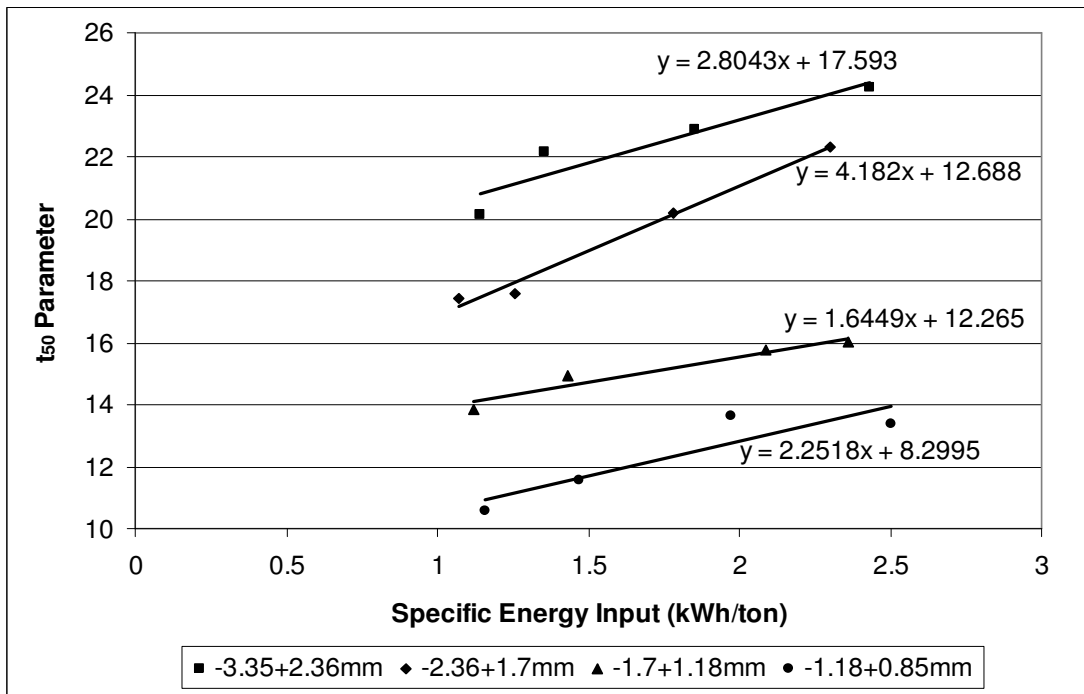
Figure 80: t_{50} parameter vs. specific energy input for different sizes of calcite samples

Furthermore, t_{10} values were calculated to develop an ore-specific relationship between energy input and size reduction (Hawkings and Manlapig, 2006). t_{10} values are plotted against their corresponding specific energy values (Ecs) to form a decaying exponential curve (Figures 81 and 82), and the slope at its origin is equal to AxB from Equation 7:

$$t_{10} = A(1 - e^{-BEcs})$$ .... (7)

The parameters "A" and "B" were calculated by using a Software program SPSS 11.5 for Windows with the method of non-linear regression (Appendix E). "A" and "B" were calculated both for quartz and calcite at all size fractions as illustrated in Table 7.

Table 7: Parameters "A" and "B", calculated by using t_{10} and specific energy input values of quartz and calcite samples at different particle sizes

Particle Size	-3.35+2.36mm		-2.36+1.7mm		-1.7+1.18mm		-1.18+0.85mm	
Parameters	A	B	A	B	A	B	A	B
Quartz	49.93	0.80	36.96	1.31	36.31	0.68	35.61	0.39
Calcite	50.67	1.78	51.37	1.53	49.03	1.60	47.75	1.49

"AxB" is a measure of a material's breakage at low energy inputs (Hawkings and Manlapig, 2006). Calcite, which is softer than quartz, has steeper gradients than quartz. 3.35+2.36mm calcite has the highest amount of "AxB", among other particle sizes which means its amount of breakage at specified energies is the highest. According to Figures 81 and 82, it can be concluded that the t_{10} value increases with increasing particle size. Calcite has higher t_{10} values when compared with quartz for all particles sizes, probably the softness of the sample effects the breakage results.
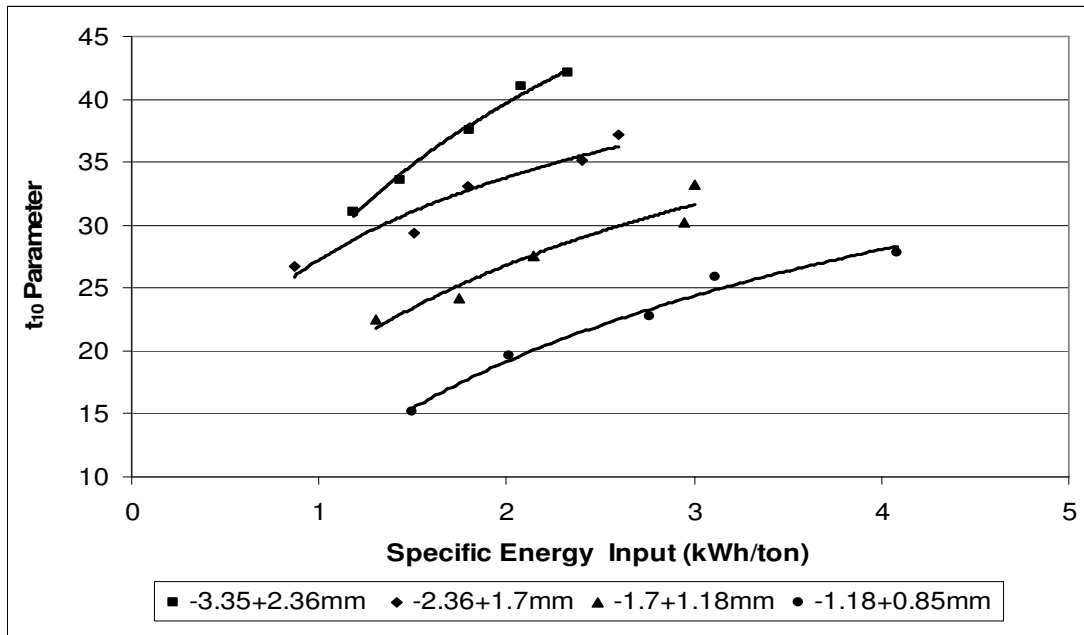
Figure 81: t_{10} parameter vs. specific energy input for different sizes of quartz samples
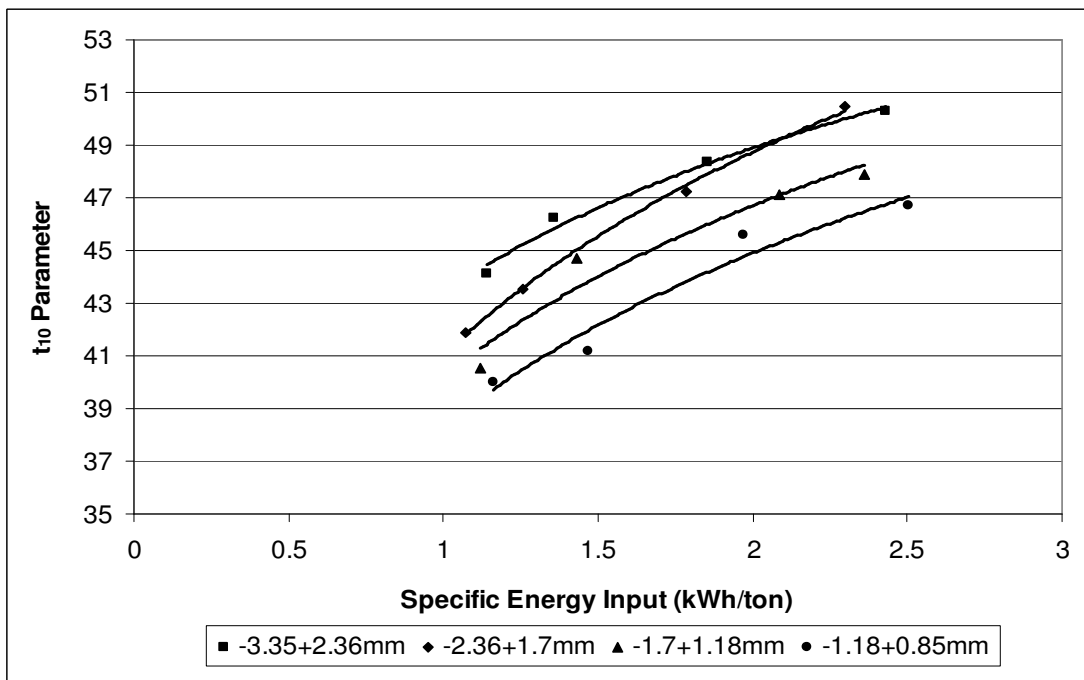
Figure 82: t_{10} parameter vs. specific energy input for different sizes of calcite samples

CHAPTER 5

CONCLUSIONS

Several experiments were conducted to investigate the principles of laboratory-scale particle bed comminution and the following conclusions can be drawn from this study.

- When product particle size distribution graphs of quartz and calcite are compared for distribution moduli of m=0.5; m=0.7 and m=0.9; it can be observed that higher amounts of fines are obtained in calcite samples. Also, at all narrow-range size fractions calcite samples have higher amounts of fines than those of quartz.

- Die-piston press product size distribution is normalisable leading to self-similar grinding curves. Indeed, for a given material, one master curve appears appropriate to describe the entire product size distribution function. To a large extent, self-similarity appears to be preserved. However, some deviations from self-similarity were observed at coarser product sizes. In addition, at low specific comminution energies self-similarity may not be preserved.

- Same magnitudes of pressures result in different specific energy inputs for quartz and calcite samples. When compared with quartz, calcite absorbs lower amounts of specific energy at all distribution moduli for all pressures. Lower pressures can be applied on calcite samples which also result in approximately the same amount of breakage with quartz samples, expending lower specific energies especially for coarse particle sizes, which means that comminution of softer sample (calcite) is more efficient in terms of energy usage.

- Specific energy input increases with increasing pressure both for quartz and calcite samples. It can generally be concluded that specific energy absorption increases with decreasing particle size; implying that fine particles are more resistant to comminution than coarser ones. For size-distributed feeds, specific energy input increases in the following order: m=0.5, m=0.7 and m=0.9. Distribution modulus of 0.9 has the highest specific energy absorption, and its reduction ratios are the highest among others.

- The compressibility of the soft mineral (calcite) in terms of the solid fraction is significantly greater than that of hard material (quartz) at all size fractions despite the fact that the energy absorption by the harder materials is considerably more.

- For distributed feed particle sizes, it can be concluded that only m=0.9 modulus gives higher amounts of reduction ratio below 1.7 kWh/ton specific energy level when compared with narrow-range size fraction samples, for calcite sample. Accordingly, coarse narrow-range size fraction (-3.35+2.36mm) gives high reduction ratios by using less energy; however, m=0.9 has higher reduction ratios at low specific energies (below 1.6 kWh/ton) than -3.35+2.36mm, especially for the harder material quartz. In addition, the quartz sample with m=0.7 gives higher reduction ratios than particle sizes of -1.7+1.18mm and -1.18+0.85mm at all energy levels.

  Energy utilization increases with decreasing porosity and m=0.5 distribution moduli samples have minimum porosity among other distribution moduli samples; however, the amount of excess fine particles in the mixture cause retardation of grinding kinetics which results in small amounts of reduction ratios and also causes excess energy consumption.

- Comparing the size fraction percentages of quartz and calcite in the product it is stated that the breakage is more effective on calcite samples since the fine size fraction amounts are higher than that of quartz at the end of comminution.

Although the amount of size reduction is higher in m=0.9 modulus quartz sample, the amount of -53+38µm size fraction in the mixture is not as much as in m=0.5 and m=0.7 moduli. Consequently, for the pressures greater than 260 MPa m=0.7 modulus results in much finer sizes at the end of comminution and followed by m=0.5 and m=0.9 moduli for quartz samples. Till 212 MPa, m=0.9 modulus of calcite has the highest amount of -53+38µm size fraction, followed by m=0.7 and m=0.5 moduli, respectively.

- The amount of size reduction achieved can also be computed by size reduction curves in addition to calculating the reduction ratios. Size reduction curves were drawn for distributed feed particle sizes and the highest reduction areas were obtained at distribution modulus of m=0.9 for quartz and calcite (acceleration of grinding kinetics).

- Distribution modulus of 0.9 has the highest size reduction area when compared with others, approximately at the same specific energy inputs for quartz and calcite samples. However, the amount of breakage is higher in calcite samples at all distribution moduli and the breakage of calcite is more energy-efficient than quartz, approximately at the same specific energy inputs

- The parameter t_{50} was suitable as global representation of the individual size distribution data and it was obtained from quartz and calcite samples with four different particle sizes at five different particle bed pressures. As a result, a linear relationship between the size distribution parameter t_{50} and specific comminution energy is achieved. Furthermore, t_{10} values were calculated to develop an ore-specific relationship between energy input and size reduction. According to t_{10} calculations, -3.35+2.36mm calcite has the highest amount of breakage at specified energies among other narrow-range particle sizes.

REFERENCES

Aziz, A., and Schönert, K., Einzelkomzerkleinerung und Gutbettbeanspruchung von Zementklinker-fraktionen, *Zement-Kalk-Gips,* 1980, **5**, 213-218.

Bazin, C., and Hodouin, D., A Graphical Method to Assess Size Reduction by Grinding, *Transactions of the Institution of Mining and Metallurgy, Section C*, *Mineral Processing and Extractive Metallurgy*, 2004, **113**, 97.

Bond, F.C., Crushing and Grinding Calculations, *British Chemical Engineering,* 1961, **6**, 378-385 and 543-548.

Clarke, A.J., and Wills, B.A., Enhancement of Cassiterite Liberation by High Pressure Roller Comminution, *Minerals Engineering*, 1989, 2, 259–262.

Fuerstenau, D.W., et. al., Comparison of Energy Consumption in the Breakage of Single Particles in a Rigidly Mounted Roll Mill with Ball Mill Grinding, *International Journal of Mineral Processing*, 1990, **28**, 109-125.

Fuerstenau, D.W., Shukla, A., and Kapur, P.C., Energy Consumption and Product Size Distributions in Choke-Fed High-Compression Roll Mills, *International Journal of Mineral Processing*, 1991, **32**, 59–79.

Fuerstenau, D.W., Kapur, P.C., and Gutsche, O., Comminution of Minerals in a Laboratory-Sized, Choke-Fed, High Pressure Roll Mill, XVIII Int. Minerals Processing Congress, Sydney, 1993, 175-180.

Fuerstenau, D.W., and Kapur, P.C., A New Approach to Assessing the Grindability of Solids and the Energy Efficiency of Grinding Mills, *Minerals and Metallurgical Processing*, 1994, 210-214.

Fuerstenau, D.W., De, A., Diao, J., and Kapur, P.C., Fine Grinding of Coal in a Two-Stage High-Pressure Roll Mill/Ball Mill Hybrid Mode. Kawatra, S.K. (Ed.), *High Efficiency Coal Preparation. Society of Mining Engineers*, Littleton, 1995, 295–305.

Fuerstenau, D.W., Gutsche, 0., and Kapur, P.C., Confined Particle Bed Comminution Under Compressive Loads, *Int. J. Miner. Process*, 1996, **44-45**, 521-537.

Fuerstenau, D.W., Kapur, P.C., and De A., Modeling Breakage Kinetics in Various Dry Comminution Systems, *KONA*, 2003, **21,** 126.

Gutsche, O., and Fuerstenau, D. W., Fracture Kinetics of Particle Bed Comminution-Ramifications for Fines Production and Mill Optimization, *Powder Technology,* 1999, **105**, 113-118.

Hanisch, J., and Schubert, H., Zum Einfluss der Beanspruchungsgeometrie auf das Zerkleinerungsverhalten von nicht allseitig begrenzten Kornschichten, *Neue Bergbautech*, 1982, **12**, 646– 649.

Hawkings, R., and Manlapig, E., Determining an Appearance Function for Compressive Bed Breakage, 23rd International Mineral Processing Congress, Sept 3-8, Congress Proceedings, Volmue II, 2006, 185-186.

Herbst, J.A., and Fuerstenau, D.W., The Zero Order Production of Fine Sizes in Comminution and its Implication in Simulation, *Transactions American Institute Mining Engineering*, 1968, **241**, 538-549.

Holland M., Seebach M. and Ranze W., Variable Speed Drives for Roller Presses, *For Presentation at the IEEE/PCA Cement Industry Technical Conference*, 1997, Hershey, PA.

Kapur, P.C., Self-preserving Size Spectra of Comminuted Particles, *Chemical Engineering Science,* 1972, **27**, 425-431.

Kapur, P.C., Modeling of Tumbling Mill Batch Process, *Crushing and Grinding Process Handbook*, Prasher, C.L., Ed., John Wiley and Sons, U.K., 1987, 323-363.

Lim, I.L., Voigt, W., Weller, K.R., Product Size Distribution and Energy Expenditure in Grinding Minerals and Ores in High Pressure Rolls, *International Journal of Mineral Processing*, 1996, **44-45,** 549-557.

Lo, Y. C., Kientzler, P. J., and King, R. P., Fundamentals and System Research in Ultrasonic Comminution Technology, *XVIII International Mineral Proceedings of Congress*, Sydney, 1993, 145–153.

Mehra, S.M., Slag Grinding by Roller Press Major Issues, *International Journal of Mineral Processing*, 1998, **53**, 87-97.

Norgate, T.N. and Weller, K.R., Selection and Operation of High Pressure Grinding Rolls Circuits for Minimum Energy Consumption, *Mineral Engineering*, 1994, **7**, 1253-1267.

Rumpf, H., Physical Aspects of Comminution and New Formulation of a Law of Comminution, *Powder Technology*, 1973, **7**, 145-159.

Rumpf, H., *Particle Technology*, English Edition, Translated by Bull, F.A., Chapman Hall, 1990, 103-114.

Sahoo, R.K., Weedon, D.M., and Roach D., Single Particle Breakage Tests of Gladstone Port Authority's Coal by a Twin Pendulum Apparatus, *Advanced Powder Technology,* 2004, **15,** 263-280.

Schönert, K., *Zement-Kalk-Gips*, 1979, **32,** 1.

Schönert, K., and Flügel, F., Zerkleinerung spro¨der Minerale im hochkomprimierten Gutbett, Prepr, *European Symposium of Particle Technology*, Dechema, Frankfurt, 1980, **A**, 82– 95.

Schönert, K., Limits of Energy Saving in Milling, *First World Congress on Particle Technology*, Nurenberg, Reprints, Part II, Comminution, 1986, 1-21.

Schönert, K., A First Survey of Grinding with High-Compression Roller Mills, *International Journal of Mineral Processing*, 1988, **22**, 401– 412.

Schönert, K., Mueller, F., and Schwechten, D., Kompression und Energie Absorption bei der Gutbett-Zerkleinerung, *Zement-Kalk-Gips*, 1990, **2**, 65-70.

Schwarz, S., and Seebach, M., Optimization of Grinding in High Pressure Grinding Rolls and Downstream Ball Mills, *In 7th European Symposium on Comminution*, Preprints, Ljubljana,. 1990, **2**, 777–788.

Schwechten, K., and Milburn, G.H., Experiences in Dry Grinding with High Compression Roller Mills for End Product Quality Below 20 microns, *Minerals Engineering*, 1990, **3**, 23-34.

Seebach, H.M., Neumann, E.W and Lohnherr, L, State-of-the-Art of Energy Efficient Grinding Systems, *Zement-Kalk-Gips*, 1996, **49**, No 2, 61-67.

Stairmand, C.J., The Energy Efficiency of Milling Processes, *4th European Comminution Symposium*, Dechema Monographien, 1975, **79**, 1-17.

Tavares, L.M., Particle Weakening in High Pressure Roll Grinding, *Minerals Engineering*, 2005, **18**, 651-657.

Vázquez-Favela, J., *The Effect of Grinding Mode on the Efficiency of Dolomite Comminution*, M.S. Dissertation, University of California at Berkeley, 1995, 51.

APPENDIX A

PREPARATION OF SIZE-DISTRIBUTED FEED SAMPLES

Gates-Gaudin-Schuhmann distribution function was used for some samples in the experiments. Table A.1 shows the required amounts of samples from each size range. For the experiments those were held in this theses, in Equation 2 $d_{max} = 3350\mu m$.

Table A. 1: Amounts of samples required from each size range to prepare size-distributed feed samples

Size (microns)	m=0.5		m=0.7		m=0.9	
	Amount of sample		Amount of sample		Amount of sample	
	W(d)	95g	W(d)	95g	W(d)	95g
-3350+2360	0.161	15.295	0.218	20.71	0.27	25.65
-2360+1700	0.127	12.065	0.16	15.2	0.187	17.765
-1700+1180	0.119	11.305	0.14	13.3	0.152	14.44
-1180+850	0.089	8.455	0.099	9.405	0.1	9.5
-850+600	0.081	7.695	0.083	7.885	0.078	7.41
-600+425	0.067	6.365	0.064	6.08	0.057	5.415
-425+300	0.057	5.415	0.051	4.845	0.042	3.99
-300+212	0.047	4.465	0.04	3.8	0.031	2.945
-212+150	0.04	3.8	0.031	2.945	0.022	2.09
-150+106	0.034	3.23	0.025	2.375	0.016	1.52
-106+75	0.028	2.66	0,.019	1.805	0.012	1.14
-75+53	0.024	2.28	0.015	1.425	0.009	0.855
-53+38	0.019	1.805	0.012	1.14	0.006	0.57
-38	0.107	10.165	0.043	4.085	0.018	1.71

APPENDIX B

EXPERIMENTAL DATA OF COMMINUTION IN PISTON-DIE-PRESS

Table B. 1: Experimental details about quartz samples

\ Name of the Sample: QUARTZ						
Experiment Number	Particle Size (mm)	Force (kN)	Pressure (Mpa)	Initial Bed Height, hi (mm)	Final Bed Height, hf (mm)	Specific Energy Input (J/g)
1	-3.35+2.36	300	106.16	20.6	13.39	4.2514
2	-3.35+2.36	400	141.54	20	13.42	5.1614
3	-3.35+2.36	600	212.31	20.3	13.89	6.4806
4	-3.35+2.36	800	283.09	20.6	13.75	7.4702
5	-3.35+2.36	1000	353.86	20.7	13.87	8.3878
6	-2.36+1.70	300	106.16	21.8	16.30	3.1223
7	-2.36+1.70	400	141.54	21.7	14.44	5.4358
8	-2.36+1.70	600	212.31	21.9	14.46	6.4589
9	-2.36+1.70	800	283.09	21.9	14.17	8.6343
10	-2.36+1.70	1000	353.86	22	14.11	9.3458
11	-1.70+1.18	300	106.16	22	14.33	4.6914
12	-1.70+1.18	400	141.54	22	13.80	6.2861
13	-1.70+1.18	600	212.31	22.3	15.00	7.7266
14	-1.70+1.18	800	283.09	22.2	14.47	10.5999
15	-1.70+1.18	1000	353.86	21.75	13.84	10.7976
16	-1.18+0.85	300	106.16	22.4	15.50	5.3830
17	-1.18+0.85	400	141.54	22.9	15.39	7.2634
18	-1.18+0.85	600	212.31	21.9	14.19	9.9636
19	-1.18+0.85	800	283.09	22	14.70	9.6666
20	-1.18+0.85	1000	353.86	22.7	14.18	14.7050
26	m=0.7	300	106.16	21.4	17.31	2.5715
27	m=0.7	400	141.54	21.5	16.84	3.7219
28	m=0.7	600	212.31	21	16.60	4.6849
29	m=0.7	800	283.09	21.25	16.43	6.9344
30	m=0.7	1000	353.86	21	15.91	8.3307

Table B.1 (continued): Experimental details about quartz samples

31	m=0.5	300	106.16	20.5	17.16	2.2505
32	m=0.5	400	141.54	20.6	17.57	3.1059
33	m=0.5	600	212.31	20.4	16.64	4.3219
34	m=0.5	800	283.09	20.9	17.07	5.0154
35	m=0.5	1000	353.86	20.8	16.69	7.1488
36	m=0.9	300	106.16	22	17	3.1462
37	m=0.9	400	141.54	23	17.54	4.1044
38	m=0.9	600	212.31	22.6	16.77	5.6954
39	m=0.9	800	283.09	22.9	17.13	6.8627
40	m=0.9	1000	353.86	22.3	16.51	8.2607

Experiments 21-25 were cancelled due to experimental errors.

Table B. 2: Experimental details about calcite sample

Name of the Sample: CALCITE						
Experiment Number	Particle Size (mm)	Force (kN)	Pressure (Mpa)	Initial Bed Height, hi (mm)	Final Bed Height, hf (mm)	Specific Energy Input (J/g)
1	-3.35+2.36	300	106.16	21	13.61	4.1030
2	-3.35+2.36	400	141.54	21.2	13.53	4.8772
3	-3.35+2.36	600	212.31	21.1	13.09	6.6772
4	-3.35+2.36	800	283.09	21.5	12.65	8.7523
6	-2.36+1.70	300	106.16	21	13.99	3.8529
7	-2.36+1.70	400	141.54	22	14.73	4.5189
8	-2.36+1.70	600	212.31	22.3	14.33	6.4186
9	-2.36+1.70	800	283.09	22.5	13.62	8.2749
11	-1.70+1.18	300	106.16	22.6	15.03	4.0307
12	-1.70+1.18	400	141.54	22.5	14.77	5.1542
13	-1.70+1.18	600	212.31	22.8	14.36	7.5180
14	-1.70+1.18	800	283.09	22	13.59	8.5073
16	-1.18+0.85	300	106.16	22.3	13.88	4.1785
17	-1.18+0.85	400	141.54	22.5	14.39	5.2831
18	-1.18+0.85	600	212.31	22.7	14.09	7.0930
19	-1.18+0.85	800	283.09	23	14.01	9.0175
21	m=0.5	300	106.16	20.2	16.03	2.5045
22	m=0.5	400	141.54	21	16.46	3.1836
23	m=0.5	600	212.31	20.2	15.39	4.7313
24	m=0.5	800	283.09	20.7	15.69	6.2862
26	m=0.7	300	106.16	22	16.21	3.0507
27	m=0.7	400	141.54	21.6	16.03	3.6362
28	m=0.7	600	212.31	21.4	15.64	5.3237
29	m=0.7	800	283.09	21.9	15.69	6.8411
31	m=0.9	300	106.16	23	16.59	3.2267
32	m=0.9	400	141.54	23	16.05	4.0126
33	m=0.9	600	212.31	23	16.16	6.7958
34	m=0.9	800	283.09	22.9	15.94	7.6110

Table B. 3: Experimental details about repeated experiments

|					Initial Bed Height, hi (mm)	Final Bed Height, hf (mm)	Specific Energy Input (J/g)
Exp. Number	Name of the Sample	Particle Size (mm)	Force (kN)	Pressure (Mpa)			
1	Quartz	-3.35+2.36	300	106.16	20.00	13.93	4.5035
2	Quartz	-2.36+1.70	300	106.16	22.00	13.88	4.7166
3	Quartz	-2.36+1.70	600	212.31	22.3	14.21	7.9645
4	Quartz	-1.70+1.18	600	212.31	22.2	14.16	8.7416
5	Quartz	-1.70+1.18	800	283.09	22.2	14.60	8.9341
6	Quartz	-1.18+0.85	800	283.09	22.4	14.57	9.6899
7	Quartz	-1.18+0.85	1000	353.86	22.3	14.69	12.4894
8	Quartz	m=0,9	600	212.31	22.3	17.92	5.5433
9	Quartz	m=0,7	600	212.31	17.4	13.23	6.6786
10	Quartz	m=0,7	800	283.09	17.6	12.40	7.1696
11	Quartz	m=0,7	1000	353.86	17.3	16.29	7.8811
12	Quartz	m=0,5	800	283.09	16.4	13.62	4.8363
13	Calcite	-3.35+2.36	400	141.54	20	12.15	4.9258
14	Calcite	-2.36+1.70	400	141.54	21.8	13.08	4.9300
15	Calcite	-1.70+1.18	600	212.31	21.3	11.93	7.3342
16	Calcite	-1.70+1.18	800	283.09	23	13.57	9.8067
17	Calcite	m=0.9	600	212.31	22.8	13.48	5.7720
18	Quartz	-2.36+1.70	600	212.31	20.7	13.85	6.4113
19	Quartz	-1.18+0.85	800	283.09	22	14.82	8.7572
20	Quartz	m=0,7	800	283.09	18	13.95	6.1652
21	Quartz	m=0,7	1000	353.86	18	14.20	7.2119
22	Calcite	-1.70+1.18	600	212.31	23	14.32	6.7807
23	Calcite	m=0.9	600	212.31	21.9	14.66	6.0222
24	Calcite	-1.70+1.18	800	283.09	23.2	14.03	8.5435

APPENDIX C

FORCE-DISPLACEMENT CURVES AND AREAS
# UNDER THE CURVES

Force-displacement curves are illustrated in this section comparing quartz and calcite samples at same particle sizes and forces. Area under the forward travel of the curve is denoted by A1 in the tables next to the figures. The forward travel of the curve becomes negative during the elastic expansion of the material and the die-piston and the area under this curve is represented by A2 in the tables.

|	Quartz	Calcite
A1	390.59	369.26
A2	71.73	61.53
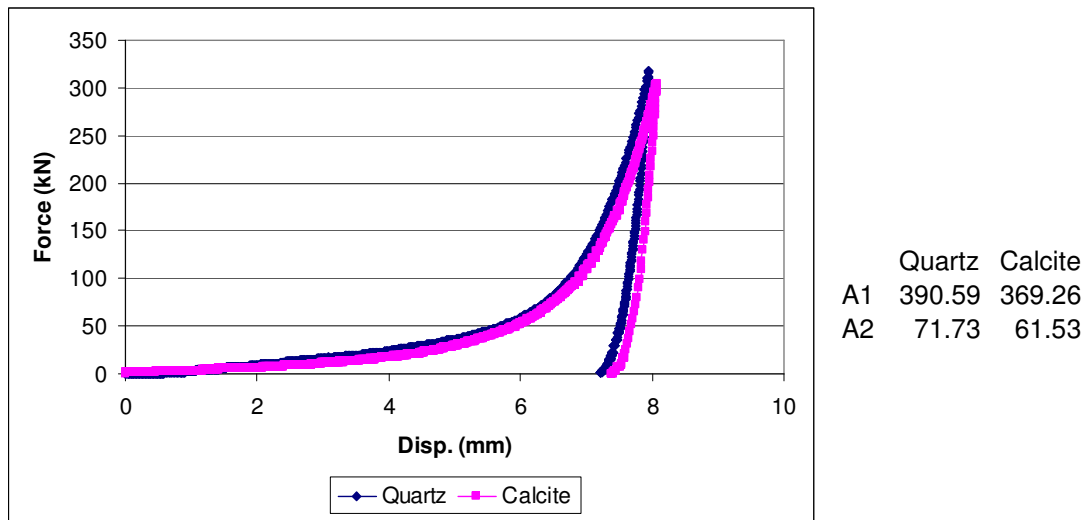
Figure C. 1: -3.35+2.36mm quartz and calcite samples comminuted in die-piston under 300kN force
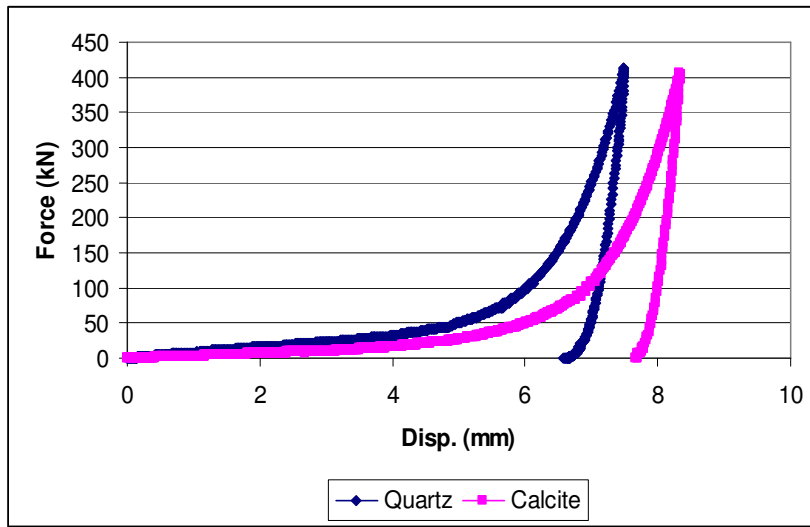
Figure C. 2: -3.35+2.36mm quartz and calcite samples comminuted in die-piston under 400kN force

	Quartz	Calcite
A1	490.90	452.85
A2	103.79	87.06
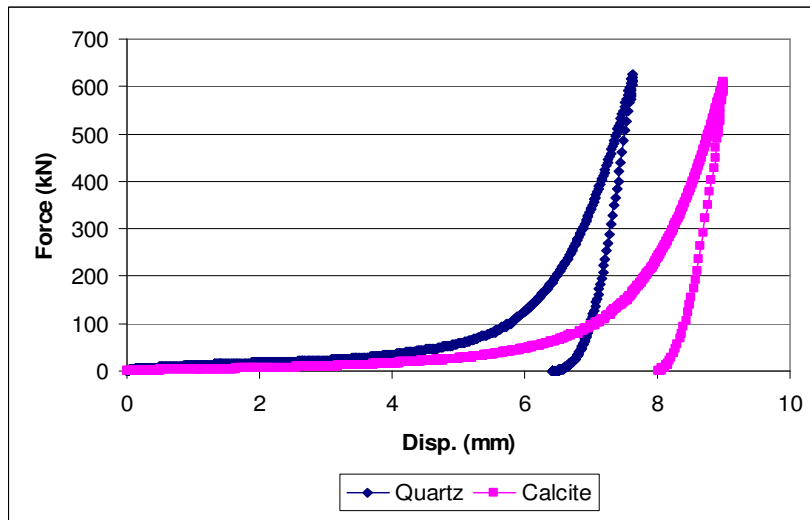
Figure C. 3: -3.35+2.36mm quartz and calcite samples comminuted in die-piston under 600kN force

	Quartz	Calcite
A1	705.33	695.41
A2	219.29	194.62
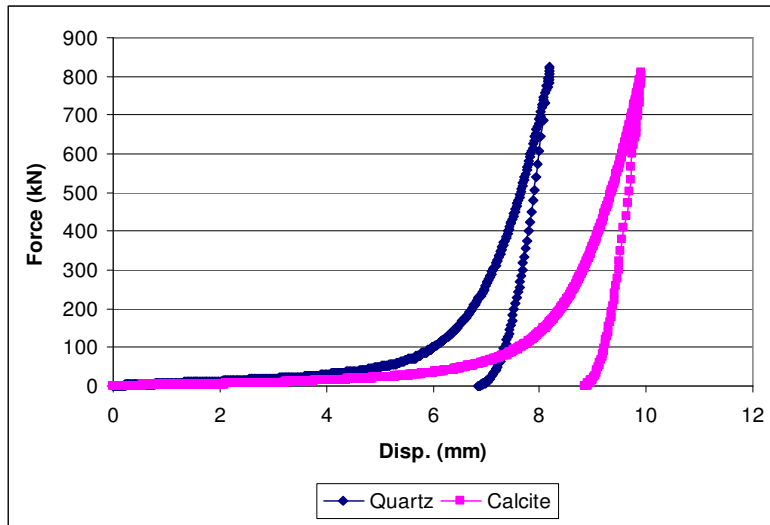
Figure C. 4: -3.35+2.36mm quartz and calcite samples comminuted in die-piston under 800kN force
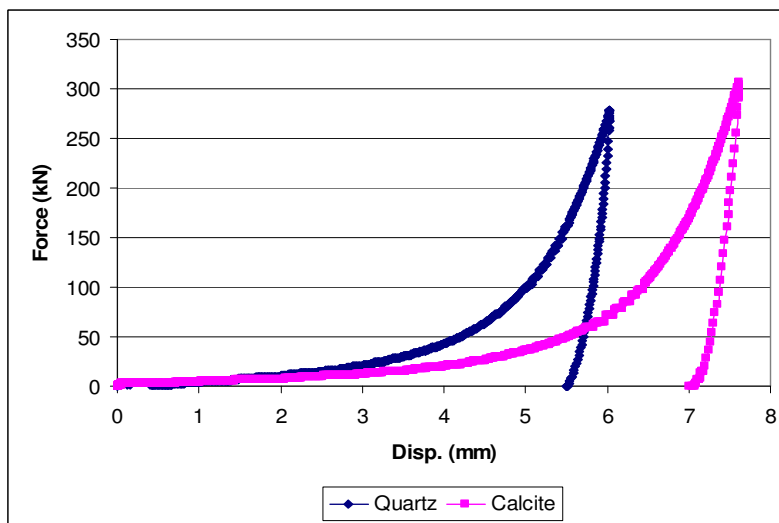
Figure C. 5: -2.36+1.7mm quartz and calcite samples comminuted in die-piston under 300kN force
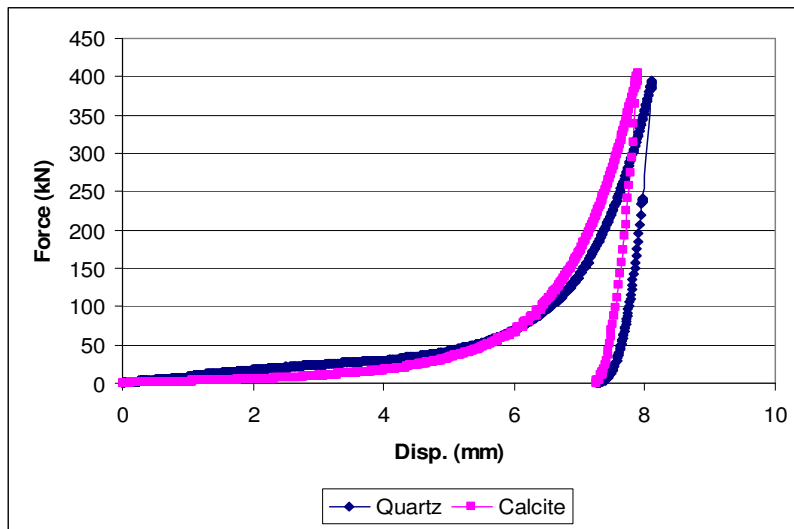
	Quartz	Calcite
A1	526.50	449.85
A2	91.63	88.34

Figure C. 6: -2.36+1.7mm quartz and calcite samples comminuted in die-piston under 400kN force
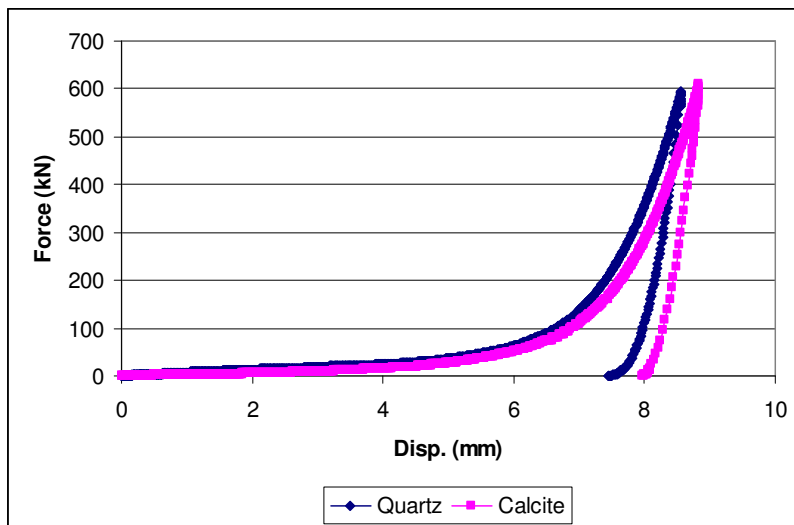
	Quartz	Calcite
A1	711.41	697.20
A2	194.70	183.72

Figure C. 7: -2.36+1.7mm quartz and calcite samples comminuted in die-piston under 600kN force

	Quartz	Calcite
A1	1008.90	956.66
A2	318.17	294.67
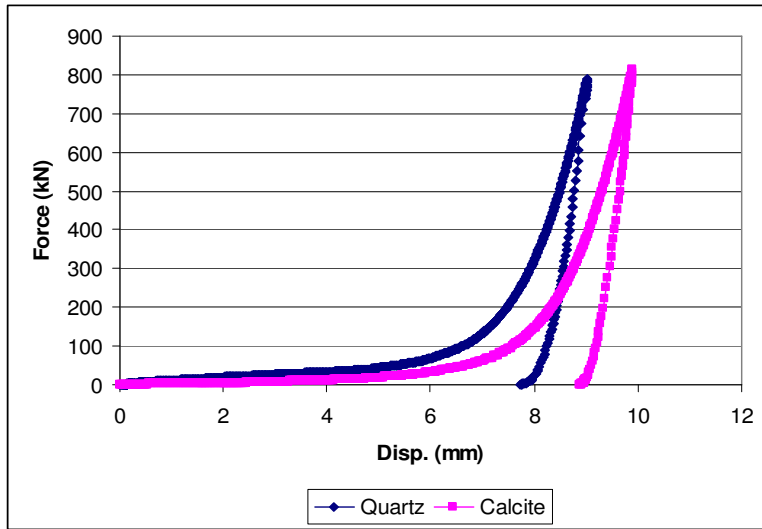
Figure C. 8: -2.36+1.7mm quartz and calcite samples comminuted in die-piston under 800kN force

	Quartz	Calcite
A1	433.38	375.36
A2	58.07	52.91
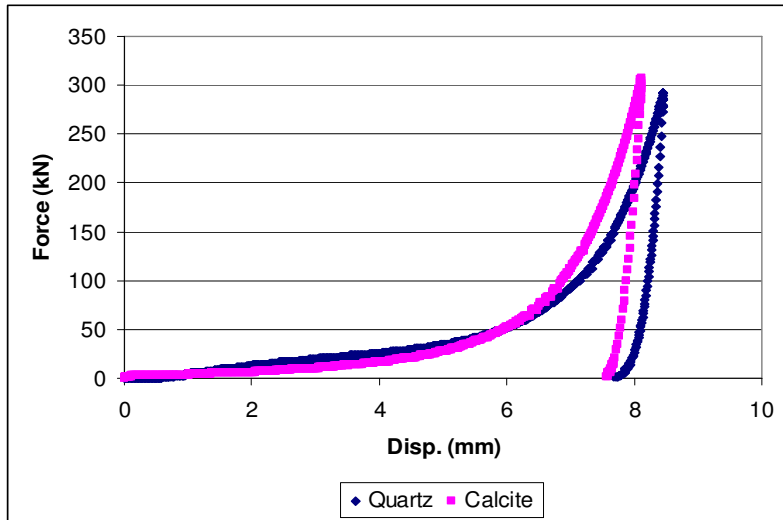
Figure C. 9: -1.7+1.18mm quartz and calcite samples comminuted in die-piston under 300kN force

91

	Quartz	Calcite
A1	598.42	504.67
A2	95.53	92.33
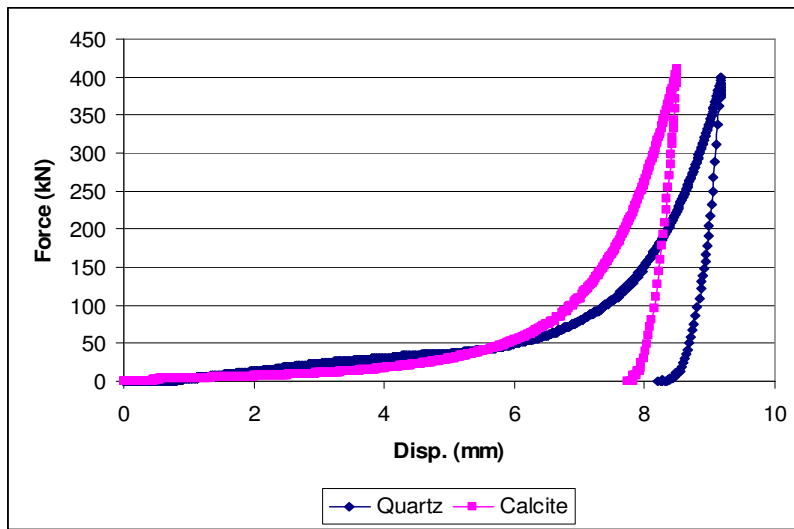
Figure C. 10: -1.7+1.18mm quartz and calcite samples comminuted in die-piston under 400kN force

|	Quartz	Calcite
A1	824.87	781.57
A2	206.75	180.13
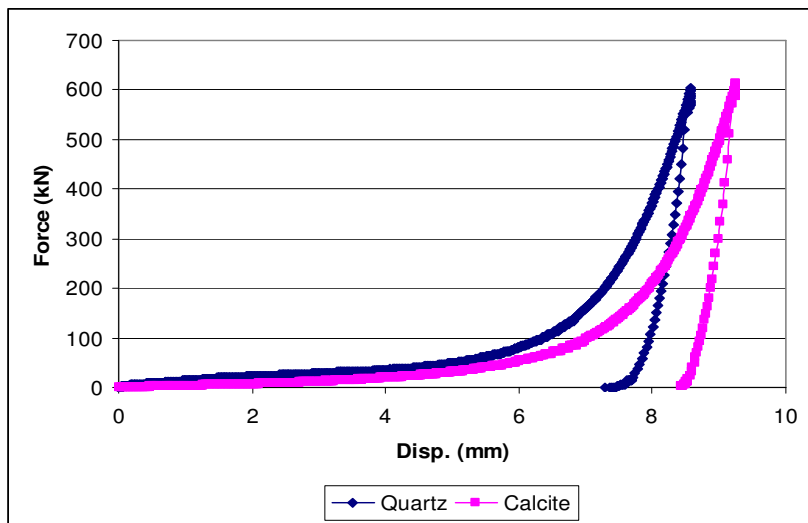
Figure C. 11: -1.7+1.18mm quartz and calcite samples comminuted in die-piston under 600kN force

	Quartz	Calcite
A1	1190.70	993.34
A2	342.75	312.76
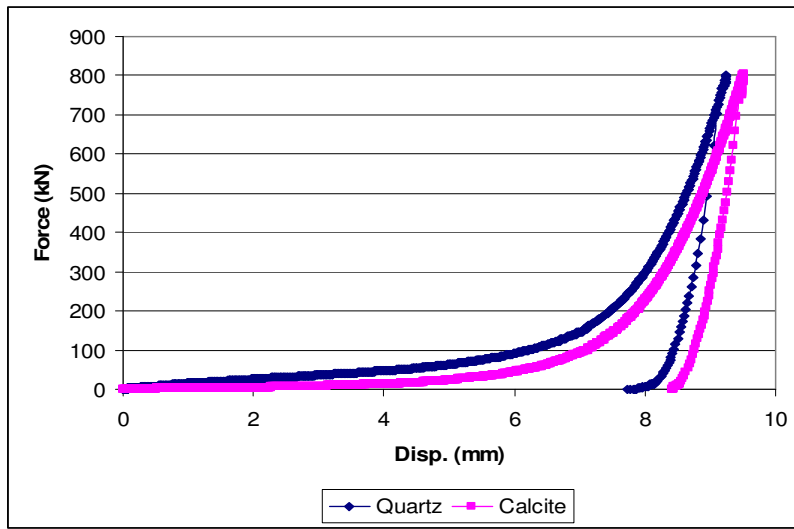
Figure C. 12: -1.7+1.18mm quartz and calcite samples comminuted in die-piston under 800kN force

	Quartz	Calcite
A1	487.80	393.11
A2	57.17	58.83
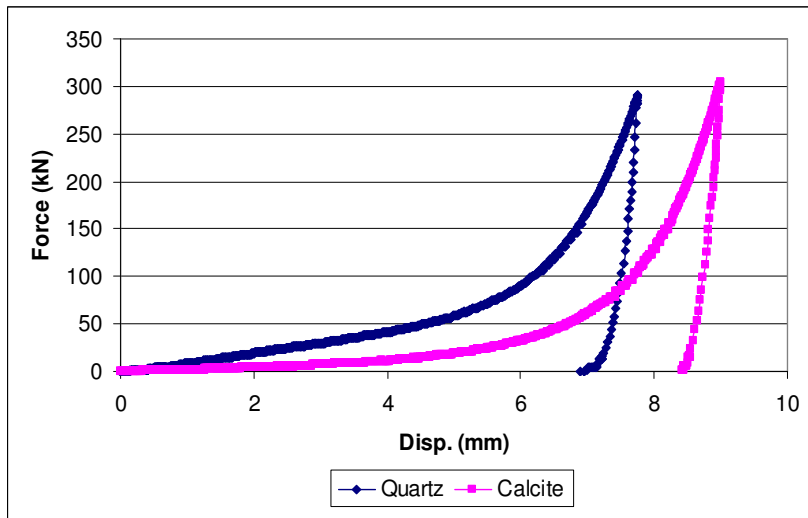
Figure C. 13: -1.18+0.85mm quartz and calcite samples comminuted in die-piston under 300kN force
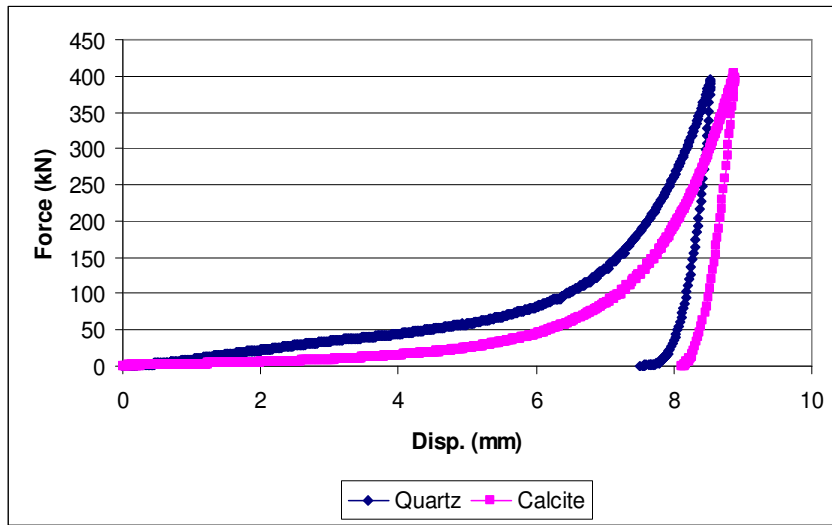
**Figure C. 14:** -1.18+0.85mm quartz and calcite samples comminuted in die-piston under 400kN force
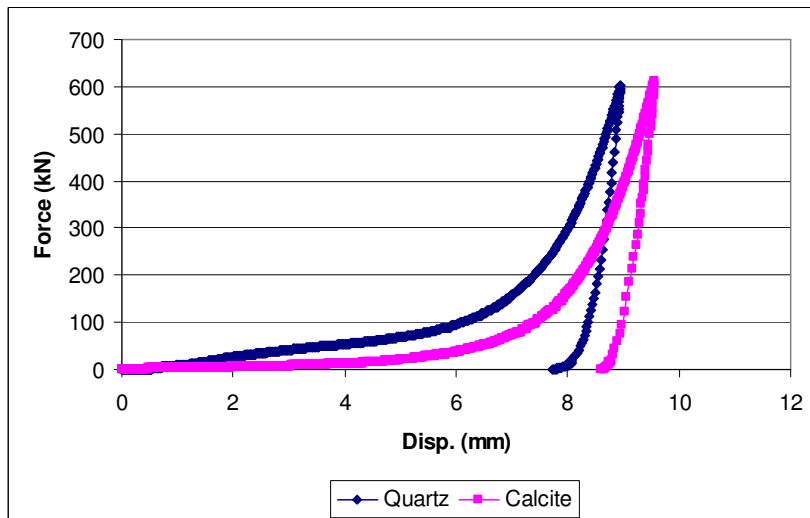

**Figure C. 15:** 1.18+0.85mm quartz and calcite samples comminuted in die-piston under 600kN force
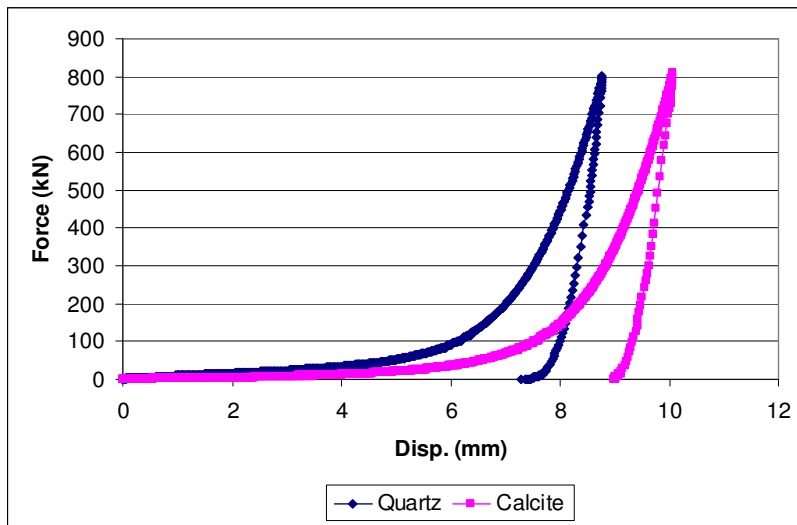
Quartz Calcite
A1 1086.80 1032.80
A2 313.52 311.41

Figure C. 16: 1.18+0.85mm quartz and calcite samples comminuted in die-piston under 800kN force
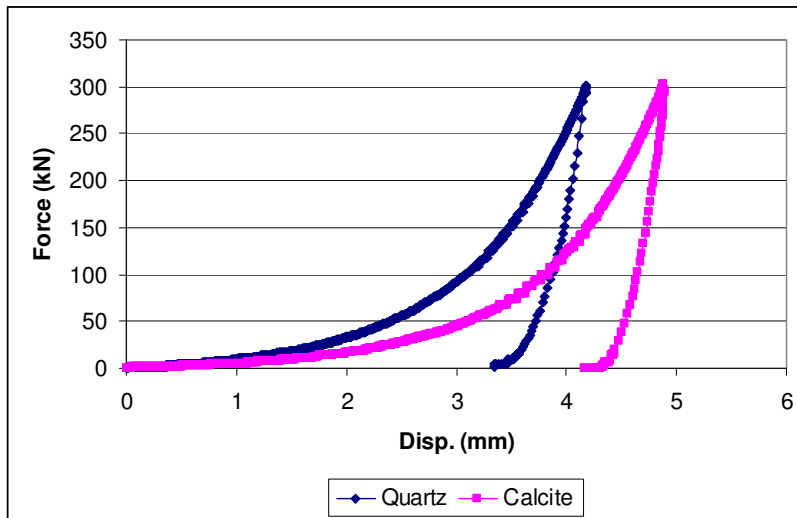
Q C
A1 289.37 293.74
A2 75.57 55.81

Figure C. 17: m=0.5 quartz and calcite samples comminuted in die-piston under 300kN force

	Q	C
A1	410.74	392.95
A2	115.68	90.51
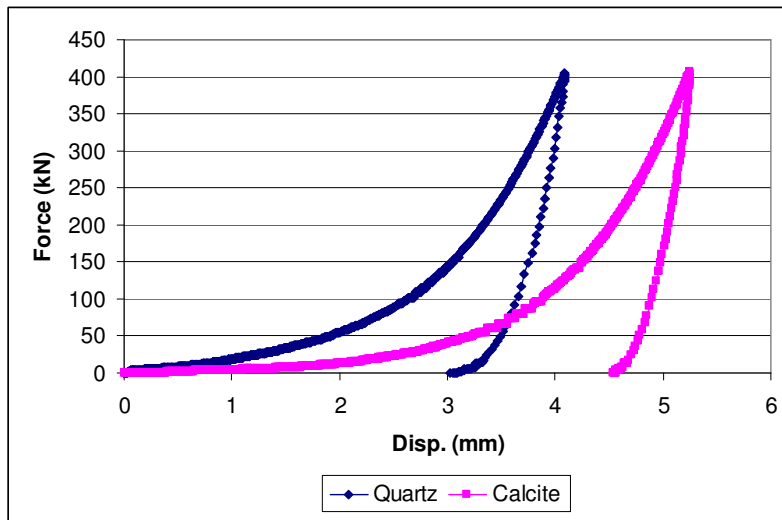
Figure C. 18: m=0.5 quartz and calcite samples comminuted in die-piston under 400kN force

	Q	C
A1	629.41	634.77
A2	218.84	185.30
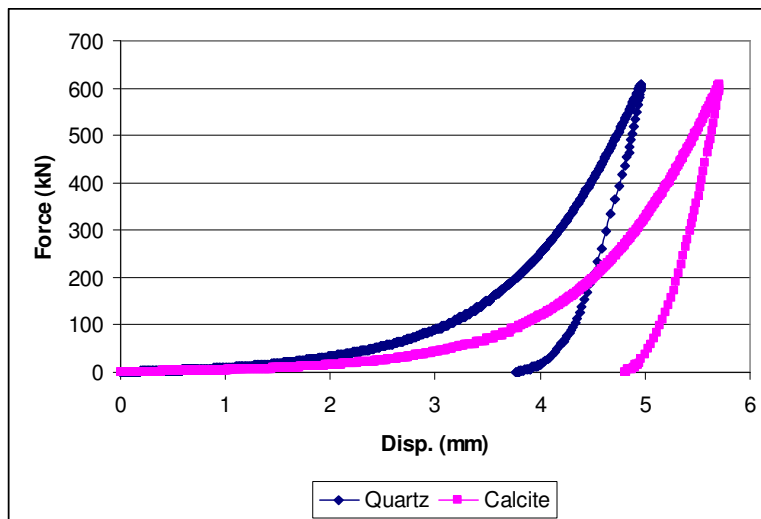
Figure C. 19: m=0.5 quartz and calcite samples comminuted in die-piston under 600kN force

96
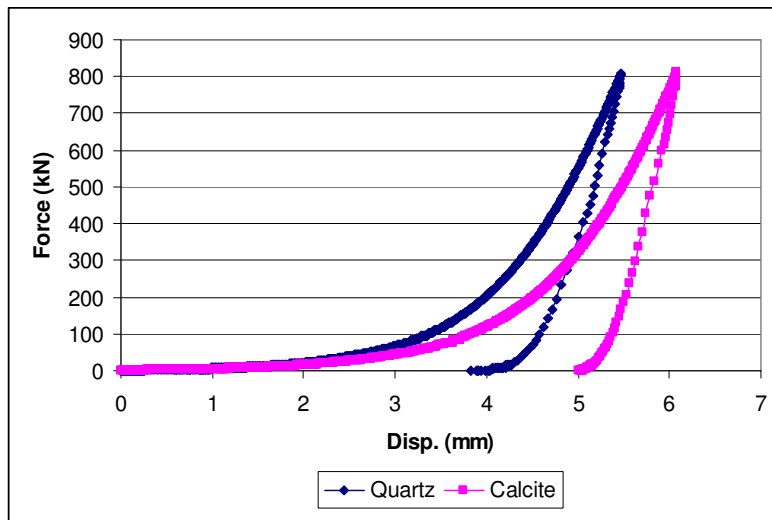
	Q	C
A1	844.75	901.30
A2	368.29	304.11

Figure C. 20: m=0.5 quartz and calcite samples comminuted in die-piston under 800kN force
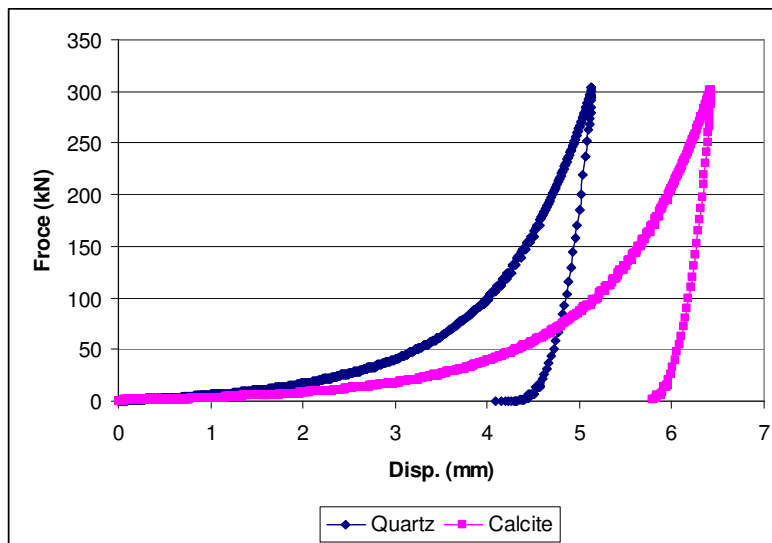
|	Q	C
A1	312.62	346.06
A2	68.33	56.24

Figure C. 21: m=0.7 quartz and calcite samples comminuted in die-piston under 300kN force
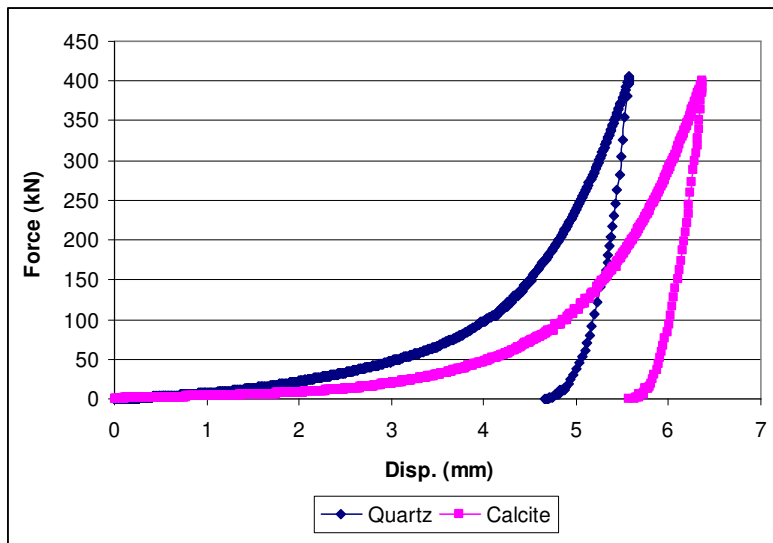
**Figure C. 22:** m=0.7 quartz and calcite samples comminuted in die-piston under 400kN force
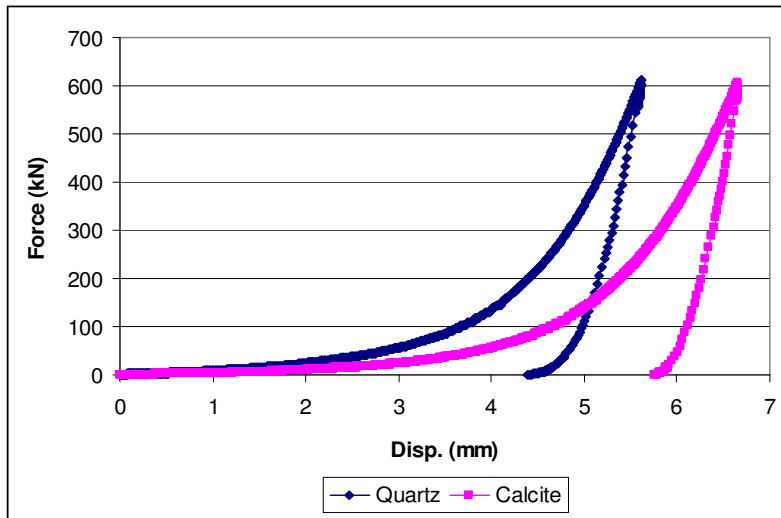
Figure C. 23: m=0.7 quartz and calcite samples comminuted in die-piston under 600kN force
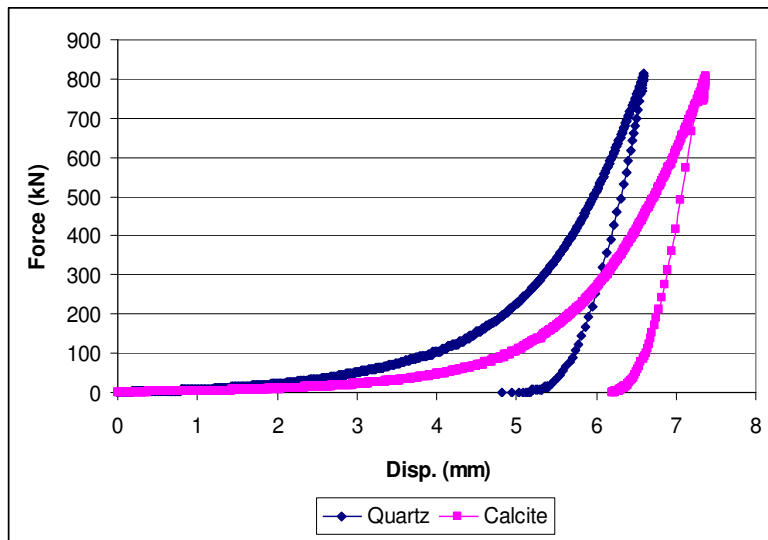
	Q	C
A1	1023.50	990.73
A2	364.78	340.83

Figure C. 24: m=0.7 quartz and calcite samples comminuted in die-piston under 800kN force
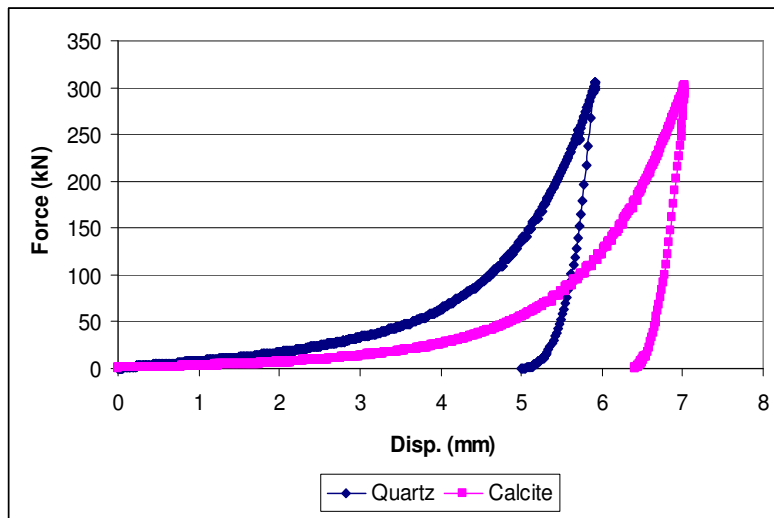
	Q	C
A1	373.21	365.53
A2	74.32	58.99

Figure C. 25: m=0.9 quartz and calcite samples comminuted in die-piston under 300kN force

	Q	C
A1	518.05	468.28
A2	128.13	87.08
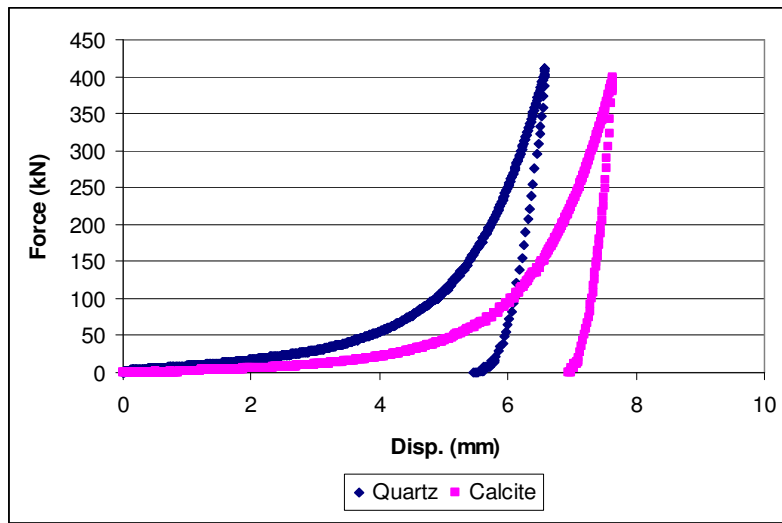
Figure C. 26: m=0.9 quartz and calcite samples comminuted in die-piston under 400kN force

	Q	C
A1	764.53	732.69
A2	223.47	187.08
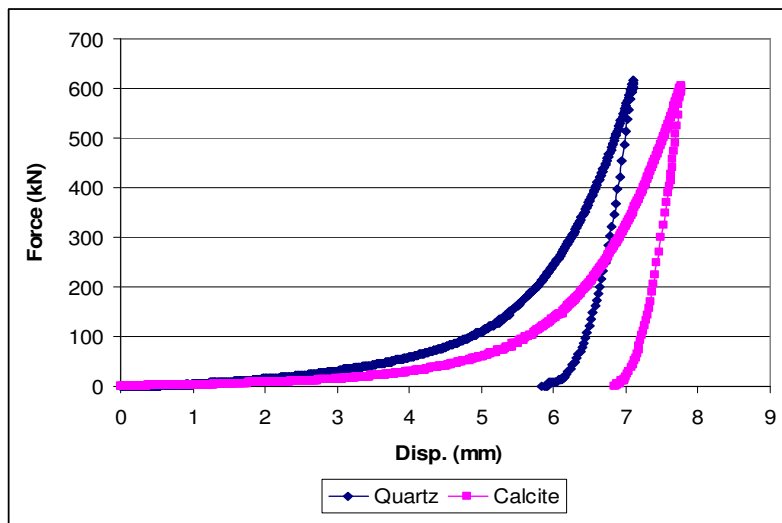
Figure C. 27: m=0.9 quartz and calcite samples comminuted in die-piston under 600kN force
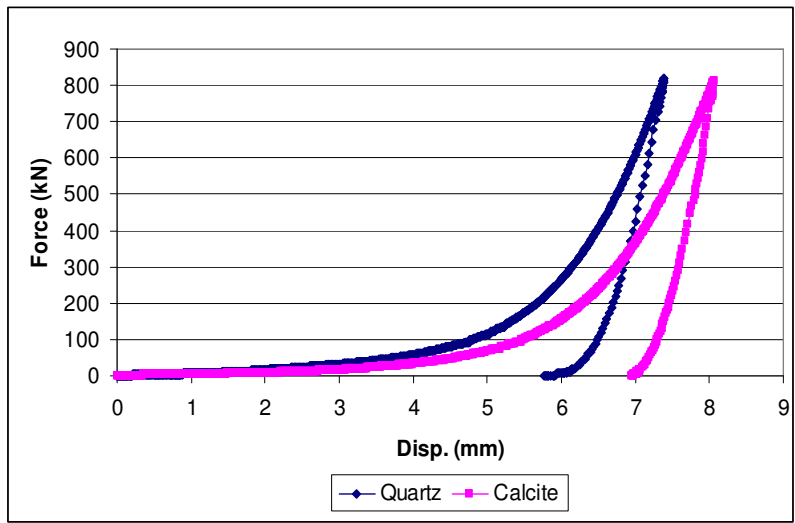
Figure C. 28: m=0.9 quartz and calcite samples comminuted in die-piston under 800kN force

APPENDIX D

## PRODUCT PARTICLE SIZE DISTRIBUTION GRAPHS
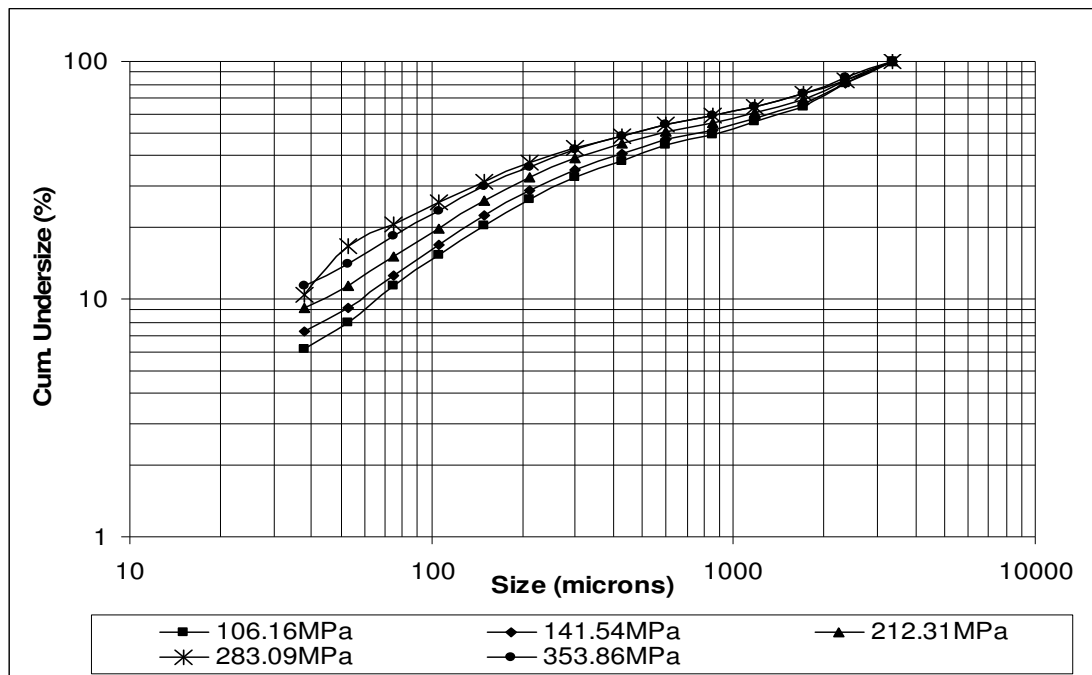
Figure D. 1: Product particle size distribution graph of -3.35+2.36mm quartz sample
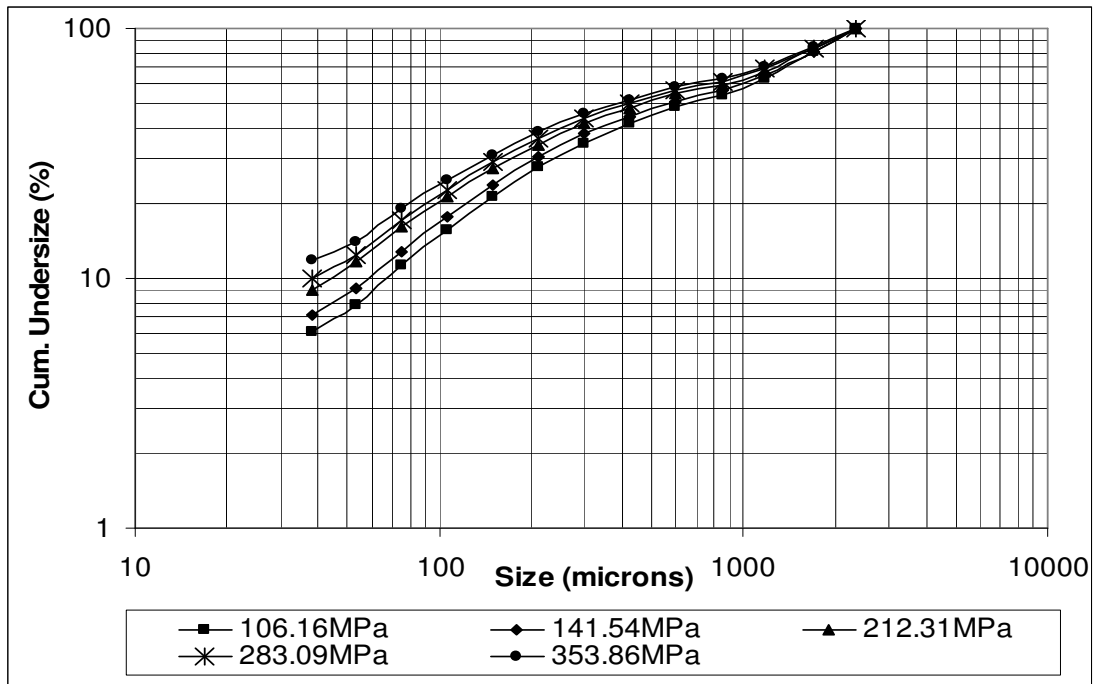
Figure D. 2: Product particle size distribution graph of -2.36+1.7mm quartz sample
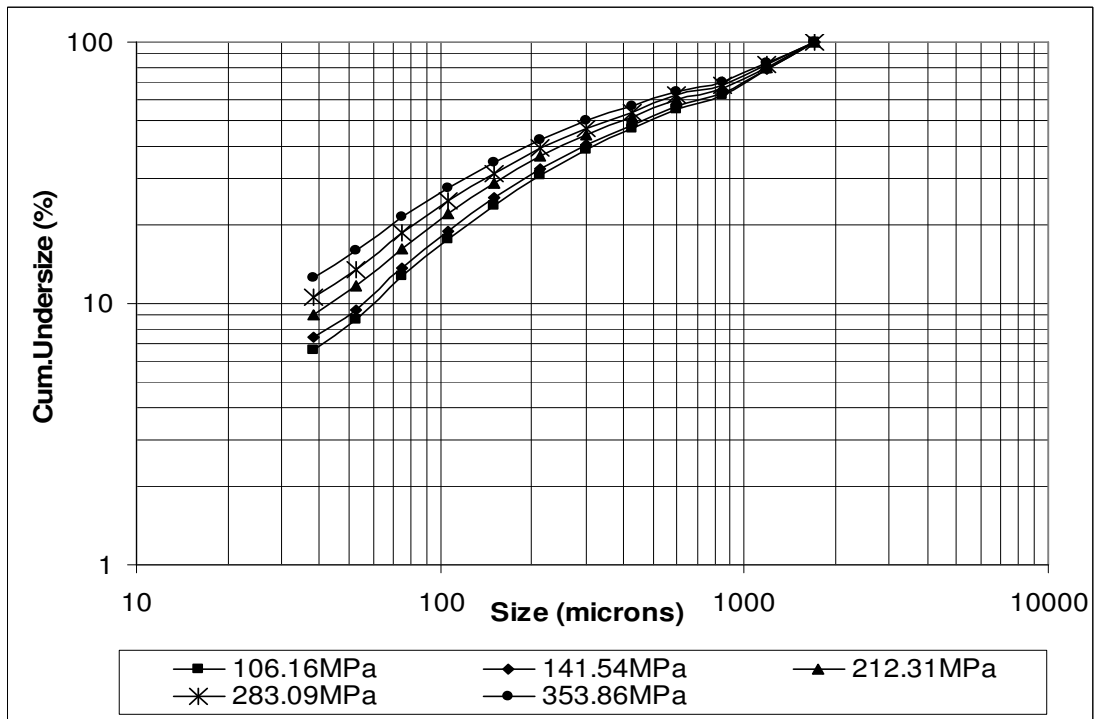
Figure D. 3: Product particle size distribution graph of -1.7+1.18mm quartz sample
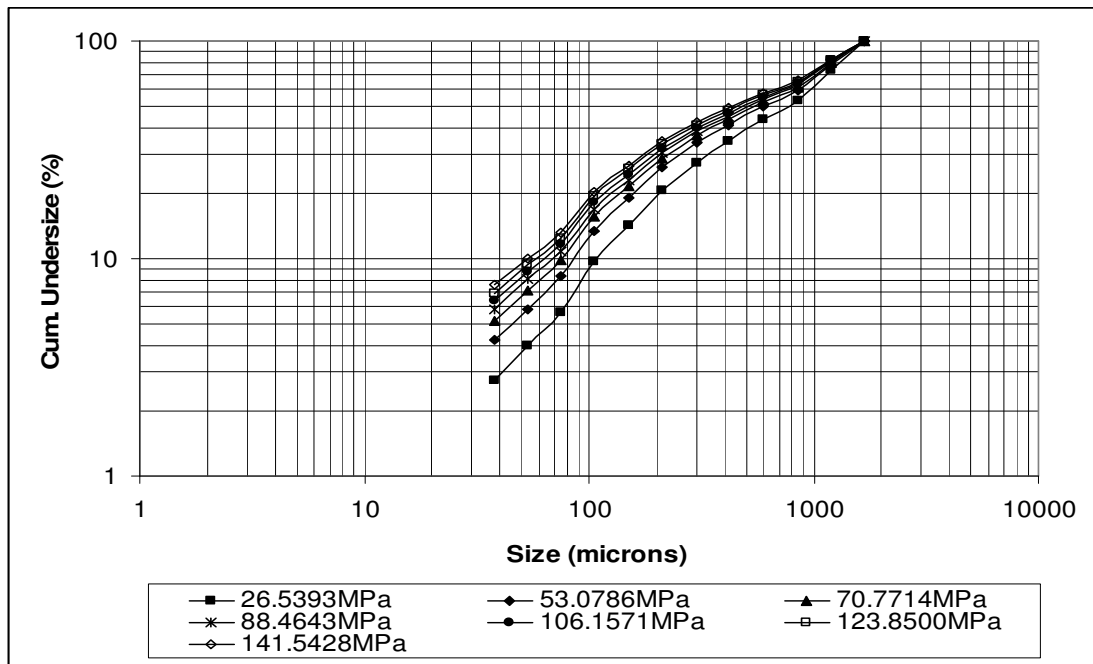
**Figure D. 4:** Product particle size distribution graph of -1.7+1.18mm quartz sample comminuted in MTS Compression Testing Machine
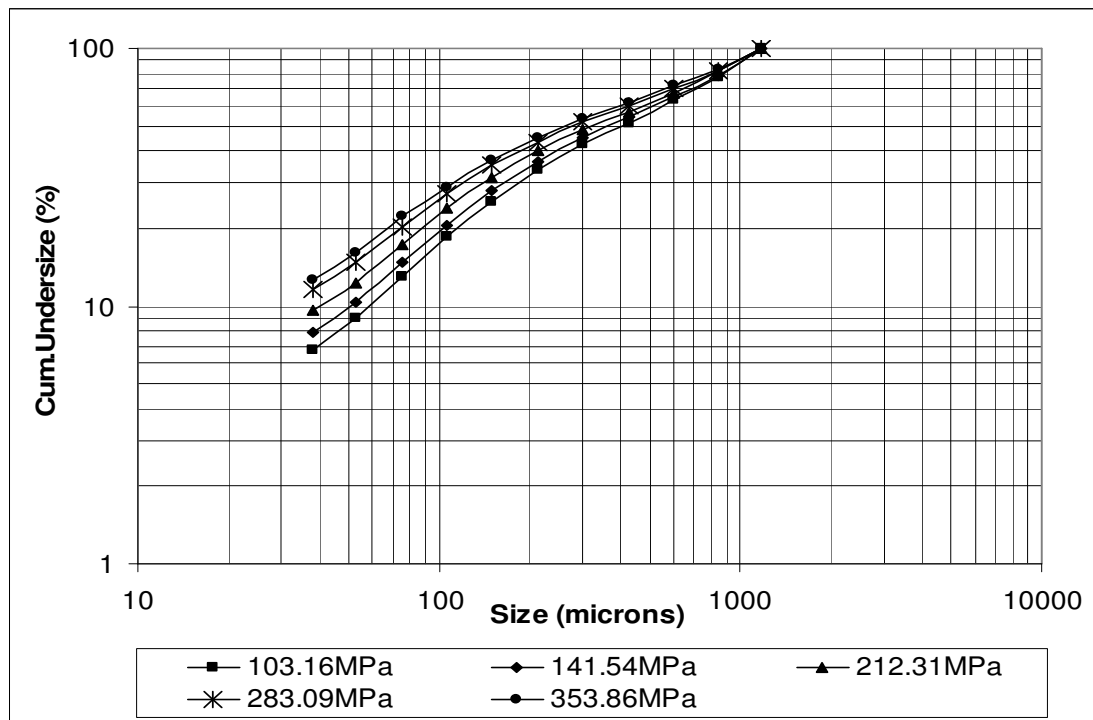
Figure D. 5: Product particle size distribution graph of -1.18+0.85mm quartz sample

104
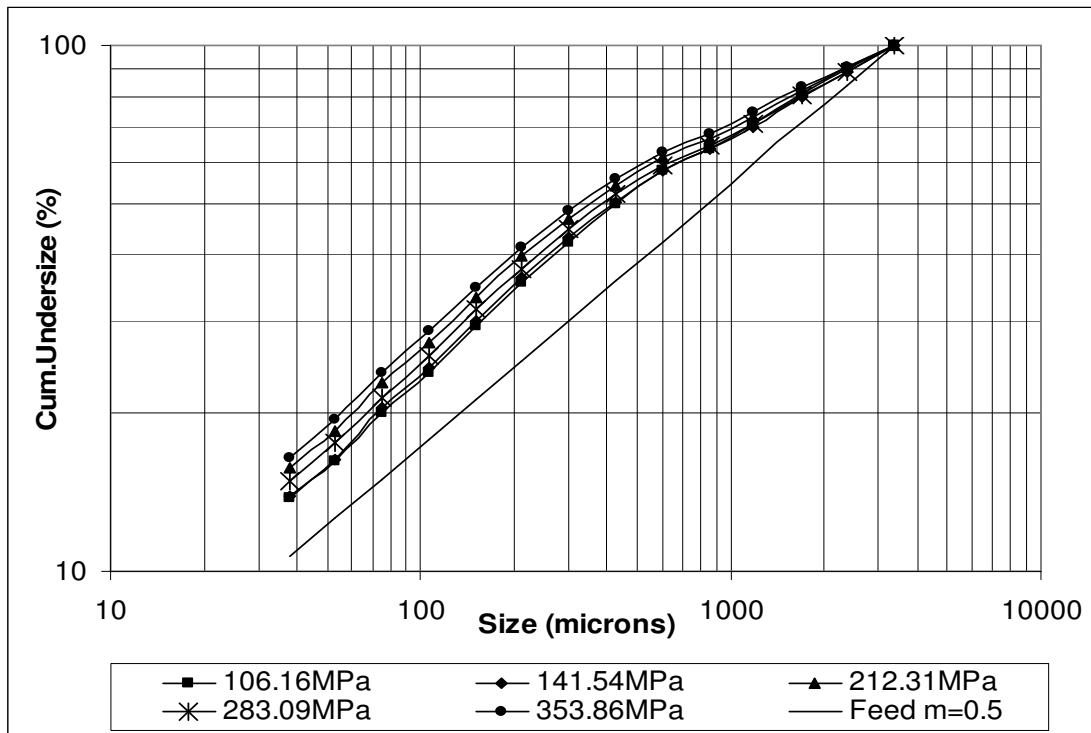
Figure D. 6: Product particle size distribution graph of m=0.5 quartz sample
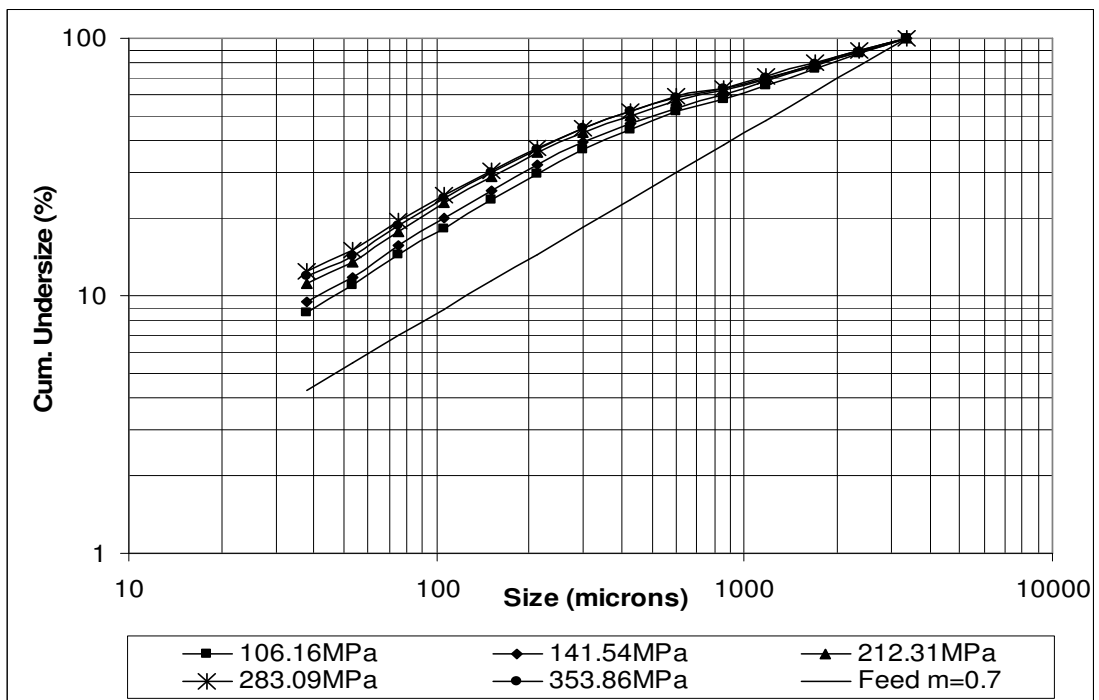
**Figure D. 7:** Product particle size distribution graph of m=0.7 quartz sample
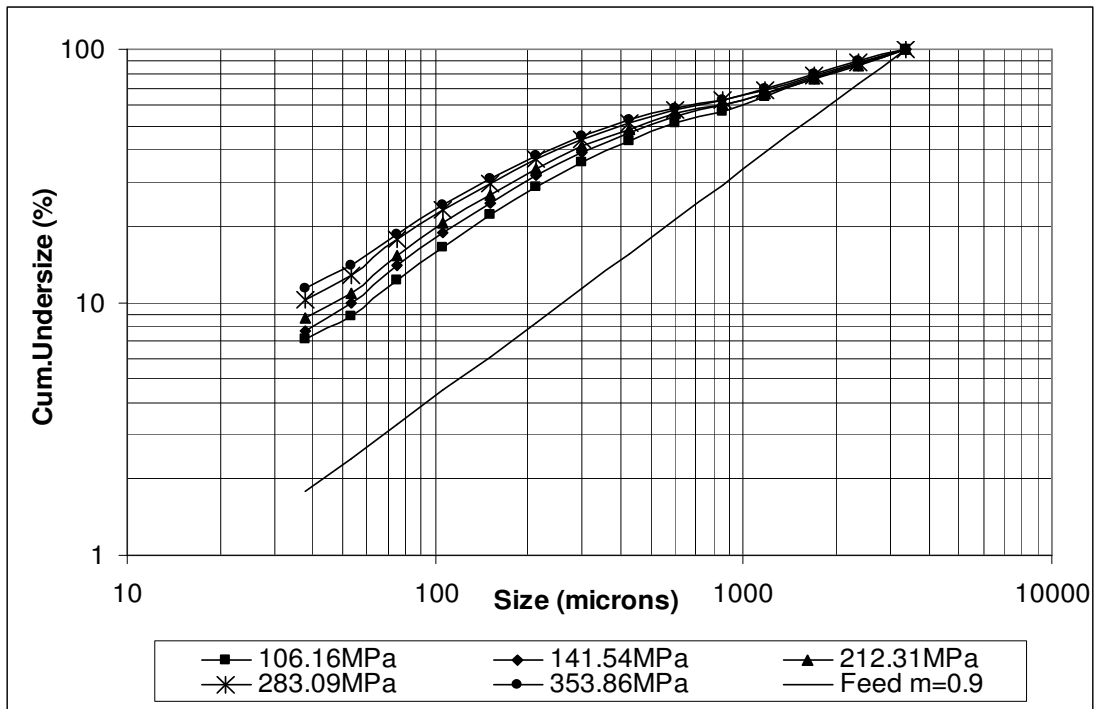
Figure D. 8: Product particle size distribution graph of m=0.9 quartz sample
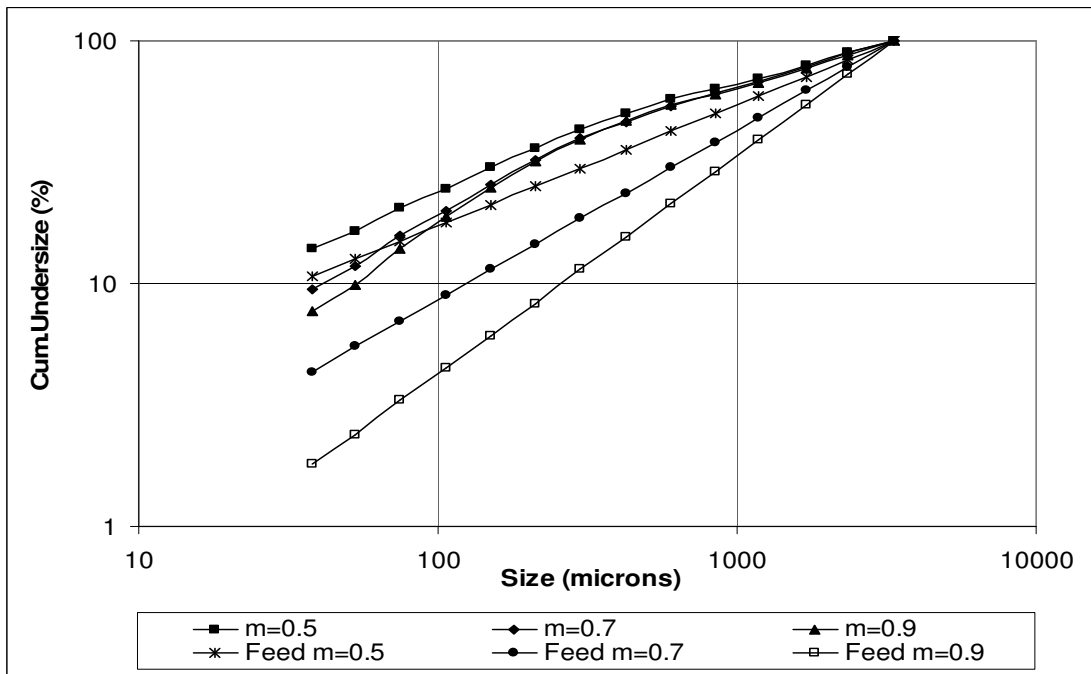

Figure D. 9: Comparison of the areas between ideal moduli lines at 0 pressure and the curves of those moduli, comminuted under 141.54 MPa pressure for quartz samples.
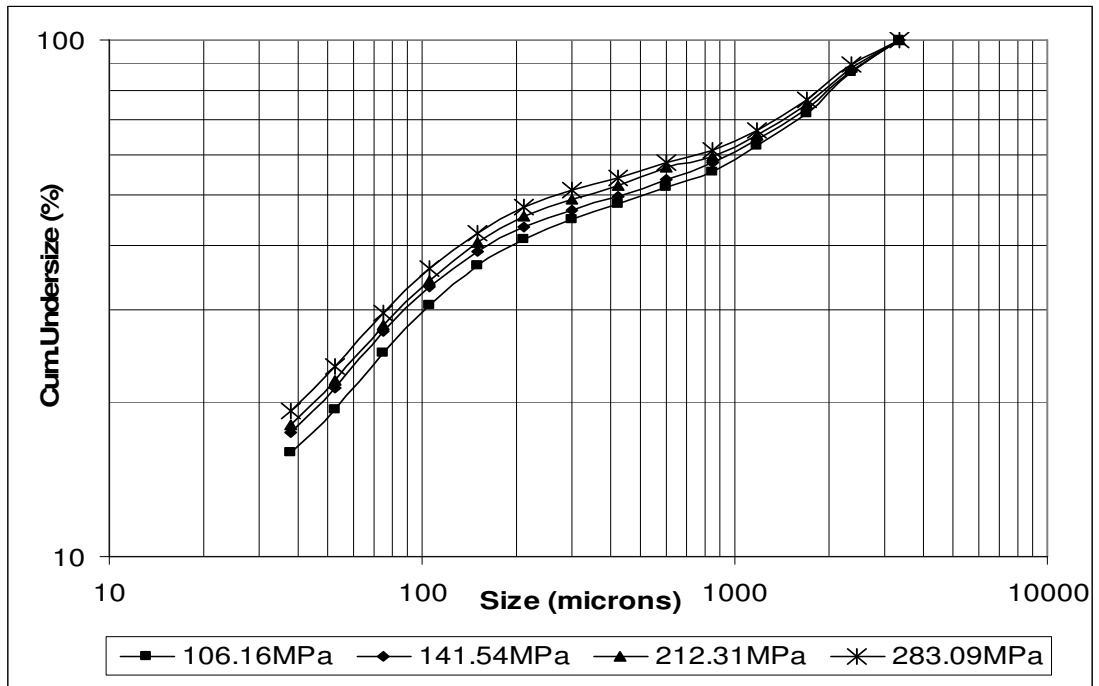
**Figure D. 10:** Product particle size distribution graph of -3.35+2.36mm calcite sample
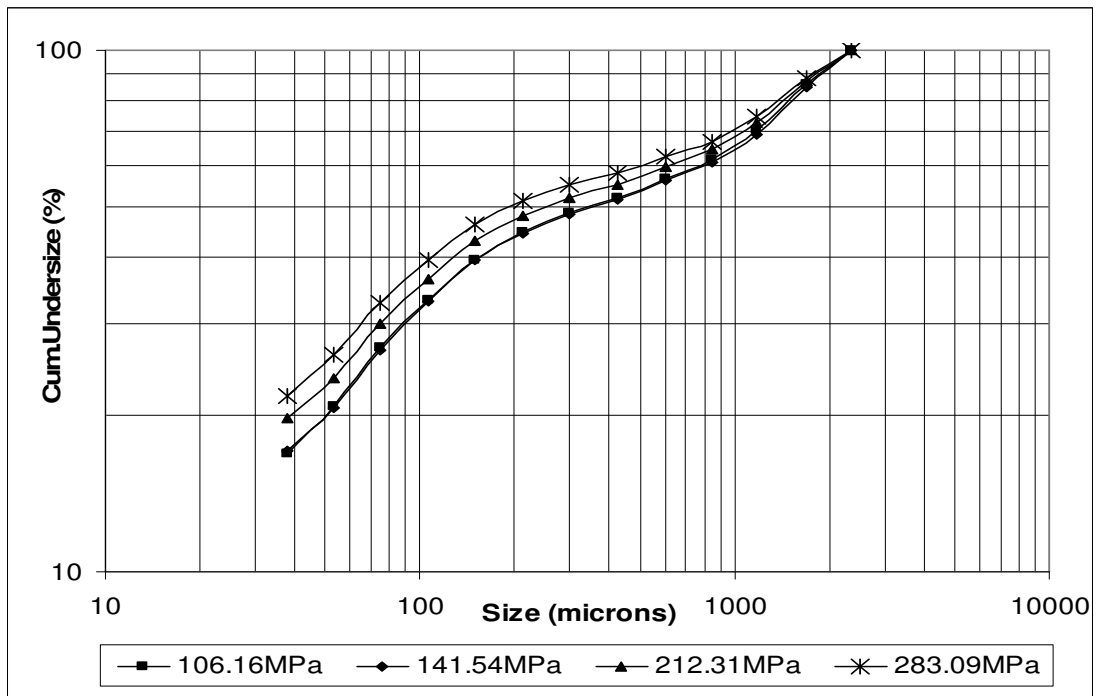
Figure D. 11: Product particle size distribution graph of -2.36+1.7mm calcite sample
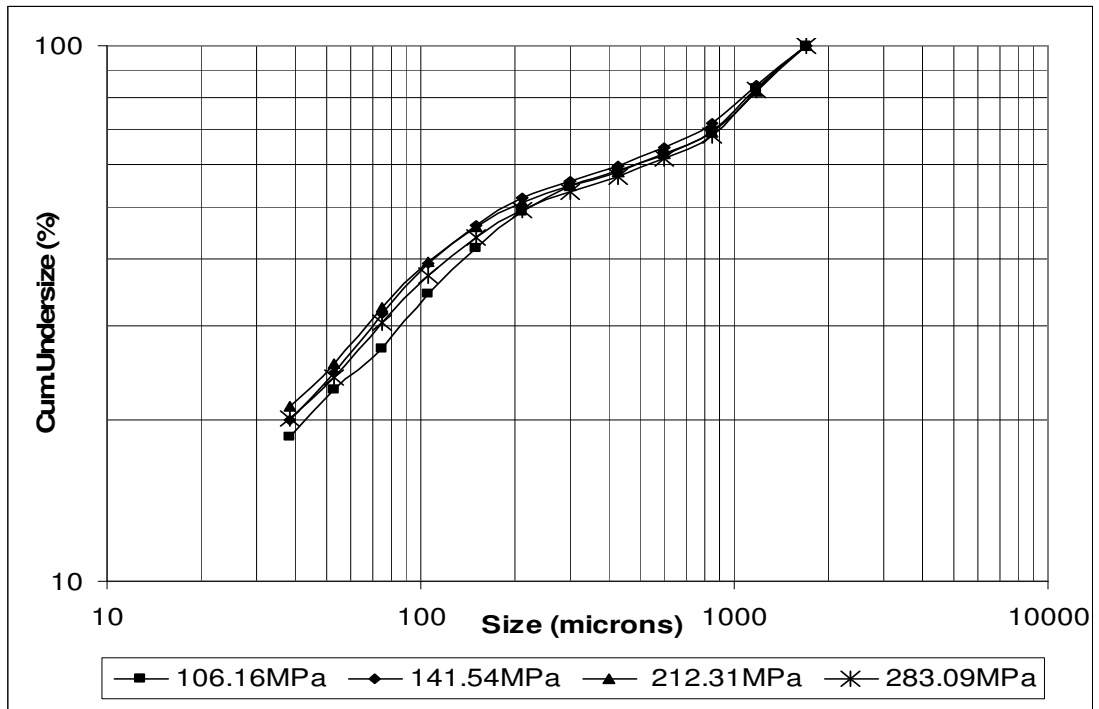
Figure D. 12: Product particle size distribution graph of -1.7+1.18mm calcite sample
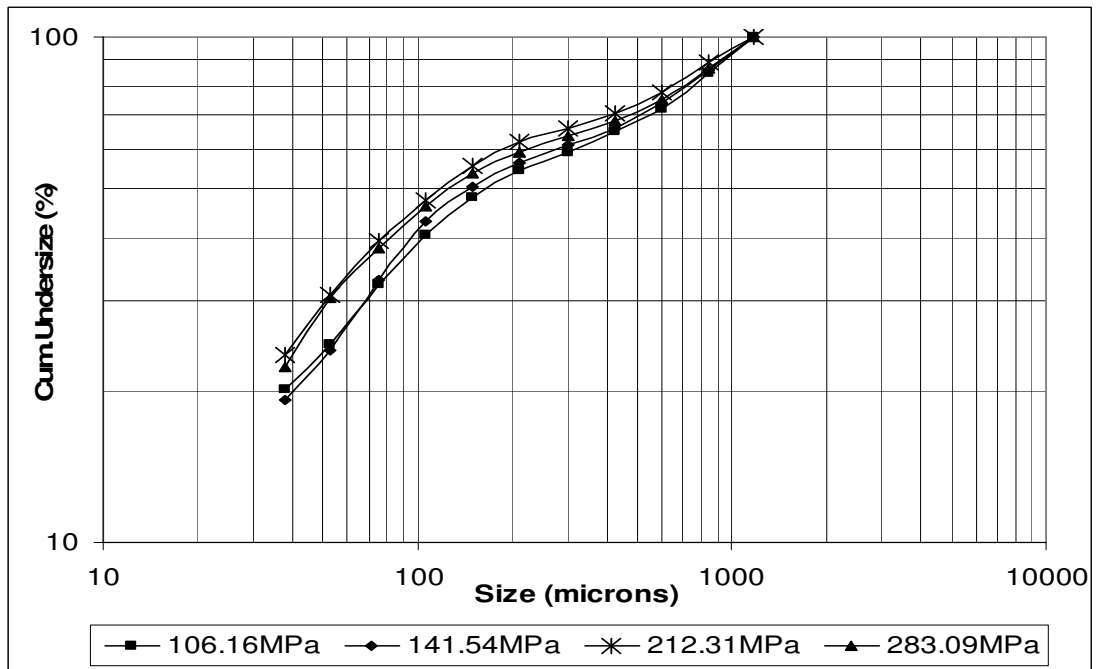

**Figure D. 13:** Product particle size distribution graph of -1.18+0.85mm calcite sample

108
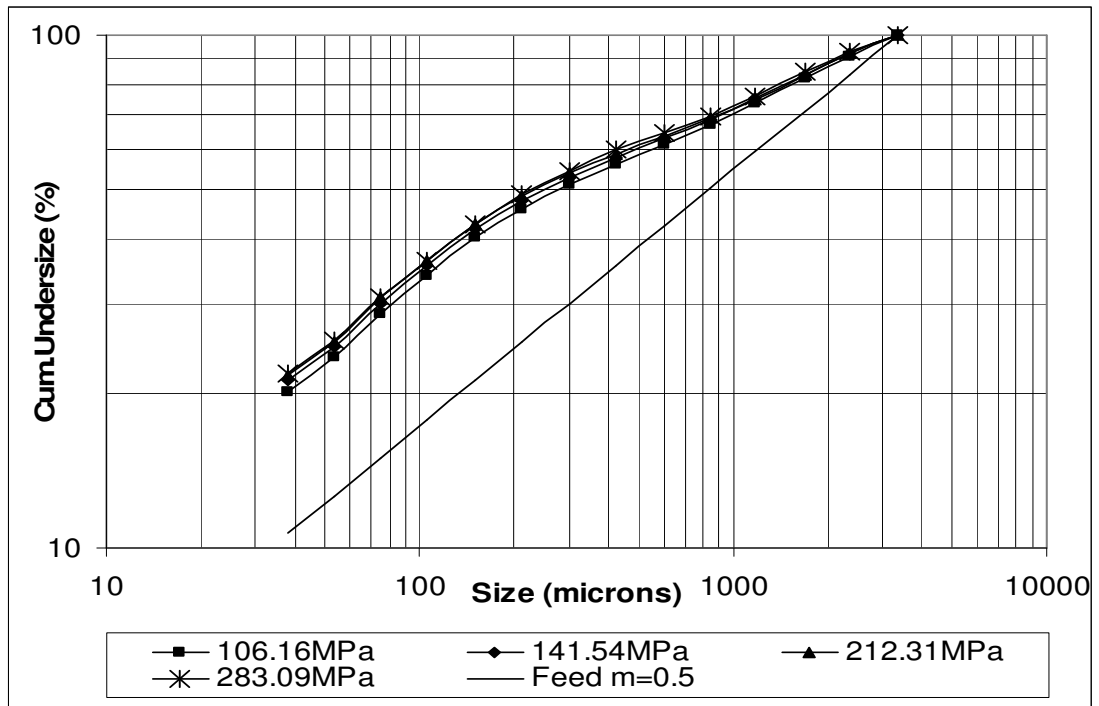
**Figure D. 14:** Product particle size distribution graph of m=0.5 calcite sample
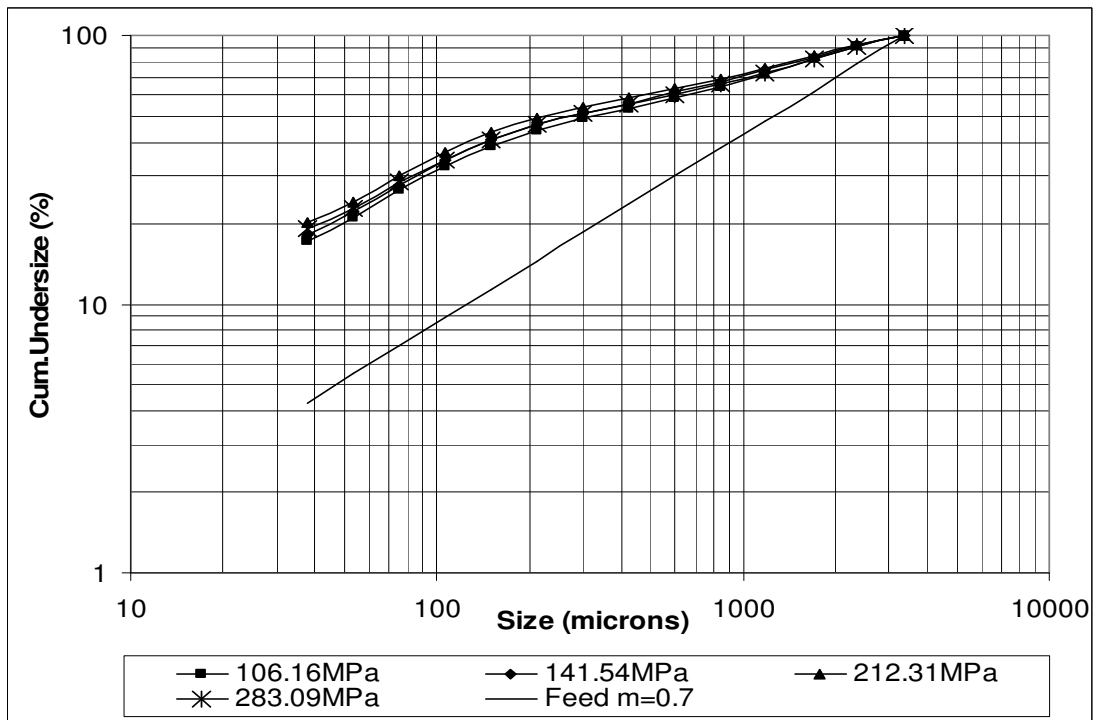
Figure D. 15: Product particle size distribution graph of m=0.7 calcite sample
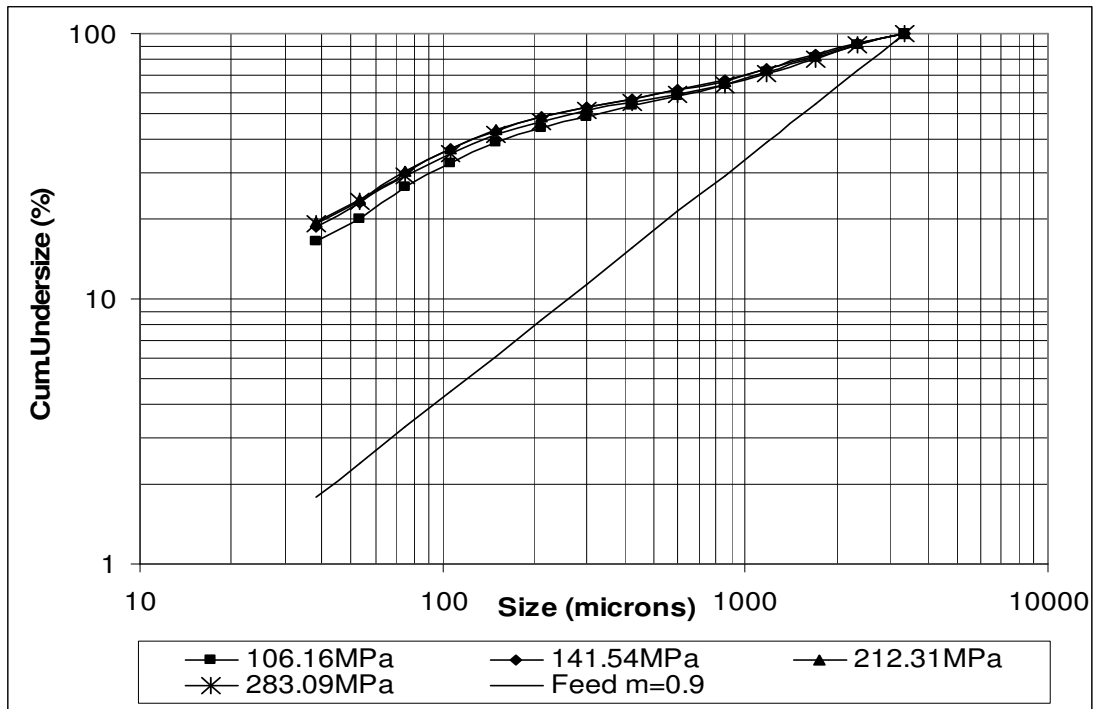
Figure D. 16: Product particle size distribution graph of m=0.9 calcite sample
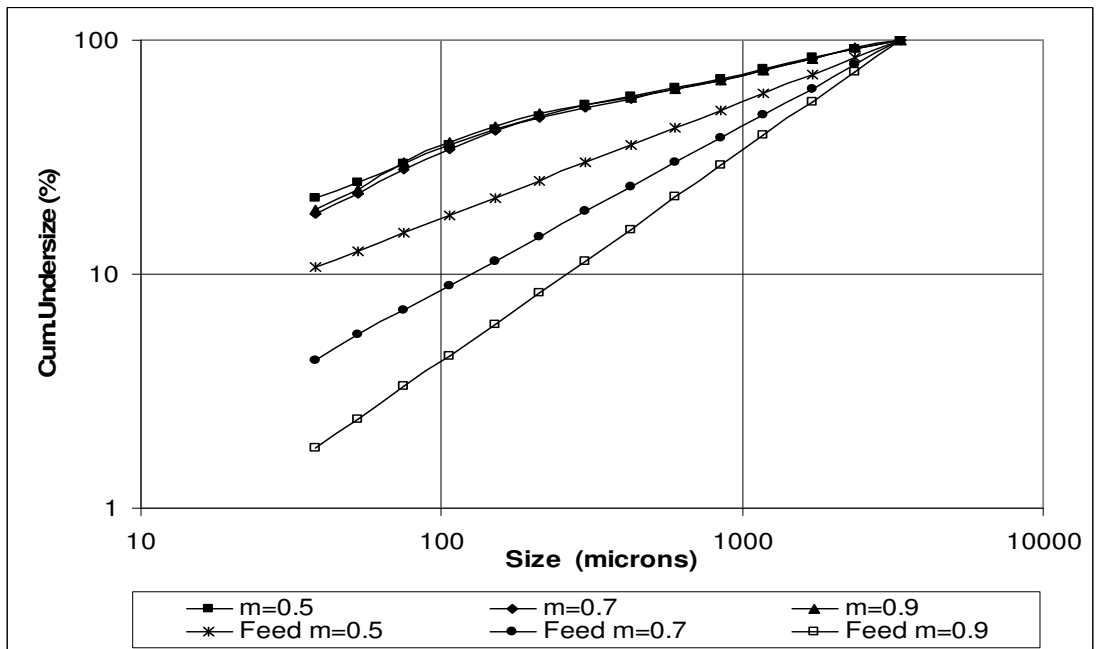
Figure D. 17: Comparison of the areas between ideal moduli lines at 0 pressure and the curves of those moduli, comminuted under 141.54 MPa pressure for calcite samples.
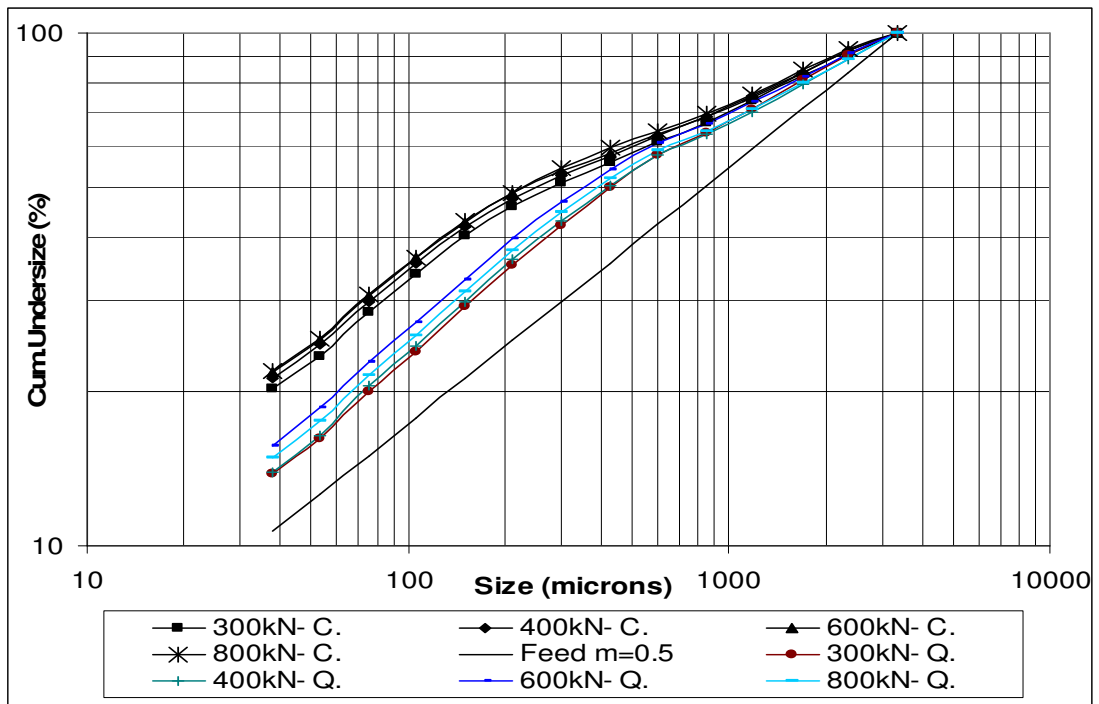
Figure D. 18: Comparison of product particle size distribution graphs of calcite and quartz samples for m=0.5 distribution modulus

APPENDIX E

NON-LINEAR REGRESSION TO CALCULATE THE PARAMETERS "A" AND "B" IN EQUATION 5

t_{10} values are plotted against their corresponding specific energy values (Ecs) to form a decaying exponential curve, and the slope at its origin is equal to A*B from Equation 5.

The parameters "A" and "B" were calculated by using a Software program SPSS 11.5 for Windows with the method of non-linear regression. "A" and "B" were calculated both for quartz and calcite at all size fractions. The following expressions are calculated for -3.35+2.36mm quartz in SPSS.

Non-linear Regression

```
All the derivatives will be calculated numerically.
```

| Iteration	Residual SS	A	B
1	4992,667065	7,00000000	1,00000000
1.1	41342,74882	49,1646227	-,39829736
1.2	3722,162693	10,3815029	2,24475680
2	3722,162693	10,3815029	2,24475680
2.1	1919,508962	18,1178452	2,86358810
3	1919,508962	18,1178452	2,86358810
3.1	147,7684714	33,6297984	3,04615738
4	147,7684714	33,6297984	3,04615738
4.1	3,0104E+16	41,5667799	-6,5350634
4.2	71,12109847	36,6575235	2,47118541
5	71,12109847	36,6575235	2,47118541
5.1	8603,819143	40,3648473	-,05438610
5.2	61,98706598	37,1993289	2,26460000
6	61,98706598	37,1993289	2,26460000
6.1	46,06097865	38,0853441	1,82423599
7	46,06097865	38,0853441	1,82423599
7.1	27,85307608	40,1151884	1,34354561

```
  8        27,85307608  40,1151884  1,34354561
  8.1      17,70528087  44,4672439  ,945362478
  9        17,70528087  44,4672439  ,945362478
  9.1      3,276894796  49,4650037  ,785970267
 10        3,276894796  49,4650037  ,785970267
 10.1      1,191415108  49,9250562  ,800405403
 11        1,191415108  49,9250562  ,800405403
 11.1      1,191409403  49,9264511  ,800406653
 12        1,191409403  49,9264511  ,800406653
 12.1      1,191409403  49,9264506  ,800406670
```

Run stopped after 27 model evaluations and 12 derivative evaluations.
Iterations have been stopped because the relative reduction between
successive
residual sums of squares is at most SSCON = 1,000E-08

Nonlinear Regression Summary Statistics   Dependent Variable T10

Source	DF	Sum of Squares	Mean Square
Regression	2	6961,17149	3480,58574
Residual	3	1,19141	,39714
Uncorrected Total	5	6962,36290	
(Corrected Total)	4	89,66062	

R squared = 1 – Residual SS / Corrected SS =   ,98671

| | | Asymptotic | Asymptotic 95 % Confidence Interval | |
Parameter	Estimate	Std. Error	Lower	Upper
A	49,926450607	1,900704023	43,877562110	55,975339104
B	,800406670	,067629435	,585179625	1,015633716

113

APPENDIX F

REPEATABILITY OF EXPERIMENTS
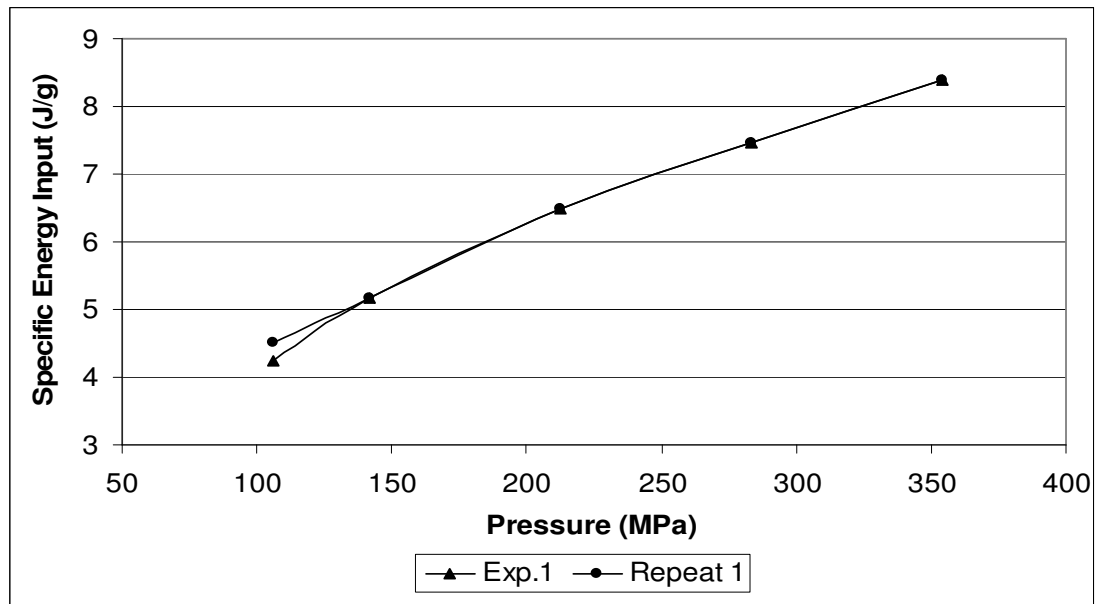
Figure F. 1: Repeatability of specific energy input values of -3.35+2.36mm quartz sample at 30 ton load in piston-die-press set-up
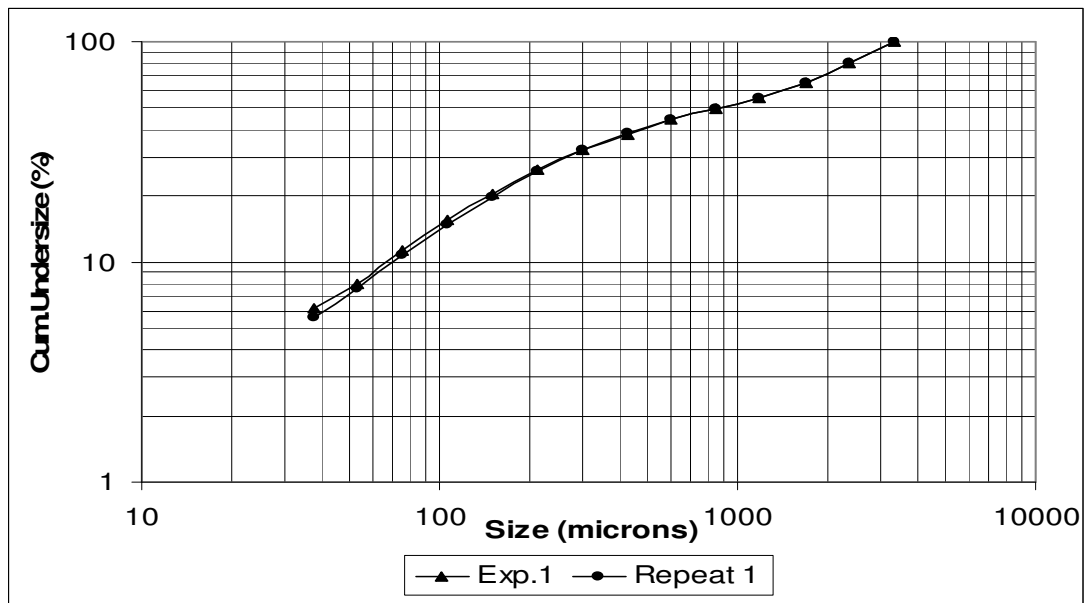
Figure F. 2: Repeatability of particle size distribution of -3.35+2.36mm quartz sample at 30 ton load in piston-die-press set-up
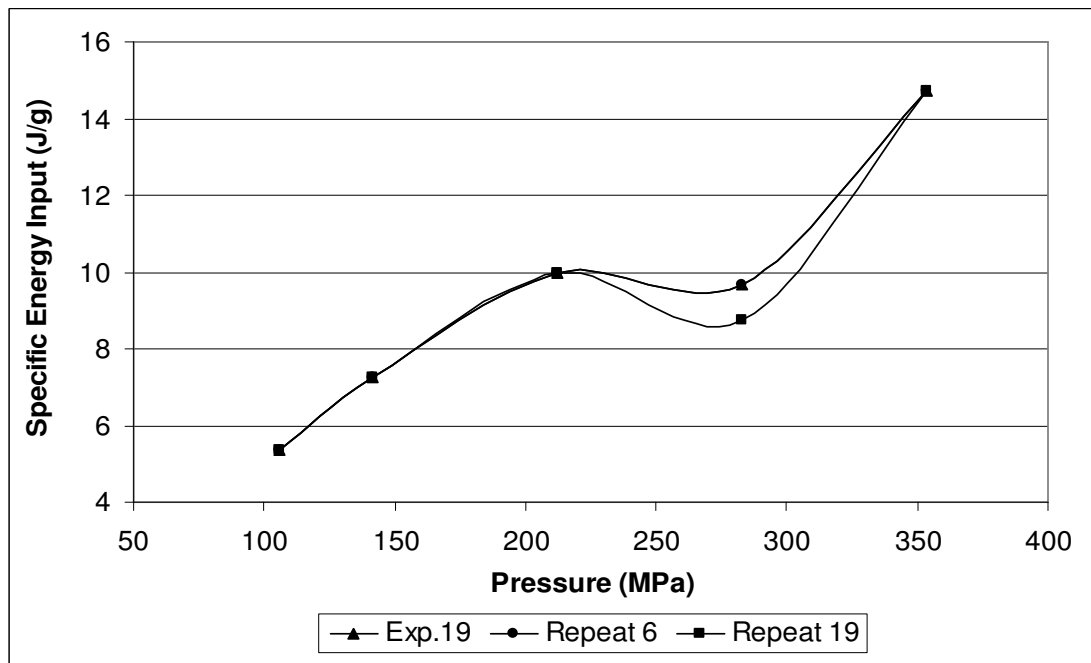

Figure F. 3: Repeatability of specific energy input values of -1.18+0.85mm quartz sample at 80 ton load in piston-die-press set-up
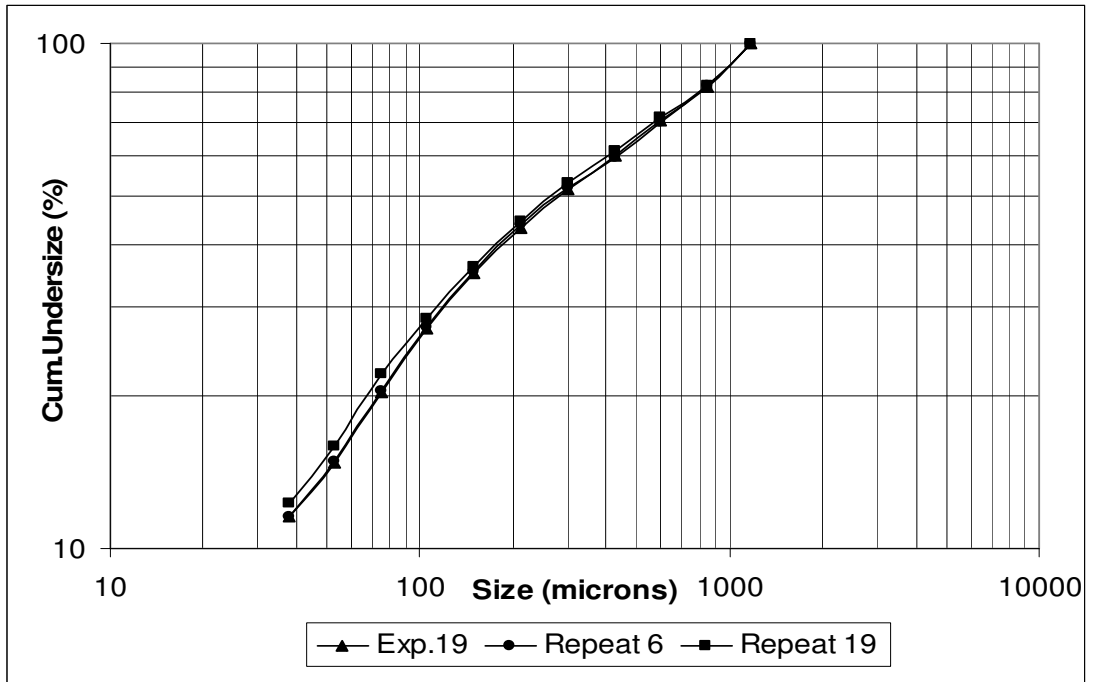
Figure F. 4: Repeatability of particle size distribution of −1.18+0.85mm quartz sample at 80 ton load in piston-die-press set-up
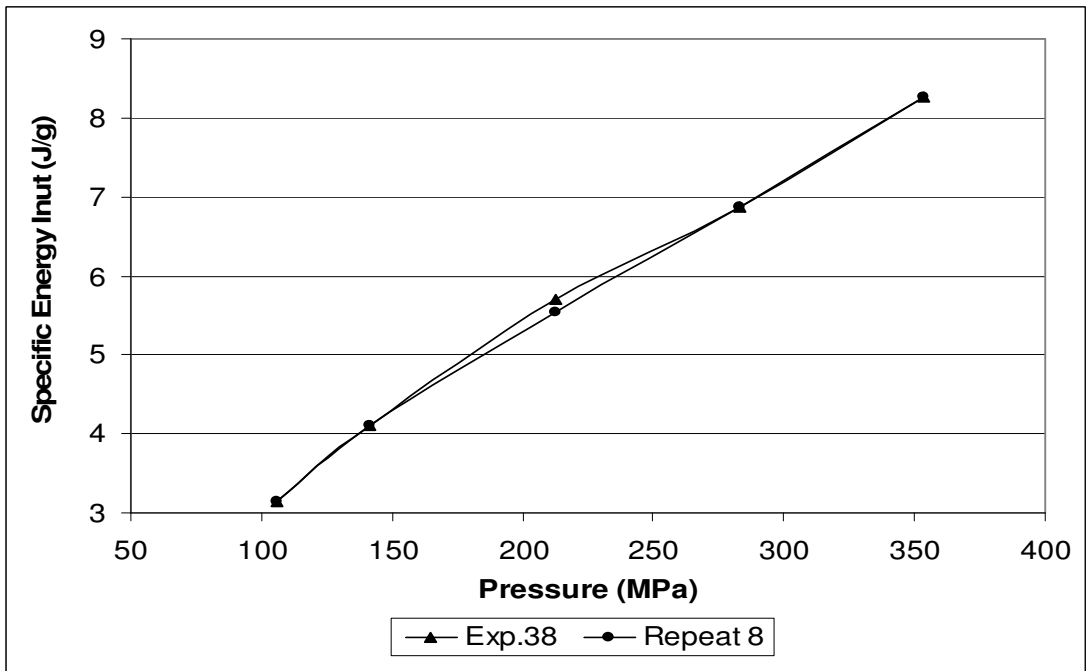

Figure F. 5: Repeatability of specific energy input values of m=0.9 quartz sample at 60 ton load in piston-die-press set-up
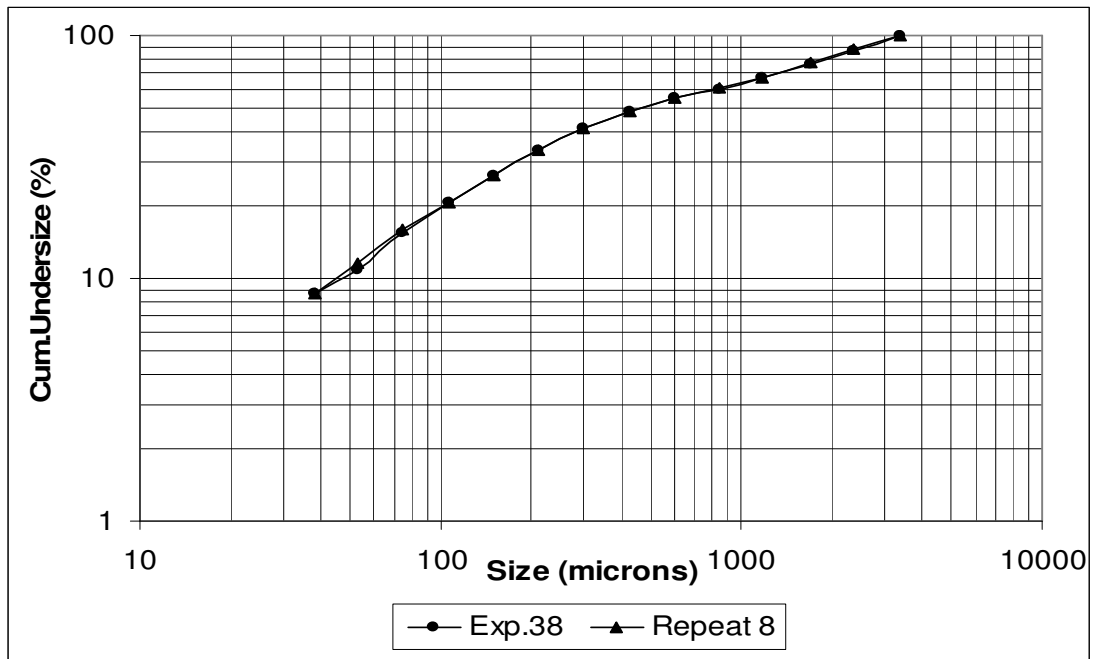
Figure F. 6: Repeatability of particle size distribution of m=0.9 quartz sample at 60 ton load in piston-die-press set-up
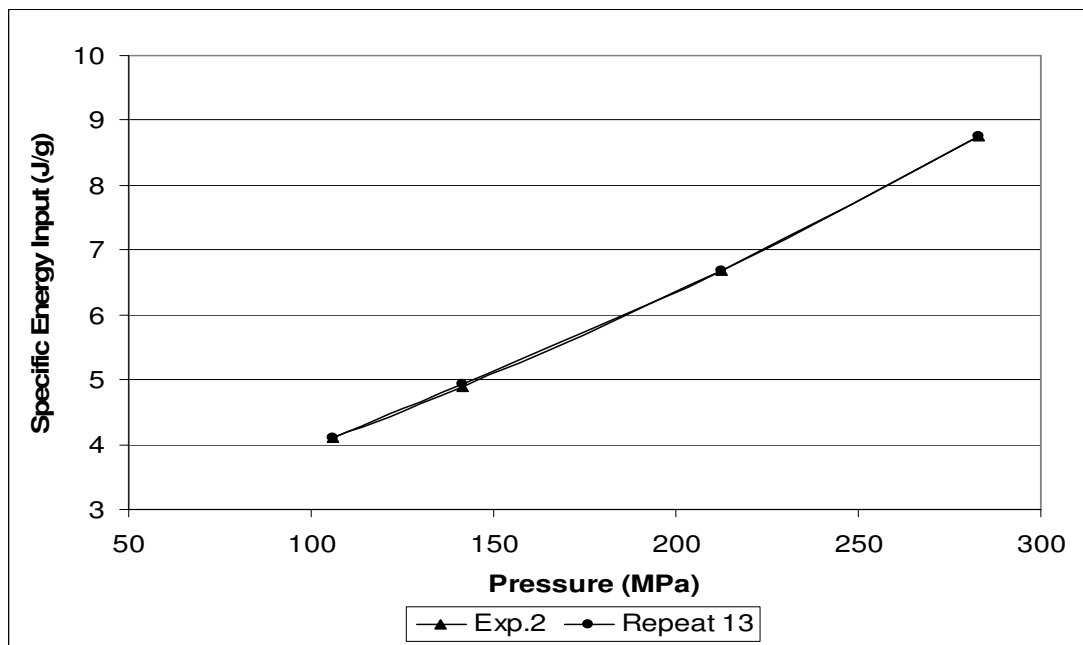

Figure F. 7: Repeatability of specific energy input values of -3.35+2.36mm calcite sample at 40 ton load in piston-die-press set-up
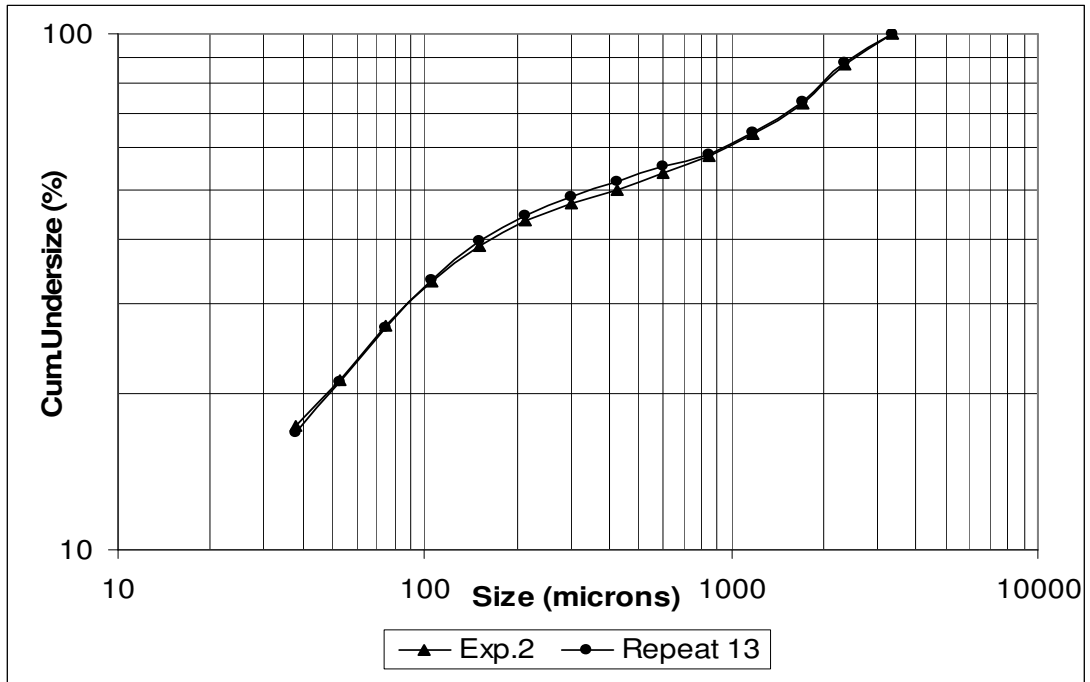
Figure F. 8: Repeatability of particle size distribution of -3.35+2.36mm calcite sample at 40 ton load in piston-die-press set-up
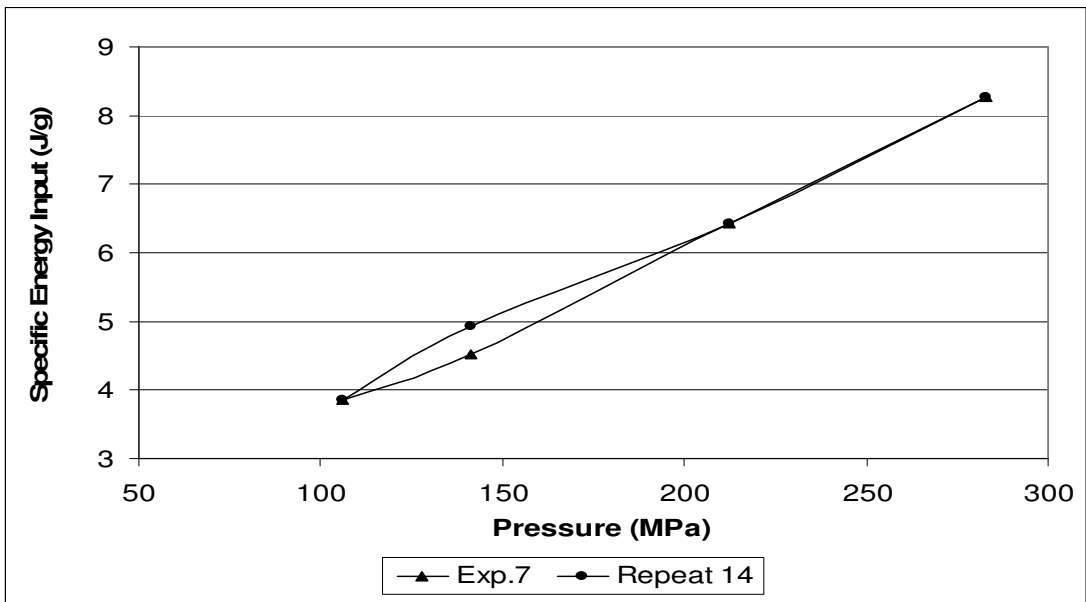
Figure F. 9: Repeatability of specific energy input values of -2.36+1.7mm calcite sample at 40 ton load in piston-die-press set-up
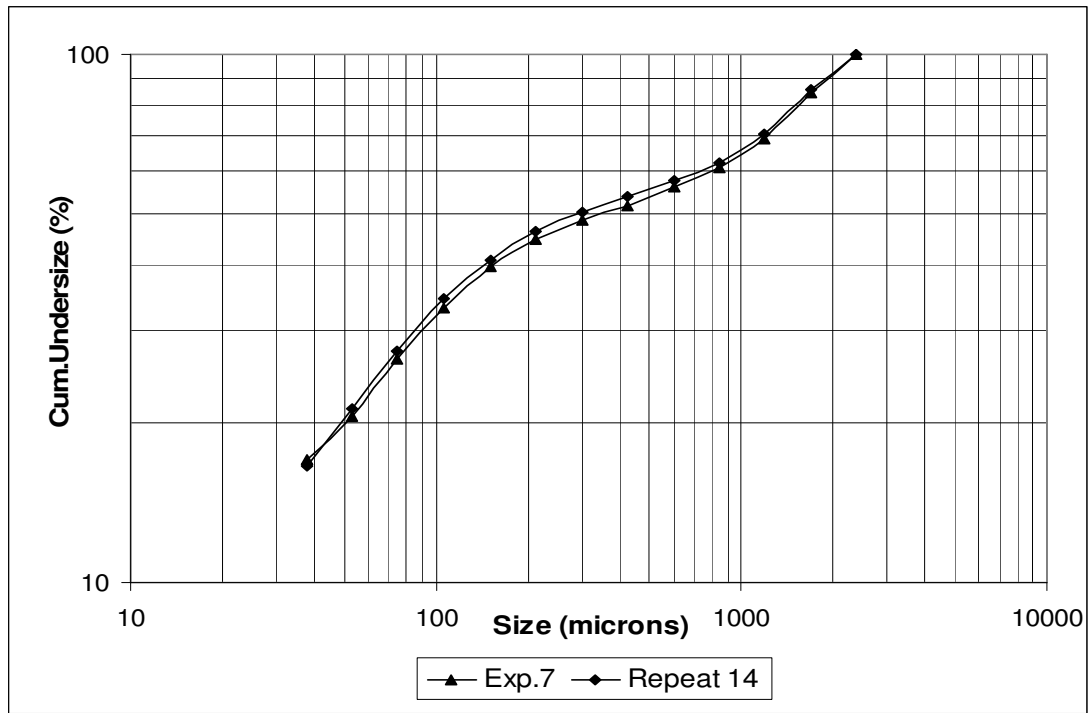
Figure F. 10: Repeatability of particle size distribution of -2.36+1.7mm calcite sample at 40 ton load in piston-die-press set-up

APPENDIX G

SIZE REDUCTION CURVES AND ENERGY UTILIZATION

Table G. 1: Specific energy inputs for unit size reduction areas, calculations based on the data in Table 3-6

	Specific Energy Input (J/g) for Unit Area							
	300kN		400kN		600kN		800kN	
	Quartz	Calcite	Quartz	Calcite	Quartz	Calcite	Quartz	Calcite
m=0.5	0.00265	0.00203	0.00381	0.00234	0.00409	0.00341	0.00558	0.00432
m=0.7	0.00205	0.00161	0.00256	0.00175	0.00292	0.00240	0.00355	0.00346
m=0.9	0.00174	0.00134	0.00208	0.00153	0.00289	0.00262	0.00317	0.00313